ISSN 2221-6413 (Print), ISSN 2223-2559 (Online)
Coden: PJSIB5 58(1) 1-58 (2015)

Pakistan Journal of Scientific and Industrial Research

Series A: Physical Sciences

Vol. 58, No.1, January-February, 2015

(for on-line access please visit web-site http://www.pjsir.org)

Published by
Scientific Information Centre
Pakistan Council of Scientific and Industrial Research
Karachi, Pakistan

Pakistan Journal of Scientific and Industrial Research
Series A: Physical Sciences

EDITORIAL BOARD

Dr. Kaniz Fizza Azhar
Executive Editor

MEMBERS

Prof. R. Amarowicz
Polish Academy of Sciences
Olsztyn, Poland
Dr. A. Chauhan
Nat. Institute of Pharma. Education and Research, Mohali, India
Dr. Debanjan Das
C.B. Fleet Company, Inc.,VA, USA
Dr. S. Goswami
Rawenshaw University, Cuttack, India
Prof. S. Haydar
University of Engg. & Technology
Lahore, Pakistan
Dr. H. Khan
Institute of Chemical Sciences
University of Peshawar, Pakistan
Prof. W. Linert
Institute of Applied
Synthetic Chemistry,
Vienna, Austria
Prof. R. Mahmood
Slippery Rock University
Pennsylvania, USA
Dr. S. K. Rastogi
Dept. of Chem. &
Biochemistry, Texas State
University, USA
Dr. I. Rezic
Faculty of Textile Technology
Zagreb, Croatia
Dr. J. P. Vicente
ETSCE, Universitat Jaume I
Spain
Prof. Z. Xie
Imperial College
London University
UK
Prof. Z. Xu
Chinese Academy of Sciences
Beijing, China

Editors: **Ghulam Qadir Shaikh** **Shagufta Y. Iqbal** **Shahida Begum** **Sajid Ali**

Pakistan Journal of Scientific and Industrial Research started in 1958, has been bifurcated in 2011 into:

Series A: Physical Sciences [**ISSN 2221-6413 (Print); ISSN 2223-2559 (online)]** (appearing as issues of January-February, May-June and September-October) and
Series B: Biological Sciences [**ISSN 2221-6421 (Print); ISSN 2223-2567 (online)]** (appearing as issues of March-April, July-August and November-December).
Each Series will appear three times in a year.

This Journal is indexed/abstracted in Biological Abstracts and Biological Abstracts Reports, Chemical Abstracts, Geo Abstracts, CAB International, BioSciences Information Service, Zoological Record, BIOSIS, NISC, NSDP, Current Contents, CCAB, Rapra Polymer Database, Reviews and Meetings and their CD-ROM counterparts etc.

Subscription rates (including handling and Air Mail postage): ***Local:*** Rs. 2500 per volume, single issue Rs. 425; ***Foreign:*** US$ 450 per volume, single issue US$ 75.

Electronic format of this journal is available with: Bell & Howell Information and Learning, 300, North Zeeb Road, P.O. 1346, Ann Arbor, Michigan 48106, U.S.A; Fax.No.313-677-0108; http://www.proquest.com

Photocopies of back issues can be obtained through submission of complete reference to the Executive Editor against the payment of Rs. 25 per page per copy (by Registered Mail) and Rs. 115 per copy (by Courier Service), within Pakistan; US$ 10 per page per copy (by Registered Mail) and US$25 per page per copy (by Courier Service), for all other countries.

Copyrights of this Journal are reserved; however, limited permission is granted to researchers for making references, and libraries/agencies for abstracting and indexing purposes according to the international practice.

Printed and Published by: PCSIR Scientific Information Centre, PCSIR Laboratories Campus, Shahrah-e-Dr. Salimuzzaman Siddiqui, Karachi-75280, Pakistan.

Editorial Address

Executive Editor
Pakistan Journal of Scientific and Industrial Research, PCSIR Scientific Information Centre
PCSIR Laboratories Campus, Shahrah-e-Dr. Salimuzzaman Siddiqui, Karachi-75280, Pakistan
Tel: 92-21-34651739-40, 34651741-43; Fax: 92-21-34651738; Web: http://www.pjsir.org, E-mail: info@pjsir.org

Pakistan Journal of Scientific and Industrial Research
Series A: Physical Sciences
Vol. 58, No.1, January-February, 2015

Contents

Pak. j. sci. ind. res. Ser. A: phys. sci. 2015 **58** (1) 1-7

Catalytic Hydrodechlorination of 2,4-Dichlorophenol Using Co-Current Down Flow Contactor Reactor

Asim Rehman[a]*, Muhammad Nawaz[b], Arshad Chughtai[c], Muhammad Arif Butt[a] and Abdul Sattar[a]

[a]Institute of Chemical Engineering and Technology, University of The Punjab, Quaid-e-Azam Campus, Lahore 54590, Pakistan

[b]School of Chemical Engineering, The University of Faisalabad, Faisalabad, Pakistan

[c]School of Chemical and Materials Engineering, National University of Sciences and Technology, H-12 Islamabad, Pakistan

(received July 1, 2013; revised February 16, 2014; accepted February 18, 2014)

Abstract. In this study, a new prospective regarding application of gas liquid reactions in the presence of catalyst was studied for pollution abatement in the novel reactor. Catalytic hydrodechlorination (CHDC) of 2,4-dichlorophenol (2,4-DCP) in aqueous system was carried out under the operating conditions at 25-75 °C, 1 atm in co-current down flow contactor reactor. Under these reaction conditions complete conversion of 2,4-DCP into less toxic products (phenol and cyclohexanone) was achieved using 5% Pd/C catalyst. At typical temperature the hydrodechlorination reaction of 2,4-DCP was completed after 10 min. 2,4-DCP was converted to 96.19% of phenol and 3.81% of cyclohexanone using 0.4 g/L of 5% Pd/C catalyst. The increase in initial concentration of 2,4-DCP resulted in the increase in time for the dechlorination of 2,4-DCP. The calculated activation energy values amounted to 43 KJ/mol for the CHDC of 2,4-DCP exhibiting that this reaction occurs mainly under the surface reaction rate controlled condition.

Keywords: catalytic hydrodechlorination, 2,4-dichlorophenol, palladium, carbon, co-current downflow contactor reactor

Introduction

Chlorophenols (CPs) are extensively used in the production of herbicides, dyes, wood protectors and plant regulators. The wastewater coming from such industries has a considerable and variable amount of CPs which is highly toxic and poorly biodegradable as reported by Czaplicka (2004). Due to their high toxicity and resistance to degradation, CPs have been listed as priority pollutants as per Proposition 65 by the Environmental Protection Agency, USA (EPA, 2005) and as per WHO guidelines (WHO, 1996) on CPs in drinking water.

CPs are widely distributed in the environment in different forms such as dissociated, non-dissociated and adsorbed on the suspended matters. Reported studies of Sithole *et al.* (1986) and Czaplicka (2001), state that CPs are present in reservoirs, surface water and in sediments. In ambient air, CPs are present as a result of vapours coming from the production related activities utilising chlorine, combustion of wastes, coal and wood. As per Berg (1990), the effect on ambient air is directly related to the local emission source. In soil, the presence of CPs is the result of wastewater discharge from the chlorinated industries, biodegradation of herbicides and pesticides. The transportation of contaminants in soil was studied by Knuutinen *et al.* (1990) which is affected by the pH of the soil, nature of contaminant, solubility in water, evaporation rates and biodegradation rates.

The catalytic hydrodechlorination (CHDC) has different advantages over the oxidation process such as the selectivity of different types of the catalysts, chemical reactors and mild reaction conditions. It offers a possible unit process having cost effectiveness in which chlorine is converted to salt (chloride ion) and phenol into saturated cyclic alcohol i.e., cyclohexanol (Vaidya and Mahajani, 2004). CHDC has a wide range of application in chlorobenzene (Meshesha *et al.,* 2009), both in gas phase (Keane and Murzin, 2001) and multiphase mixture (Murena and Giogia, 2004), chloroethylenes (Concibido *et al.,* 2005; Nishijima *et al.,* 2004), chlorobiphenyls (Gryglewicz *et al.,* 2006), carbon tetrachloride (Gomez-Sainero *et al.,* 2002; 2000) and chloroethanes (Mori *et al.,* 2004). The precious metal Pd, Pt, and Rh exhibited

*Author for correspondence; E-mail: asim_rehman@live.com

the highest activity in the CHDC reaction with a wide range of supported metals such as Pd/C, Pd/Al_2O_3 and Rh/C (Yuan and Keane, 2003), Ru-Pd/TiO_2 (Vaidya and Mahajani, 2004), Pd/Mg(Al)O (Meshesha *et al.,* 2009), Pd, Pt, Rh/Al_2O_3 (Diaz *et al.,* 2008), Pd/SiO_2 (Jujjuri *et al.,* 2009), Pd/Fe (Graham *et al.,* 2005) and Pd/ activated carbon (Xia *et al.,* 2009; Da-Silva *et al.,* 2007; Calvo *et al.,* 2004).

The co-current downflow contactor reactor (CDCR) was initially used for the hydrogenation of Iatonic acid by Lu *et al.* (1996) and 2-butyne 1,4-diol by Winterbottom *et al.* (2003). The reactor exhibited excellent gas liquid mass transfer characteristics as a slurry reactor with the following characteristics i.e., high gas holdup, high mass transfer efficiencies, improved selectivity and process intensive. During the evaluation of mass transfer characteristics of CDCR in a fermentation broth (Dursun *et al.,* 1999), the result indicates that K_{La} and gas holdup increases with increasing liquid and gas flow rate and is suitable for biotechnological processes. Due to significant advantages over conventional bubble column reactor, the CDCR was used in the photocatalytic oxidation reactions of chlorophenols by Ochuma and Fishwick (2007a) and Ochuma and Osibo (2007b). The results indicate that inherit characteristics of CDCR resulted in complete demineralisation in the short reaction time.

The objective of this study was to carry out CHDC reaction of 2,4-DCP in CDCR in the presence of Pd/C catalyst under mild reaction conditions. It is the first time that CDCR was used for CHDC reaction studies.

Materials and Methods

Materials. Pd/C catalyst 5% was purchased from GFS chemicals and used without further treatment. In all the experiments 2,4-DCP (purity>99%) of Alfa Aesar, 2-CP (purity>98%) of Fluka and following chemicals of Merck 4-CP (purity>98%), cyclohexanol (purity>98%), cyclohexanone (purity>98%), phenol (purity>99%) and sodium hydroxide (purity 99-100%) were used. For preparation of solutions during the experimentation, deionised water was used and hydrogen and nitrogen gases having 99.99% purity were used in experimentations.

Hydrodechlorination reactor (CDCR). All experiments were carried out in the CDCR and schematic diagram of reactor is represented in Fig. 1. In the CDCR hydrogen gas and reaction mixture (2,4-DCP, 5% Pd/C catalyst & NaOH) were introduced at the top of a fully flooded column co-currently through an orifice having diameter 0.5 mm. As a result, in the upper section of the fully flooded column, vigorous gas-liquid dispersion was formed by the high velocity liquid jet which prevents the formation of gas pockets at the top section. During the whole reaction, the gas bubble rise velocity was at higher side with reference to the down flow liquid velocity in the CDCR which prevents, at the bottom, the entrainment of gas bubbles. Due to this, nearly uniform sized bubble dispersion was formed throughout the column. At the bottom of the CDCR and throughout the dispersion, the coalescence occurd producing larger bubbles to rise up which were smashed up by the incoming high velocity inlet liquid stream having the fresh inlet gas which then impulsively merged in the inlet region to give the distinctive and uniform bubble size. The total volume of the system was 6 L with QVF glass column having dia 0.0381 m and length 2.43 m. The flow rate of liquid was 1.8 L/min, whereas the flow of H_2 gas was kept constant in all the experiments.

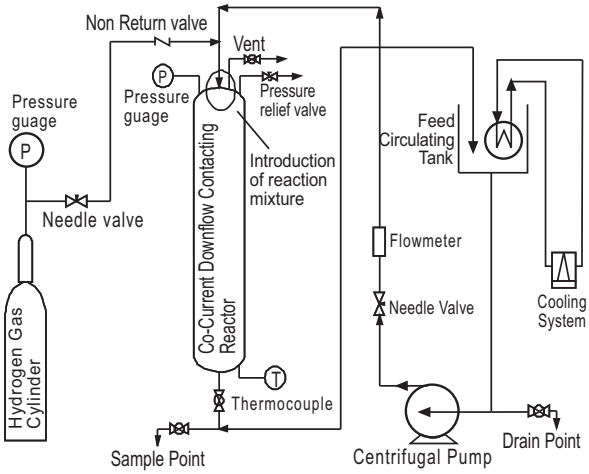

Fig. 1. Schematic diagram for CHDC reaction in CDCR.

Product analysis. The concentration of 2,4-DCP and reaction products was determined by gas chromatograph having model VARIAN CP 3800 in flame ionisation detector mode and VF-5ms column (30 m in length, 0.25 μm film thickness and Ø 0.25 mm). The temperature of column was programmed from 60 °C to 110 °C (2 min held) at the rate of 5 °C/min and then to 220 °C (3 min held) at a rate of 10 °C/min. Nitrogen gas was used as a carrier gas having flow rate of 1.4 mL/min under pressure of 8.5 psi. The injector and detector temperature was set at 250 °C. The identification of components of product mixture was carried

out by comparing the retention times of the solutes with standard chemicals and also with the help of co-injection technique.

Results and Discussion

In order to establish optimum conditions for CHDC of 2,4-DCP, the effect of pressure, temperature of the reaction media, the effect of catalyst loading and initial concentration of 2,4-DCP was investigated.

Effect of pressure. The effect of pressure was investigated by applying different pressures in CDCR. The effect of pressure was studied by using 489 mg/L of 2,4-DCP, 0.3 g/L of 5% Pd/C at 25 °C with the dispersion height of 40 cm. At 1 bar pressure the hydrodechlorination of 2,4-DCP was achieved in 45 min with the 0.52% of cyclohexanone and 99.48% of phenol. With the increase of pressure (at 2 bar) the conversion was very rapid as shown in Fig. 2(a-b) that, after 10 min, 2,4-DCP was totally hydrodechlorinated with the 4.46% of cyclohexanone and 95.54% of phenol. Identical results were reported by Calvo *et al.* (2004) conforming that the CHDC reaction can be carried out under mild pressure (2.4-3 bar) in fixed bed reactor however for CDCR the optimum pressure range is 1-2 bar. The increase in pressure resulted in high activity of the reaction and the reaction completed in the shortest time (~ 10 min) as the solubility increases the rate of reaction increases.

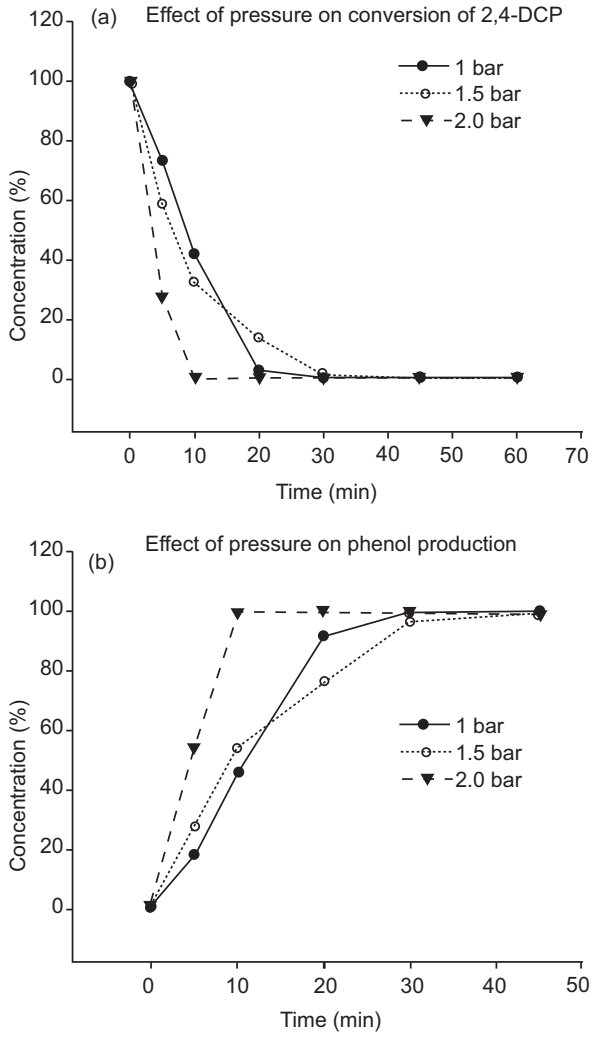

Fig. 2(a-b). The effect of pressure on the CHDC of 2,4-DCP.

Effect of temperature. The reaction was carried out at 25 °C, 35 °C and 45 °C by using initial concentration of 2,4-DCP as 489 mg/L, 0.3 g/L of 5% Pd/C, dispersion height 40 cm and at 1 bar of pressure. At 25 °C the reaction was completed within 30 min whereas the complete conversion of 2,4-DCP was achieved within 20 min at 45 °C and 2.47% of cyclohexanone was produced as the end product. The 2-CP and 4-CP were formed as the intermediate products but after 60 min of reaction, phenol and cyclohexanone were the end products as shown in Fig. 3(a-c). With the increase in temperature the conversion of 2,4-DCP improved, similar results were reported by Calvo *et al.* (2004).

The influence of temperature on the rate constant of a reaction is represented by the original equation of Arrhenius $k = A_{exp}\left(\frac{E_a}{RT}\right)$. The parameter of this relation activation energy (E_a) and pre exponent frequency factor (A) will be calculated using the linear regression analysis and applying the results presented in Fig. 4 (graph of 1/T along x-axis and ln-k along Y-axis) and the calculated activation energy is 43 KJ/mol indicating that the reaction occurred under surface reaction rate controlled conditions with negligible resistance to mass transfer as described by Satterfield (1970) and it is in accordance with the energy of activation for 2,4-DCP over Pd/C calculated by Yuan and Keane (2003).

Effect of catalyst loading. The change/variation in catalyst loading was carried out to investigate the optimum value for the treatment of 2,4-DCP. The experiments were carried out at different amounts of catalyst loading under the reaction conditions i.e., initial concentration of 2,4-DCP was 489 mg/L, 5% Pd/C, 25 °C and at 1 bar. As per result (Fig. 5), the increase in catalyst loading results in increased removal of 2,4-DCP. The top sketch of Fig. 6(a-c) depicts that 2-CP and 4-CP were intermediate products but the ultimate conversion was predominantly phenol with minor

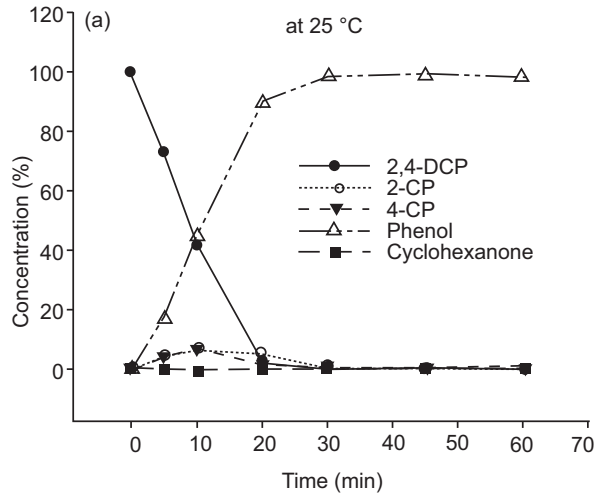

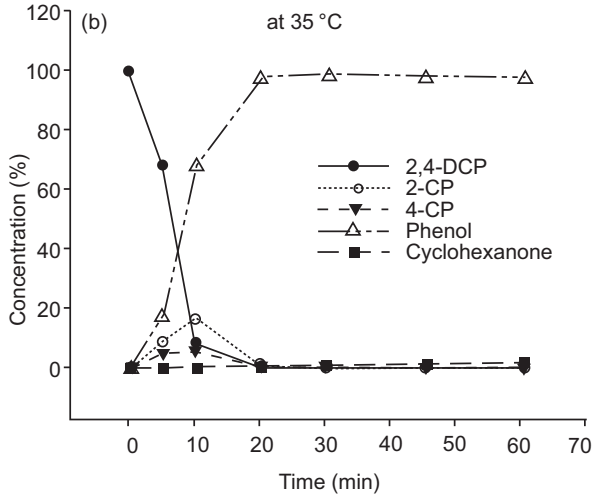

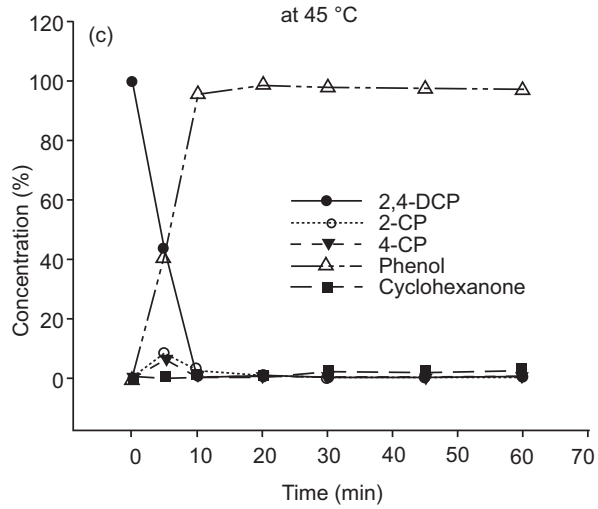

Fig. 3(a-c). The effect of temperature on the hydro-dechlorination of 2,4-DCP (a) at 25 °C, (b) 35°C and (c) at 45 °C.

amount of cyclohexanone. As reported by Yuan and Keane (2003) the cyclohexanone was formed over Pd/C catalyst on the completion of hydrodechlorination after phenol with the 2-CP as the only intermediate product. However, in the present study, both 2-CP and 4-CP were formed as the intermediate products but end products were only phenol and cyclohexanone.

Effect of initial concentration. The influence of initial concentration of 2, 4-DCP on hydrodechlorination was studied with 5% Pd/C catalyst loading at 25 °C under atmospheric pressure and at dispersion height of 40 cm. Figure 6(a-c) shows the effect of initial concentration on the catalytic hydrodechlorination of 2,4-DCP. With the increase in the initial concentration of 2, 4-DCP the time required for CHDC reaction was

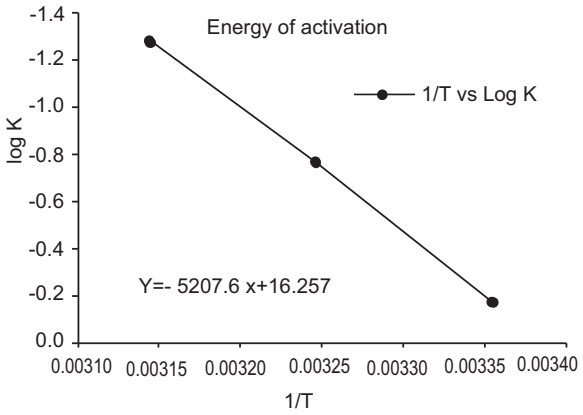

Fig. 4. Arrhenius plot of the rate constant measured in the range 298-318 K.

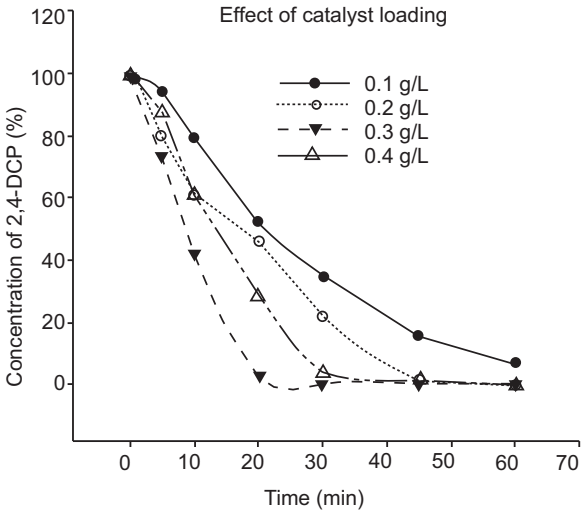

Fig. 5. The effect of catalyst loading on CHDC of 2,4-DCP at 25 °C.

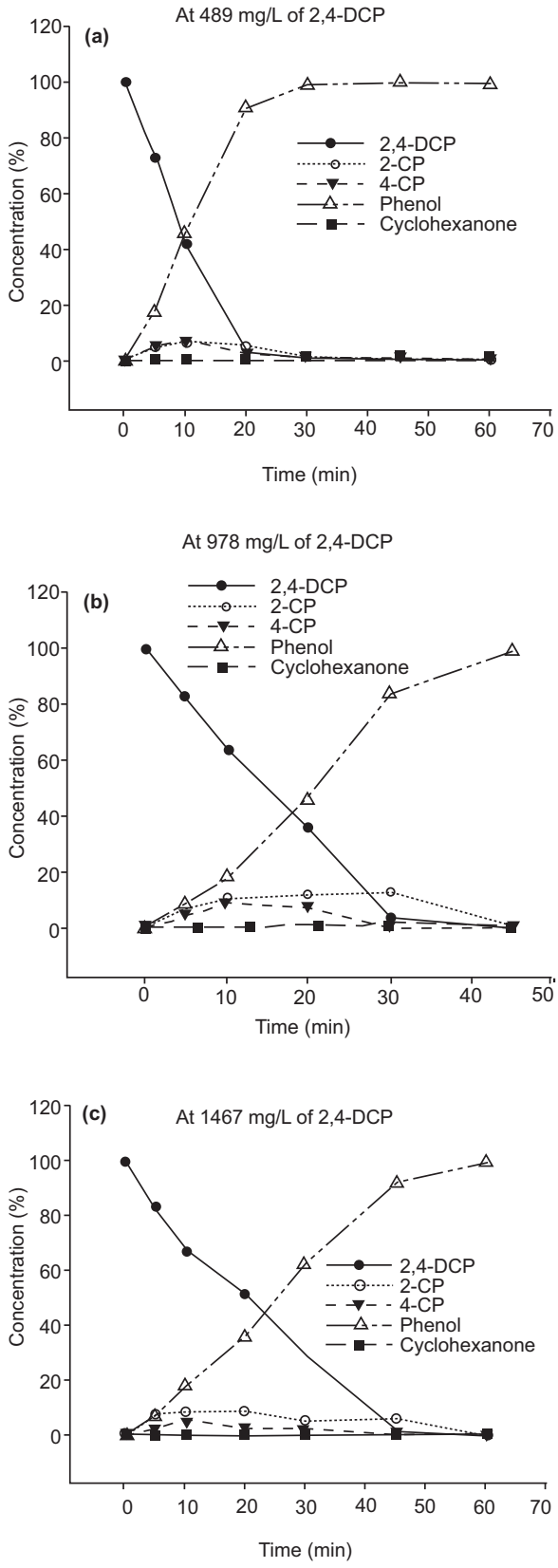

Fig. 6(a-c). The effect of initial concentration on the CHDC of 2,4-DCP.

also increased. More cyclohexanone was produced when 978 mg/L of 2, 4-DCP was used and in case of 1467 mg/L of 2,4-DCP, more phenol was produced in the end products.

Conclusion

The goal of this research was to develop optimum reaction parameters for the CHDC of 2, 4-DCP and suitability of CDCR as an efficient reactor technology. It was shown that 2, 4-DCP was almost completely hydrodechlorinated predominantly to phenol and fractions of this phenol was further hydrogenated to cyclohexanone at 25 °C under 1 atmospheric pressure in water with 5 % Pd/C catalyst loading with respect to reactant. The results indicate that the application of CDCR reactor in the CHDC is the promising and efficient technique for pollution abatement. The inherent characteristics of CDCR facilitates the reaction and in batch reactors offers less time to degrade the 2, 4-DCP. The calculated activation energy is 43 KJ/mol which indicates surface reaction rate controlled exhibiting efficient mass transfer in CDCR.

Acknowledgement

This study was supported by the Higher Education Commission of Pakistan vide NRPU P-1811/RND/119245 and University of the Punjab, Lahore, Pakistan.

References

Berg, L.G., Glas, B., Swanson, S.E., Rappe, C., Paul, K.G. 1990. Peroxidase-catalyzed oxidation of chlorophenols to polychlorinated dibenzo-p-dioxins and dibenzofurans. *Archive of Environmental Contamination and Toxicology,* **19:** 930-938.

Czaplicka, M. 2004. Sources and transformations of chlorophenols in the natural environment. *Science of the Total Environment,* **322:** 21-39.

Czaplicka, M. 2001. Determination of phenols and chlorophenols in bottom sediments. *Chromatographia,* **53:** 470-473.

Concibido, N.C., Okuda, T., Nakano, Y., Nishijima, W., Okada, M. 2005. Enhancement of the catalytic hydrodechlorination of tetrachloroethylene in methanol at mild conditions by water addition. *Tetrahedron Letters,* **46:** 3613-3617.

Calvo, L., Mohedano, A.F., Casas, J.A., Gilarranz, M.A., Rodrýguez, J.J. 2004. Treatment of chlorophenols bearing wastewaters through hydrodechlori-

nation using Pd/activated carbon catalysts. *Carbon,* **42:** 1377-1381.

Da-Silva, J.W., Bruns, R.E., Cobo, A.J.G. 2007. Study of the reaction conditions for the hydrodechlorination of pentachlorophenol on palladium catalysts. *Chemical Engineering Journal,* **131:** 59-64.

Dursun, G., Ozer, A., Elibol, M., Ozer, D.1999. Mass transfer characteristics of a fermentation broth in a reactor: co-current downflow contacting reactor. *Process Biochemistry,* **34:** 133-137.

Diaz, E., Casas, A., Mohedano, A.F., Calvo, L., Gilarranz M.A., Rodriguez, J.J. 2008. Kinetics of the hydrodechlorination of 4-chlorophenol in water using Pd, Pt, and Rh/Al_2O_3 catalysts. *Industrial & Engineering Chemistry Research,* **47:** 3840-3846.

EPA, 2005. *Proposition 65,* Office of Environmental Health Hazard, EPA, California, USA.

Gomez-Sainero, M.L., Seoane, X.L., Tijero, E., Arcoya, A. 2002. Hydrodechlorination of carbon tetrachloride to chloroform in the liquid phase with Pd/carbon catalyst. Study of mass transfer steps. *Chemical Engineering Science,* **57:** 3565-3574.

Gomez-Sainero, M.L., Seoane, X.L., Tijero, E., Arcoya, A., Cirtis, A. 2000. Hydrodechlorination of carbon tetrachloride to chloroform in the liquid phase with metal supported catalysts. Effect of catalyst components. *Industrial and Engineering Chemistry Research,* **39:** 2849-2854.

Graham, L.J., Atwater, J.E., Jovanovic, G.N. 2005. Chlorophenol Dehalogenation in a Magnetically. Stabilized Fluidized Bed Reactor. *AIChE Journal,* **52:** 1083-1093.

Gryglewicz, G., Stolarski, M., Gryglewicz, S., Klijanienko, A., Piechocki, W., Hoste, S., Driessche, V.I., Carleer, R., Yperman, J. 2006. Hydrodechlorination of dichloro-biphenyls over Ni–Mo/Al_2O_3 catalysts prepared by spray-drying method. *Chemosphere,* **62:** 135-141.

Jujjuri S., Keane, M.A. 2009. Catalytic hydrodechlorination at low hydrogen partial pressures: Activity and selectivity response. *Chemical Engineering Journal,* **157:** 121-130.

Knuutinen, J., Palm, H., Hakala, H., Haimi, J., Huhta, V., Salminen, J.1990. Polychlorinated phenols and their metabolities in soil and earthworms of sawmill environment. *Chemosphere,* **20:** 609-623.

Keane, M.A., Murzin, D.Y. 2001. A kinetic treatment of the gas phase hydrodechlorination of chlorobenzene over nickel/silica: beyond conventional kinetics. *Chemical Engineering Science,* **56:** 3185-3195.

Lu, X.X., Boyes, A.P., Winterbottom, J.M.1996. Study of mass transfer characteristics of co-current downflow bubble column reactor using hydrogenation of iatonic acid. *Chemical Engineering Science,* **51:** 2715-2720.

Meshesha, B.T., Chimentao, R.J., Medina F., Sueiras, J.E., Cesteros, Y., Salagre, P., Figueras, F. 2009. Catalytic hydrodechlorination of 1,2,4-trichlorobenzene over Pd/Mg(Al)O catalysts. *Applied Catalysis B: Environmental,* **87:** 70-77.

Murena, F., Gioia, F. 2004. Diffusional kinetics in the catalytic hydrodechlorination of chlorobenzene in multiphase aqueous mixtures. *Applied Catalysis A: General,* **271:** 145-151.

Mori, T., Kubo, J., Morikawa, Y. 2004. Hydrodechlorination of 1,1,1-trichloroethane over silica supported palladium catalyst. *Applied Catalysis A: General,* **271:** 69-76.

Nishijima, W., Ochi, Y., Tsung-Yuech, T., Nakano, Y., Okada, M.2004. Catalytic hydrodechlorination of chlorinated ethylenes in organic solvents at room temperature and atmospheric pressure. *Applied Catalysis B: Environmental,* **51:** 135-140.

Ochuma, I. J., Fishwick, R. P. 2007a. Photocatalytic oxidation of 2,4,6-trichlorophenol in water using a cocurrent downflow contactor reactor (CDCR). *Journal of Hazardous Materials,* **144:** 627-633.

Ochuma, I.J., Osibo, O.O. 2007b. Three-phase photocatalysis using suspended titania and titania supported on a reticulated foam monolith for water purification. *Catalysis Today,* **128:** 100-110.

Satterfield, C.N. 1970. *Mass Transfer in Heterogeneous Catalysis,* Chapter No.1. pp. 3-5, MIT Press, USA.

Sithole, B.B., Williams, D.T.1986. Halogenated phenols in water at forty Canadian potable water treatment facilities. *Journal of Association of Official Analytical Communities,* **69:** 807-810.

Vaidya, P.D., Mahajani, V.V. 2004. Studies in hydrotreatment as a unit process to destroy 4-chlorophenol in aqueous stream over Ru-Pd/TiO_2 catalyst. *Applied Catalysis B:*

Environmental, **51:** 21-31.

WHO, 1996. *Guideline for Drinking-Water Quality,* vol. **2**, 2nd edition, World Health Organization, Geneva, Switzerland.

Winterbottom, J.M., Marwan, H., Stitt, E.H., Natividad, R. 2003. The palladium catalysed hydrogenation of 2-butyne-1,4-diol in a monolith bubble column reactor. *Catalysis Today,* **79-80:** 391-399.

Xia, C., Liu, Y., Zhou, S., Yang, C., Liu, S., Guo, S., Liu, Q., Yu, J., Chen, J. 2009. The influence of ion effects on the Pd-catalyzed hydrodechlorination of 4-chlorophenol in aqueous solutions. *Catalysis Communications,* **10:** 1443-1445.

Yuan, G., Keane, M.A. 2003. Liquid phase catalytic hydrodechlorination of chlorophenols at 273 K. *Catalysis Communications,* **4:** 195-201.

Pak. j. sci. ind. res. Ser. A: phys. sci. 2015 **58** (1) 8-16

Assessment of the Intrinsic Vulnerability to Groundwater Contamination in Lahore, Pakistan

Khalid Mahmood*, Rabia Munsaf Khan, Mudabbar Ashfaq, Haseeb Ahsan, Zernain Shakoor and Muhammad Tanveer
Department of Space Science, University of the Punjab, Lahore, Pakistan

(received November 27, 2013; revised February 4, 2014; accepted March 13, 2014)

Abstract. This study was intended to map intrinsic vulnerability of groundwater contamination in Lahore using GIS based DRASTIC model. The final output of DRASTIC model was reclassified into three equal interval classes, corresponding to low, moderate and high vulnerability regions. Most of the study area was found to have low to moderate vulnerability, with 27.48% area of low, 66.48% of moderate and only 6.04% area of high vulnerability. Most of the drinking water wells are installed in the residential area of the city, which shows low chances of contamination due to deep water table and almost no recharge. However, an industrial drain is located in the high vulnerable area in the southeastern part of the study area. The previous studies are in agreement with vulnerability zones. Further to remove any doubt in the suitability of assigned weight, map removal sensitivity analysis had been carried out. The assessment of the sensitivity analysis had been made through visual as well as quantitative methods. Priority order for contribution of the parameters in the vulnerability for the study area is D>I>C>R>A>T>S.

Keywords: groundwater, intrinsic vulnerability, DRASTIC, weighted overlay, sensitivity analysis

Introduction

Water, the matrix of life, is essential for human existence over face of the earth. Fresh water constitutes only 2.5% of Earth's total water and only one third of it is available for human use (Mahmood *et al*., 2011). In this regard, groundwater serves as a major source of fresh drinking water in rural and urban areas (Mahmood *et al*., 2013). This source of fresh water is prone to contamination, that can cause many of the water borne diseases such as cholera, diarrhoea, typhoid, paratyphoid, hepatitis A, dermatitis and enteric fever (Butt and Ghaffar, 2012; Mahmood *et al*., 2011; Rehman, 2008). Considering importance of the source of freshwater, environmental protection policies give highest priorities to monitor groundwater quality (Mahmood *et al*., 2011).

Groundwater has self-purification capacity but the system is not strong enough to separate all kind of contaminations (Wang *et al*., 2012; Saidi *et al*., 2011). Even with the advances in technology, rehabilitation of polluted groundwater is very difficult and need heavy investment for a long period of time (Majandang and Sarapirome, 2013; You-Hailin *et al*., 2011). One of the possibilities to avoid groundwater contamination is through the identification of vulnerable areas followed by their remedial monitoring.

*Author for correspondence; E-mail: khalid.spsc@pu.edu.pk

The concept of groundwater vulnerability is very popular for the assessment of groundwater contamination risk and hence to preserve groundwater quality (Almasri, 2008) and exists since 1960. The term groundwater vulnerability is well defined by National Research Council (NRC, 1993), as the tendency or likelihood for contaminants to reach a specified position in the groundwater system after introduction at some location above the uppermost aquifer. This vulnerability largely depends upon the geological structure of the area as it controls the time for surface water to filter through the layers before reaching the aquifer (Rahman, 2008) but there are other factors as well.

Main problem of vulnerability based analysis is the handling of large heterogeneous data for the analysis (Rahman, 2008). Use of the geographic information system (GIS), in this regard, is very helpful as it facilitates spatial data management, analysis and mapping (Almasri, 2008). Studies mostly made use of weighted overlay and result into a map, produced by overlaying a series of layers, each correspond to a parameter for groundwater contamination (Majandang and Sarapirome, 2013). Among many types of vulnerability analysis, intrinsic vulnerability is a process independent of the nature of specific contaminants and takes into account the geological, hydrogeological and hydrological characteristics of an area (Shirazi *et al*., 2013). Each of the

parameters is assigned a weight or multiplier to show its relative importance as compared to other parameters. The index is calculated by summing all layers into an overall numerical score. On the basis of their attained value, the areas are classified into major classes such as areas having low, moderate and high vulnerability to groundwater contamination.

DRASTIC, acronym of seven input map hydro-geological parameters, is the most popular of the Overlay Indexed Methods and the most common method for aquifer sensitivity assessment (Shirazi *et al*., 2013; Wang *et al*., 2012; Pathak and Hiratsuka, 2011; Leone *et al*., 2009; Almasri, 2008; Rahman, 2008). It was developed by Aller *et al*. (1987) as a joint project with National Water Well Association (NWWA) and US Environmental Protection Agency, for aquifer sensitivity using depth to water table, aquifer material, soil composition, recharge rates, topography, vadose zone and saturated hydraulic conductivity (Shirazi *et al*., 2013). The results of DRASTIC are mainly dependent upon the weight and rating assigned to the input data layers. As the weight multiplier and assigned ratings are subjective so there exists doubt in the accuracy of the final output (Rahman, 2008). Usually in order to remove this doubt, sensitivity analysis is performed that assess the participation of each of the parameters to the vulnerability index (Huan *et al*., 2012; Saidi *et al*., 2011; Rahman, 2008; Almasri, 2008).

Materials and Methods

Study area. Lahore, the second largest city of Pakistan and provincial capital of Punjab, is an entirely groundwater dependent city (Mahmood *et al*., 2013). Like many other cities of Pakistan, Lahore is facing serious issues of groundwater quantity and quality degradation due to groundwater overexploitation and discharging of untreated sewage and industrial effluents (World Bank, 2006). The situation has pushed the communities to the risk of acquiring waterborne infection like water borne hepatitis A, E, cholera, diarrhoea, dysentery, typhoid and parasitic diseases, etc.

With a population of about 10 million, Lahore is 217 m above sea level and lies between 31°15′-31°45′N and 74°01′-74°39′E (Mahmood *et al*., 2011). It is bounded on the north and west by the Sheikhupura district, on the east by India and on the south by Kasur district. The river Ravi flows on the northern side of Lahore as shown in Fig. 1. Lithologically it lies in alluvial plain composed of quaternary sediments which are mainly of deltaic and alluvial origins (Farooqi *et al*., 2007). The thickness of sediments reaches several hundreds of meters and they comprise of coarse sand and a high concentration of fine to very fine sand and silt.

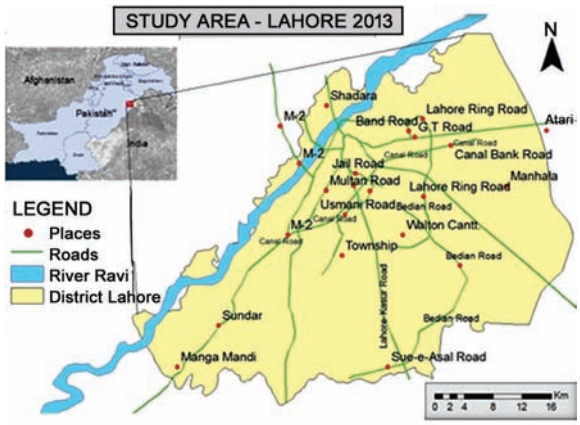

Fig. 1. Study area.

Data sets. Most of the input data like depth to water, aquifer media, soil media, vadose zone and hydraulic conductivity had been taken from water and power development authority (WAPDA), Lahore. The obtained data was in the vector format whereas the weighted overlay required data in raster format, so the data had been converted to raster with cell dimensions of 26 m. In addition to data obtained from WAPDA, some of the data like topography (slope) was generated for this study using freely available, 30 m ASTER DEM. The land cover map, used for recharge measurements, had been taken from WWF and an improved version of water table depth had been taken from a study by Mahmood *et al*. (2013).

Processing. After conversion of all the datasets to raster, each of the parametric layers has been reclassified, where smallest number represents lowest impact and largest number represents the highest. The scheme of classification is based on the Delphi technique which made use of the expert's opinion extracted from their practical and research work. As all the parameters never participate equally in controlling groundwater vulnerability so relative weights to each of them had been assigned, again using the Delphi technique. The used reclassification scheme and the assigned weights are shown in Table 1.

Table 1. Reclassification of used parameters and relative importance scheme

Parameter	Range	Assigned value	Numerical multiplier	Weight (%)
Water table depth (meter)	<6.9	10	5	22
	6.9-10.8	9		
	10.8-14.7	8		
	14.7-18.6	7		
	18.6-22.5	6		
	22.5-26.4	5		
	26.4-30.3	4		
	30.3-34.2	3		
	34.2-38.1	2		
	>40	1		
Recharge (Land cover types)	Built-up	1	4	17
	Sparsely built-up	2		
	Open/barren lands	3		
	Water bodies	8		
Aquifer media	Fine to medium sand	6	3	13
	Sand and kankar (granules)	5		
	Coarse sand	8		
Soil media	Sandy loam	5	2	9
	Loam	6		
	Clay loam	7		
	Silty clay loam	8		
Topography (degree slope)	<5	10	1	4
	5-10	5		
	>10	1		
Impact of the Vadose zone	Hard clay	5	5	22
	Surface clay	8		
	Clay kankar (granules)	6		
	Sandy clay	9		
	Fine to medium sand	7		
Hydraulic conductivity (1000 G.P.D./ft^2)	<20	2	3	13
	20-40	4		
	>40	8		

In case of water table depth 10 classes have been formed, higher rating is given to the areas with shallow water table because lower the water table, rare is the chance of water to be polluted. The depth > 42m is assigned a rating of 1, the depth < 3m is assigned a rating of 10 and all other intermediate values are rated accordingly. As different land covers respond differently to the rain water in context of its seepage therefore, the net recharge to groundwater is estimated using land cover classification. The land cover had been classified into four classes built-up area, sparsely built-up area, vegetation and water. Areas near water bodies are assigned a highest possible rating because water recharge mostly occurs in these areas and so the vulnerability is high. The existence of fine size particles in aquifer media, like clay, reduce the chances of contamination, thus are assigned a lower rating. The presence of fine textured material as soil media decreases the permeability and hence the vulnerability to contamination. Four classes of soil media has been formed and rated from 4 to 8 as shown in Table 1. Similarly topography, vadose zone and hydraulic conductivity have been classified into 3, 5 and 3 classes, respectively.

Finally, the DRASTIC index is calculated by applying a linear combination of all the factors using the following equation:

$$\text{DRASTIC index} = D_rD_w + R_rR_w + A_rA_w + S_rS_w + T_rT_w + I_rI_w + C_rC_w$$

where:

D, R, A, S, T, I, and C are the seven parameters; r and w are the corresponding rating and weights, respectively. The original weights of DRASTIC as defined by Aller *et al*. (1987) and used by many other experts as well, had been used in the equation and are shown in Table 1. Weighted overlay analysis results into a map showing spatial distribution of the vulnerability index in the study area. To make this interpretable the map is reclassified in three classes which are: low, moderate and high vulnerability. Reclassification process is based upon equal interval classification which emphasizes the relative amount of attribute values in comparison with other values.

Sensitivity analysis has also been performed to clarify relative importance of DRASTIC parameters (Fig. 2). For this purpose map removal sensitivity analysis is used for which single input layer from the final output is removed to observe the change it causes. All the seven parameters were removed one by one and effect of the removal is compared with the actual DRASTIC map. This change is observed in two different ways,

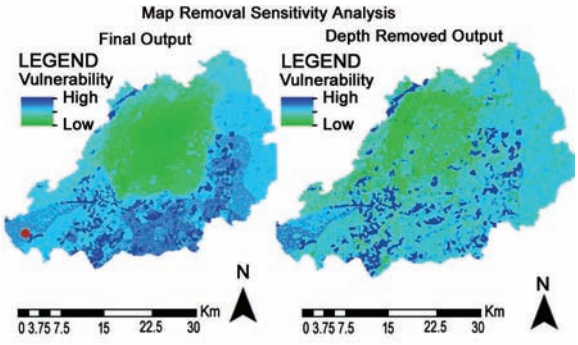

Fig. 2. Visual sensitivity analysis.

visually and through quantitative measure. For the visual change single layer removed map is observed in contrast to the DRASTIC map as shown in Fig. 2 (for water table depth only). Quantitative analysis is performed by calculating area for each of the vulnerability class after removing layers one by one and then comparing the measurements with that of the DRASTIC.

Results and Discussion

The aquifer level is lower in central part of the city as shown in Fig. 3, due to high growth of population and consequently high rate of groundwater consumption. It implies that water contamination chances in central part of the city are very low due to deep groundwater, ranges from 22.5 m to 40 m. The amount of net recharge is low in built-up areas due to concrete structures, thus further reducing the vulnerability to contamination here, shown in Fig. 4. Figure 5 shows that major portion of the study area is composed of coarse sand, causing high vulnerability.

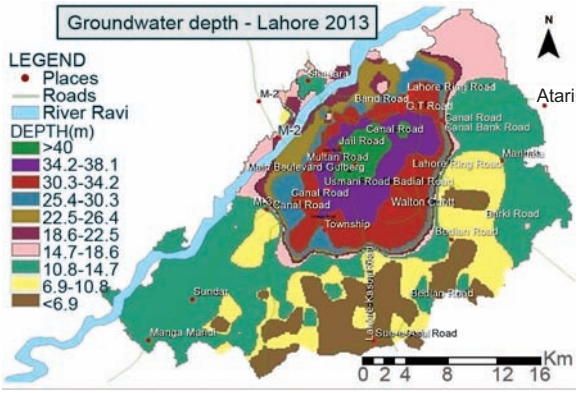

Fig. 3. Spatial distribution of groundwater depth.

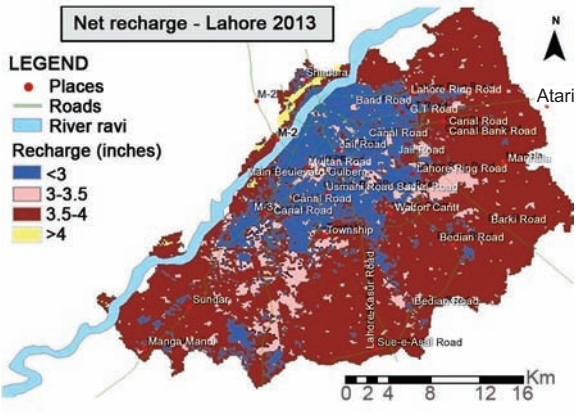

Fig. 4. Spatial distribution of groundwater recharge.

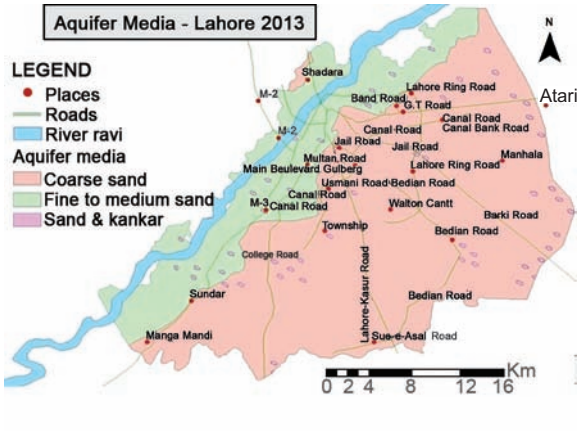

Fig. 5. Spatial distribution of aquifer media.

Spatial distribution of the soil media is shown in Fig. 6. Along the river bed, there is loam and sandy loam which allows more seepage hence increasing the vulnerability. Whereas central portions of the urban area are entirely made up of silty clay loam. Clay loam is dominating in the outer regions as well, especially in the southern part of the study area. The other built-up patches like Township, Sundar etc. also comprises of silty clay loam. Presence of clay loam within the built-up area is greatly reducing the vulnerability. No sharp variation in topography has been found (Fig. 7) and the slope varies between 5-10 m. Gentle slopes have low runoff rates and allow more and more seepage of the water, thus providing an overall increase in the vulnerability index of the study area.

With reference to Fig. 8, the river bed is clearly dominated by fine to medium sand with two small patches of clay and kankar (granules). Apart from the river bed, the study area is dominated by the presence of hard clay

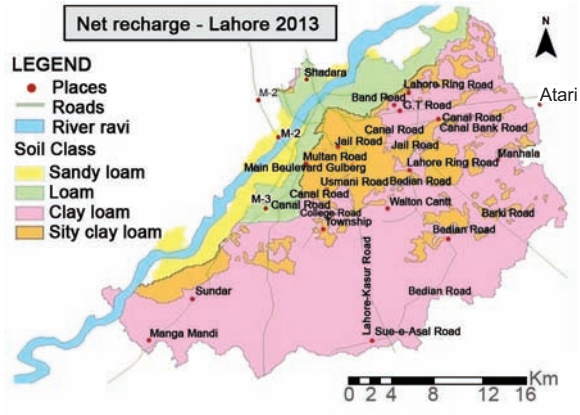

Fig. 6. Spatial distribution of soil media.

which decreases the vulnerability of the study area. Very small part of the study area constitutes of sandy clay giving higher vulnerability. Hydraulic conductivity had been divided into three classes and most of the study area was found with low hydraulic conductivity and hence, in less vulnerable conditions as shown in Fig. 9.

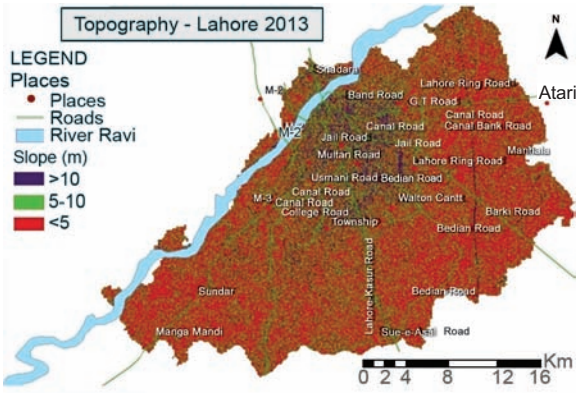

Fig. 7. Spatial distribution of slope.

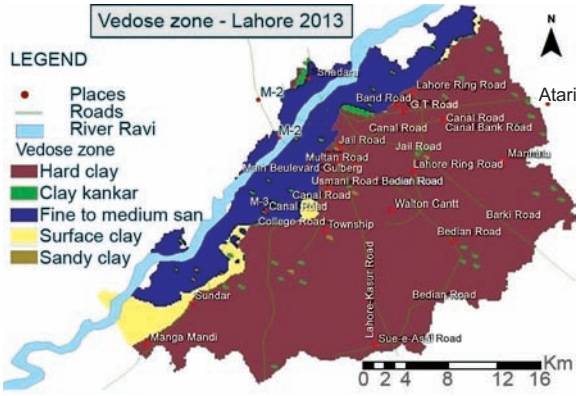

Fig. 8. Spatial distribution of Vadose zone media.

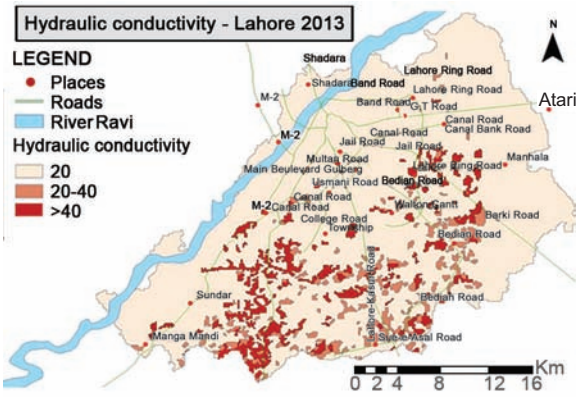

Fig. 9. Spatial distribution of hydraulic conductivity.

DRASTIC vulnerability index. The result of overlay analysis, DRASTIC vulnerability map, is shown in Fig. 10. Whereas, reclassification into three major categories of low, moderate and high vulnerable areas and is shown in Fig. 11. The ranges of classes and quantitative measures are given in Table 2.

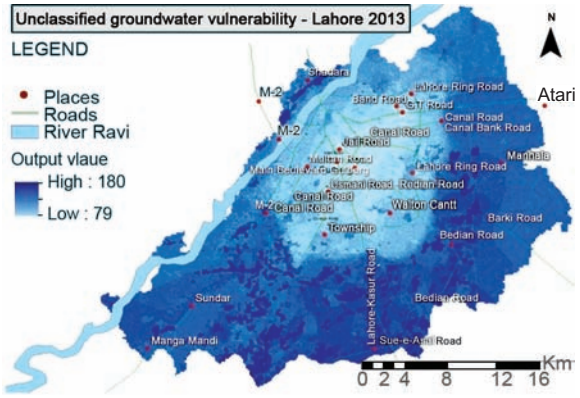

Fig. 10. Spatial distribution of groundwater vulnerability index.

Table 2. DRASTIC index classification scheme

Vulnerability zone	DRASTIC index value range	Area (Sq. km)	Area (%)
Low	79 – 113	446	27.48
Moderate	113 – 146	1079	66.48
High	146 – 180	98	6.04

The low vulnerable regions covered an area of about 446 sq.km (27.48% of the study area) are grouped in the centre of map, which is actually the residential area of Lahore. These are the regions with maximum depth to water table, a major contributor in assessing vulnerability, and its higher values has tend the vulnerability to decrease. The other important factor is the impervious land cover type which reduces water infiltration and hence the possibility of the contaminations to reach groundwater.

The areas with vegetation and open lands have mostly been identified as moderately vulnerable regions. This is the vulnerability class that covers maximum of the study area, an area of 1079 sq. km, which is 66.48% of the area of Lahore, Pakistan. These regions are located in the outskirts of the city; the exceptions include open grassy plots, barren land and parks that exist in residential area of the city. The other common factors about

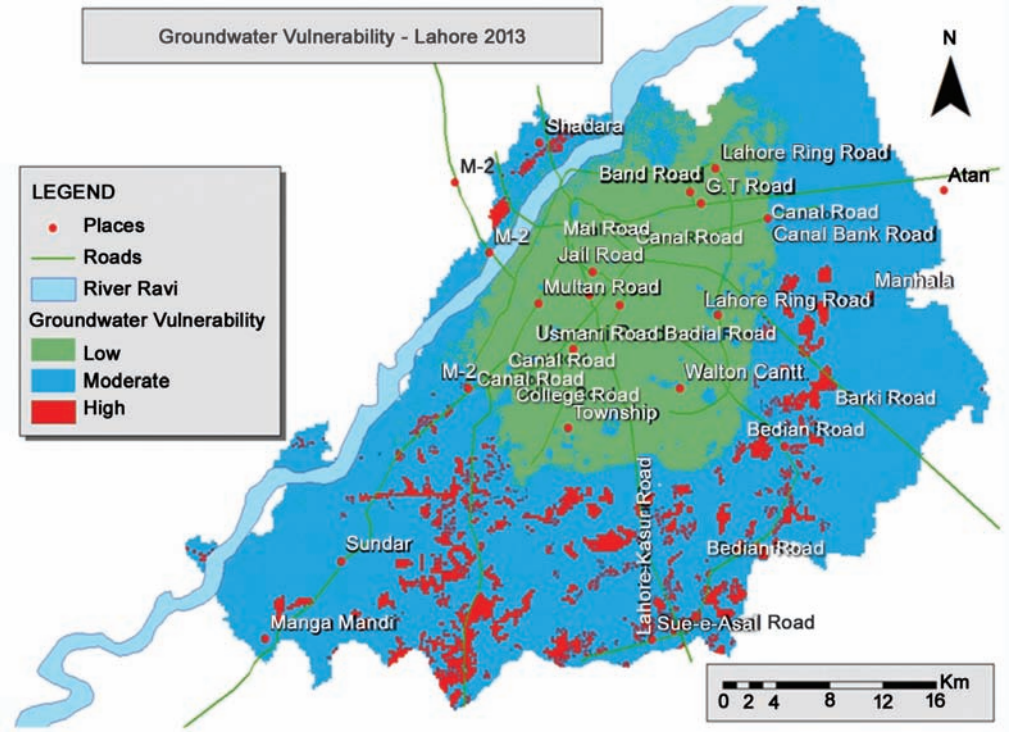

Fig. 11. Reclassified output map.

these regions are: moderate depth to water table, higher recharge rates and coarse sand as the aquifer media. Regions of high vulnerability are found along the river Ravi and there small chunks are papered in eastern to southwestern outskirts of the urban area. High water table and hydraulic conductivity is the common factor for these regions. Whereas aquifer media, recharge rates and soil media are almost same as that for the moderate vulnerable class.

Sensitivity analysis. All the seven parameters were removed one by one and compared with the DRASTIC output to observe their individual participation.

Visual analysis. On removal of D-layer (water table depth layer) a visual increase in the vulnerability index of the central part of the study area has been observed and is shown in Fig. 2. On contrary, addition of D-layer tends to increase vulnerabilities of the outer regions. Reasons for this effect is the higher multiplier associated with D-layer and the large variation in the depth of residential and non-residential areas. Visual effect of the removal of the R-layer is very prominent just like it was found in the case of D-layer. The major variation after removing this layer was found along the river Ravi and other water bodies, as they are major contributors of recharge to groundwater. A moderate change is found in outer regions of the city, which are either barren lands or are covered with vegetation. Removal of the A-layer increase vulnerability at the river site because these are the areas with fine and medium sand layers on contrary to other regions with comparatively more permeable coarse sand.

As the values of S-layer and the T-layer are same throughout the area, so there removal cause no major geographical changes in the vulnerability classes and the only impact is the overall decrease in the value of the measurement. Visual impact of removing I-layer is almost uniform except the river bed where vadose zone comprises of sandy clay. Hydraulic conductivity is the second largest contributor in vulnerability index after depth to water table. Removal of HC-layer results into the conversion of many highly vulnerable small chunks found at outskirts of the area into low vulnerable regions.

Quantitative analysis. There are some parameters that cannot be accurately observed visually. Therefore, quantitative analysis is being carried out to understand the effect of map removal for each of the parameter. Contributing percentages of low, medium and high vulnerable regions, after removing layers one by one,

were calculated and compared with that of the DRASTIC as shown in Fig. 12.

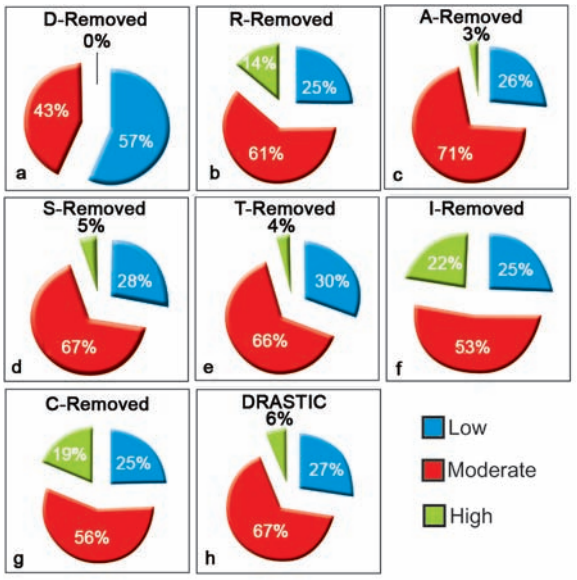

Fig. 12. Results of the map removal sensitivity analysis.

Very small or almost no change in the contributing percentiles of low, moderate and high vulnerable classes have been found by removing the recharge (b), aquifer media (c), soil media (e) and topography (d) layers. In contrary, the removal of depth to groundwater (a), impact of vadose zone (f) or hydraulic conductivity (g) have greatly impact the measured areas of the vulnerability classes. Among these highly sensitive parameters, depth to groundwater has emerged as the most significant parameter in controlling vulnerability in the area. Addition of this layer increases the low vulnerable regions, reduces moderate vulnerable regions and tends high vulnerable area almost to zero. The overall contributing hierarchy of all the parameters is D>I>C>R>A>T>S

Results verification. The study output is showing that low vulnerable areas are actually the residential regions. Here, drinking water supply is made through groundwater and it is responsibility of Water and Sanitation Authority (WASA), Lahore. WASA, Lahore periodically assesses the groundwater quality of these water supply tubewells and has reported that all the samples are safe for drinking. In this way personal communication with

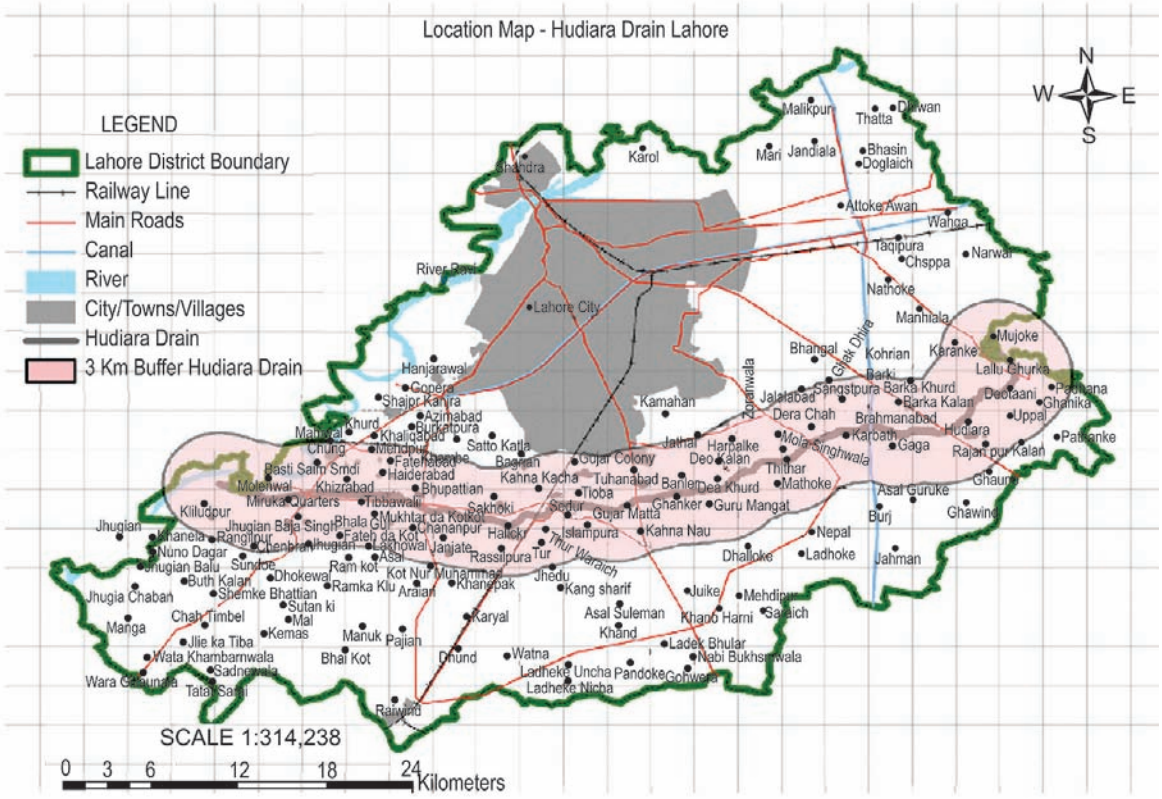

Fig. 13. Study area for Khatak *et al*. (2012).

WASA, Lahore officials is well in agreement with the results for low vulnerable areas.

The exception, as reported by WASA officials, is found along the bank of river Ravi close to Shahdra. Here the groundwater is found contaminated even at deep levels. These areas are already mapped under highly vulnerable regions.

The major portion of the high vulnerable class is found in eastern and south western out skirts of the city, as shown in Fig. 11. Here two studies are found, showing unsuitability of the groundwater for irrigation purpose, mainly due to high concentration of chloride and presence of *E. coli*. One of the studies is conducted by Ali *et al*. (2009) where they have found that out of 60 groundwater samples, 76.6% were unfit, 11.7% were marginally fit and only 11.7% were fit for irrigation. The other study was conducted by Khatak *et al*. (2012) in the same region (study area map is shown in Fig. 13) and have found 21% of the samples marginally fit and all the remaining 79% unfit for irrigation (Fig. 13), study area for Khatak *et al*. (2012).

Conclusion

The results of this study confirm the operational criterion of the GIS based DRASTIC model for the vulnerability assessment of Lahore metropolitan. The results are well in agreement with the factual situation in the area as reported by local authorities and previous studies. The land use information is found to be very important in the assessment, as the existence of densely populated area in the region of study has greatly influenced the parameters of recharge and depth to groundwater. Vulnerability index is found to be varying from 79 to 180 in the study area. When divided into three vulnerability classes of equal interval, 27.5 % (446 sq. km) of the area falls in the low vulnerable ranking; 66.5% (1078.9 sq.km) in moderate and 6% (97.9 sq.km) in high vulnerable class. The major distinction found in the moderate and high vulnerability classes is the difference in groundwater depth and hydraulic conductivity. On the other hand the difference between low vulnerable and other classes is marked by the groundwater depth and recharge rates.

The study has also highlighted the importance of the weight multiplier, which may varies area to area, that should be selected by assessing their actual contribution in DRASTIC, exclusively for the area under investigation. It is found that quantitative measurement for assessing importance of each parameter is better than the ordinary visual analysis. Ground water depth is found to be the strongest contributor in calculating DRASTIC as its removal from the final output causes all the three classes to vary greatly. Impact of vadose zone is ranked second in this regard as its contribution has decreased the area under high vulnerable class.

References

Ali, M.S., Mahmood, S., Chaudhary, M.N., Sadiq, M. 2009. Irrigation quality of ground water of twenty villages in Lahore district. *Soil & Environment*, **28:** 17-23.

Aller, L., Bennet, T., Leher, J.H., Petty, R.J., Hackett, G. 1987. *DRASTIC: A Standardized System for Evaluating Groundwater Pollution Potential Using Hydrogeologic Settings.* 622 pp., Environmental Protection Agency EPA-600/2-87-035, USA.

Almasri, M.N. 2008. Assessment of intrinsic vulnerability to contamination for Gaza coastal aquifer, Palestine. *Journal of Environmental Management*, **88:** 577-593.

Butt, I., Ghaffar, A. 2012. Groundwater quality assessment near Mahmood Boti landfill, Lahore, Pakistan. *Asian Journal of Social Sciences & Humanities*, **1:** 13-24.

Farooqi, A., Masuda, H., Firdous, N. 2007. Toxic flouride and arsenic contaminated groundwater in the Lahore and Kasur Districts, Punjab, Pakistan and possible contaminant sources. *Environmental Pollution*, **145:** 839-849.

Huan, H., Wang, J., Teng, Y. 2012. Assessment and validation of groundwater vulnerability to nitrate based on a modified DRASTIC Model: A case study in Jilin city of Northeast China. *The Science of the Total Environment*, **440:** 14-23.

Khattak, M.A., Ahmed, N., Qazi, M.A., Izhar, A., Ilyas, I., Chaudhary, M.N., Khan, M.S.A., Iqbal, N., Waheed, T. 2012. Evaluation of ground water quality for irrigation and drinking purposes of the areas adjacent to Hudiara industrial drain, Lahore, Pakistan. *Pakistan Journal of Agricultural Sciences*, **49:** 549-556.

Leone, A., Ripa, M.N., Uricchio, V., Deak, J.,Vargay, Z. 2009. Vulnerability and risk evaluation of agricultural nitrogen pollution for Hungary's main aquifer using DRASTIC and GLEAMS Models. *Journal of Environmental Management*, **90:** 2969-2978.

Mahmood, K., Rana, A.D., Tariq, S., Kanwal, S., Ali, R., Haider, A., Tahseen, T. 2013. Groundwater levels susceptibility to degradation in Lahore metropolitan. *Science International (Lahore)*, **25:** 123-126.

Mahmood, A., Muqbool, W., Mumtaz, M.W., Ahmad, F. 2011. Application of multivariate statistical techniques for the characterization of groundwater quality of Lahore, Gujranwala and Sialkot (Pakistan). *Pakistan Journal of Analytical and Environmental Chemistry*, **12:** 102-112.

Majandang, J., Sarapirome, S. 2013. Groundwater vulnerability assessment and sensitivity analysis in Nong Rua, Khon Kaen, Thailand using a GIS-based SINTACS Model. *Environmental Earth Science*, **68:** 2025-2039.

NRC, 1993. *Ground Water Vulnerability Assessment, Contamination Potential Under Conditions of Uncertainty*. 210 pp., National Research Council, National Academy Press, Washington, DC., USA.

Pathak, D.R., Hiratsuka, A. 2011. An integrated GIS based fuzzy pattern recognition model to compute groundwater vulnerability index for decision making. *Journal of Hydro-environment Research*, **5:** 63-77.

Rahman, A. 2008. A GIS based DRASTIC model for assessing groundwater vulnerability in shallow aquifer in Aligarh, India. *Applied Geography*, **28:** 32-53.

Saidi, S., Bouri, S., Dhia, B., Anselme, B. 2011. Assessment of groundwater risk using intrinsic vulnerability mapping: Application to Souassi aquifer, Tunisian Sahel. *Agricultural Water Management*, **98:** 1671-1682.

Shirazi, S.M., Imran, H.M., Akib, S., Yusop, Z., Harun, Z.B. 2013. Groundwater vulnerability assessment in the Melaka state of Malaysia using DRASTIC and GIS techniques. *Environmental Earth Science*, **70:** 2293-2304.

Wang, J., He, J., Chen, H. 2012. Assessment of groundwater contamination risk using hazard quantification, a modified DRASTIC model and groundwater value, Beijing Plain, China. *Science of The Total Environment*, **432:** 216-226.

World Bank. 2006. *Pakistan-Strategic Country Environmental Assessment*. Main Report Washington, DC., World Bank.http://documents.worldbank.org/curated/en/2006/08/7100383.

You-Hailin, Xu-Ligang, Ye-Chang, Xu-Jiaxing, 2011. Evaluation of groundwater vulnerability with improved DRASTIC method. *Procedia Environmental Sciences*, **10:** 2690-2695.

Pak. j. sci. ind. res. Ser. A: Phys. sci. 2015 **58**(1) 17-25

Role of Biodiesel-Diesel Blends in Alteration of Particulate Matter Emanated by Diesel Engine

Asad Naeem Shah[a b]*, Ge Yun-Shan[b], Tan Jian-Wei[b] and Ejaz Mahmood Shahid[a]

[a]Department of Mechanical Engineering, University of Engineering and Technology, Lahore-54000, Pakistan

[b]National Laboratory of Auto Performance and Emission Test, School of Mechanical and Vehicular Engineering, Beijing Institute of Technology, Beijing100081, China

(received June 4, 2013; revised April 11, 2014; accepted April 15, 2014)

Abstracts: The current study is focused on the investigation of the role of biodiesel in the alteration of particulate matter (PM) composition emitted from a direct injection-compression ignition. Two important blends of biodiesel with commercial diesel known as B20 (20% biodiesel and 80% diesel by volume) and B50 were used for the comparative analysis of their pollutants with those of 100% or traditional diesel (D). The experiments were performed under the auspices of the Chinese 8-mode steady-state cycle on a test bench by coupling the engine with an AC electrical dynamometer. As per experimental results, over-50 nm aerosols were abated by 8.7-47% and 6-51% with B20 and B50, respectively, on account of lofty nitrogen dioxide to nitrogen oxides (NO_2/NO_x) ratios. In case of B50, sub-50 nm aerosols and sulphates were higher at maximum load modes of the test, owing to adsorption phenomenon of inorganic nuclei leading to heterogeneous nucleation. Moreover, trace metal emissions (TME) were substantially reduced reflecting the reduction rates of 42-57% and 64-80% with B20 and B50, respectively, relative to baseline measurements taken with diesel. In addition to this, individual elements such as Ca and Fe were greatly minimised, while Na was enhanced with biodiesel blended fuels.

Keywords: biodiesel, unregulated emissions, trace metals, nanoparticles, sulphates, diesel engine

Introduction

Today biodiesel is considered as one of the most attractive and environmentally benign fuels on account of its better physicochemical properties and combustion as compared to conventio-nal diesel fuel. It is a readily available clean burning fuel which can be used both in blended as well as neat forms without major changes in the engine hardware. Regulated emissions such as carbon monoxide (CO), hydrocarbons (HC) and PM are greatly reduced with biodiesel (He *et al.,* 2009; Shah *et al.,* 2009a; Rehman and Ghadge, 2007; Turrio-Baldassarri *et al.,* 2004; Dorado *et al.,* 2003). Moreover, smoke opacity and other unregulated emissions comprising aldehyde and ketones, polycyclic aromatic hydrocarbons (PAHs), and volatile organic compounds (VOCs) are also decreased with this alternative fuel (Shah *et al.,* 2009b; Shah *et al.,* 2008; Jha *et al.,* 2008; Lin *et al.,* 2006). However, oxides of nitrogen (NO_x) and nuclei mode particles have been reported to be increased with biodiesel (Shah *et al.,* 2014; Shah *et al.,* 2009a, 2009b; Karabektas *et al.,* 2008; Szybist *et al.,* 2007; Usta, 2005).

The performance of engines in terms of brake power, thermal efficiency, and brake specific energy consumption is more or less same with biodiesel or its blends (Shah *et al.,* 2009a, 2009b; Agarwal and Das, 2001). In addition to this, study of combustion parameters such as ignition delay, maximum combustion pressure (MCP), maximum rate of pressure rise, start of injection angle, heat release rate, and combustion zones endorse the superiority of this renewable and biodegradable fuel over the petroleum diesel (Shah *at al.,* 2009a; Tsolakis, 2006; Lee *et al.,* 2005). Further, macroscopic spray characteristics of biodiesel-diesel blended fuel have revealed that both the spray tip penetration and cone angle are increased with biodiesel, relative to diesel (Shah *et al.,* 2010). This reflects the better quality of biodiesel blended fuel, than the neat diesel.

In general, PM is constituted by ashes or trace elements, volatile organic fraction or soluble organic fraction, sulphates and carbon soot, while the composition is affected by several parameters such as engine category, sampling technique, lubricating oil, composition of fuel and type of driving cycle (Zhao *et al.,* 2010). Agarwal (2007) is of the view that PM consists of 40% unburned lubricating oil, 31% elemental carbon, 14% sulphates, 7% unburned fuel, and 8% metals along with some other substances. Metals in the emitted particulate matter originate from lube oil, fuel, and engine

*Authour for correspondence; E-mail:naeem_138@hotmail.com

wear along with the gaseous sulphite at higher temperature during the combustion (Lim *et al.,* 2007).

Particulate matter brought forth by a diesel engine exhaust is composed largely of nuclei, accumulation, and coarse mode particles with their respective diameters typically between 5 and 50 nm, 50 and 1000 nm, and higher than 2.5 μm (Liu *et al.,* 2011; Wong *et al.,* 2003). Burtscher (2005) had reported that the typical diesel particles are agglomerates comprising spherical particles of diameter 15 to 40 nm. Further, the mean diameter of these agglomerated particles (accumulation mode) remains always in the range of 60 to 100 nm. The substantial numbers of nuclei (sub-50 nm) particles typically contribute just few percent to total mass, and their contribution to the number depends on their size distribution. The size distributions are affected by many parameters including engine operating conditions, exhaust after treatment, fuels, etc. Nuclei mode particles comprise primarily of metallic compounds, carbonaceous nuclei, sulphur compounds and soluble organic fraction, some of which are formed during cooling or dilution processes (Wong *et al.,* 2003; Kittleson, 1998). The probability of nuclei mode particles to be inhaled by human beings is higher owing to their smaller sizes and larger numbers. This may cause respiratory diseases and even lungs cancer (Donaldson *et al.,* 1998). European regulations (Euro 5/6), therefore, have already included particle number measurements along with the total mass of PM.

The objective of the current study is to investigate the influence of biodiesel on the PM composition including nuclei and accumulation mode particles, sulphates and trace metal emissions (TME). Biodiesel-diesel blends B20 and B50 have been used to gain a deep insight into the biodiesel role in above discussed emissions. Earlier, authors (Shah *et al.,* 2014) have reported that accumulation mode particles, total TME, and individual elements such as iron and calcium are greatly reduced, while nuclei mode particles and sodium are increased with neat biodiesel (B100). In addition to this, it has also been pointed out that sulphates are slightly, only 8%, increased with B100 as compared to petroleum diesel. Thus the current study will characterise the PM composition, and will provide the comparative analysis of B20 and B50 with conventional diesel. The emission measurements taken with diesel fuel are known here as baseline measurements.

Materials and Methods

Test engine, operating cycle, fuels and lubricant. A turbocharged inter-cooled DI-CI engine of 4.752 L capacity was run on an AC electrical dynamometer (Schenck HT350, Germany) on a test bench following an 8 Mode steady-state cycle ISO 8178 Type C1 (Shah *et al.,* 2011). The engine has four cylinders with compression ratio of 16.8: 1. The bore and stroke are 110 and 125 mm, respectively, while the injector has 6 holes/nozzles of 0.23 mm diameter each. The maximum torque and power of the engine are 580 N-m and 117 kW at crankshaft speeds of 1400 and 2300 rpm, respectively. The engine test bench is shown in Fig. 1.

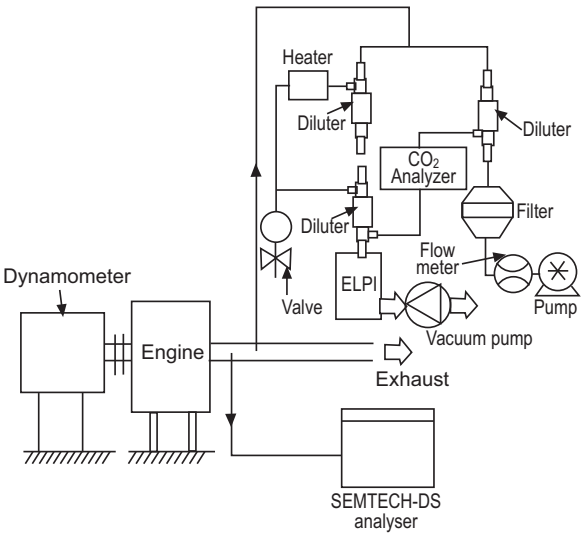

Fig.1. Schematic diagram of test bench.

During the first 4 modes of the cycle, i.e., Mode 1-4, engine was operated at 100, 75, 50 and 10% of full load at 2300 rpm. During the next three modes i.e. Modes 5-7, engine was run at 100, 75 and 50% of full load at 1400 rpm, while the 8th Mode was an idle mode. The baseline measurements were taken by fuelling the engine with locally available (higher sulphur) petroleum diesel. The engine was then fuelled with soybean oil-based biodiesel blended fuels B20 and B50 to get the subsequent measurements. Biodiesel was purchased from the market and its properties were provided by the vender. The sulphur content of 160 ppm and oxygen enrichment are deemed to be the inherited properties of biodiesel depending on its source and origin. The detail of fuel properties are given in Table 1, while the composition of lubricant is as follows: 0.6 ppm Fe; 1.6 ppm Al; 3.3 ppm Na; 15.3 ppm Mg; 63.9 ppm Mo; 353 ppm Zn; and >1000 ppm Ca.

Sampling methodology. The sampling was carried out first for the measurement of nitric oxide (NO) and NO_2

Table 1. Fuel properties and test method

Property	Diesel	Biodiesel	Method[a]	≈ ASTM
Viscosity (mm^2/s) at 20 °C	4	7.1	GB/T265	D445
Cetane number	52	60.1	GB/T386	D6890
Sulphur content (ppm)	350	160	GB/T380	D4294
Density (kg/m^3) at 20 °C	841	875	GB/T1884-85	D1298/4052
Calorific value (MJ/kg)	42.8	37.3	-	-
Oxygen content (wt %)	0.0	11.0	-	-
C : H	87 : 13	77 : 12	SH/T 0656-1998	-

[a] = standard method used in China.

separately through SEMTECH-DS (USA), then for the analysis of particles, sulphates and TME as per schematic diagram shown in Fig.1. In order to collect the exhaust for the estimation of sub-50 nm and over-50 nm aerosoles, 2 tandem ejector diluters each with a dilution ratio of almost 8:1 were arranged in series, first at 200 °C and then at ambient temperature. The exhaust was then passed through an ELPI (Dekati, Finland) having a corona charger, an electrometer, and a cascade (Shah *et al.,* 2014). A sampling pump was used to provide flow, while the flow rate was controlled by a controller at about 10 L/min. The samples for analysis of sulphates and TME were trapped in Teflon membrane filter (Teflo, Pall Corporation), having diameter and pore size of 47 mm and 0.2 µm, respectively. Prior to the filter, exhaust was led to pass through an ejector diluter similar to that discussed earlier at a temperature of about 100 °C. A battery operated pump was engaged there to keep the volume flow rate of the sample at 80 L/min. The filters containing the trapped pollutants were stored for further processing. Total 3 samples (n = 3) were collected for each analysis of sulphates and TME, while 3 measurements were also taken for each category of sub-50 nm and over-50 nm aerosols and the NO_2/NO_x ratios. Thus pollutants in the current study are calculated and subsequently discussed on the basis of their mean values.

Analysis of pollutants. One half part of the sampled material was put into Teflon vessel after cutting it into several pieces which were then soaked up into 2 mL nitric acid (HNO_3) for 5 mins. This sample was finally dissolved into 1 mL distilled hydrochloric acid (HCl) to get a solution of 10 mL in a standard flask. The trace metal emission (TME) such as sodium (Na), potassium (K), aluminum (Al), calcium (Ca), magnesium (Mg), chromium (Cr), titanium (Ti), manganese (Mn), iron (Fe), sulphur (S), strontium (Sr), nickel (Ni), zinc (Zn), lead (Pb) and copper (Cu) were analysed using the inductively coupled plasma (ICP)-atomic emission, spectroscopy, (VARIN VISTA-MPX).

The second half part of the filter was taken into a centrifuge tube after cutting it into numerous pieces. The sampled material was immersed into 15 mL distilled and deionised water, and then sonicated (agitated for particles) for 20 mins. For the purification of the extract, a microcellular membrane filter (Pall Corporation) was used. The same procedure was repeated to get another extract of the sampled material. Finally, both extracts were mixed together for the subsequent analysis of pollutants. The sulphates were then quantified by using the ion chromatography (Dionex USA).

Results and Discussion

The size of the particles measured by an ELPI ranges from 0.03 to 10 µm aerodynamic diameters available from12 channels. The particle sizes in these 12 categories are as follows: 0.021, 0.039, 0.072, 0.121, 0.203, 0.317, 0.486, 0.766, 1.234, 1.96, 3.10, and 6.32 µm. In the current study, aerosols of first 2 sizes i.e. 0.021 µm and 0.039 µm are discussed as sub-50 nm aerosols (nuclei mode), while the subsequent 6 sizes ranging from 0.072 µm to 0.766 µm are summed up under over-50 nm aerosols (accumulation mode) category. However, their number-size distributions have been addressed elsewhere (Shah *et al.,* 2009c)

Emissions of aerosols. Over-50 nm aerosols were generally reduced with both B20 and B50 fuels as compared to petroleum diesel during the whole cycle of operation as shown in Fig. 2. The rate of reduction is 8.7-47% with B20 and 6-51% with B50, relative to baseline measurements. B50 blend gave more control on this category of pollutants as compared to B20. The reduction rate is remarkably high during the medium load modes such as Mode 3 and Mode 7 with both the blends of biodiesel. Moreover, these pollutants are predominant at higher loads as compared to lower ones with all the three fuels. In addition to this, particles are dominant at maximum speed (2300 rpm) modes, relative to lower speed (1400 rpm) modes.

The higher reduction rates with biodiesel blended fuels in general, and with B50 in particular are most likely due to the elevated NO_2/NO_x ratios with the blended fuels relative to neat diesel, as shown in Fig. 2. The

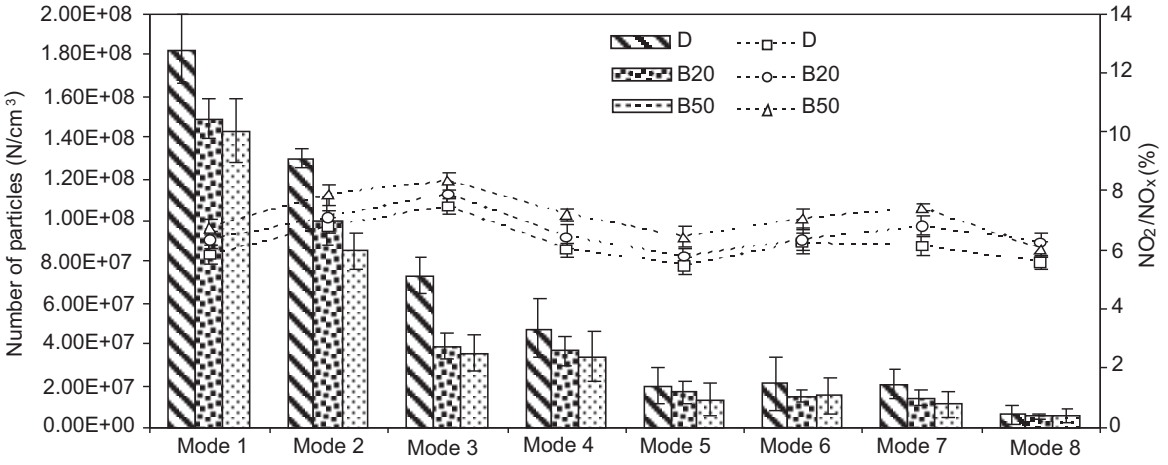

Fig. 2. Over-50 nm aerosols and NO_2/NO_x ratio comparisons at different test modes.

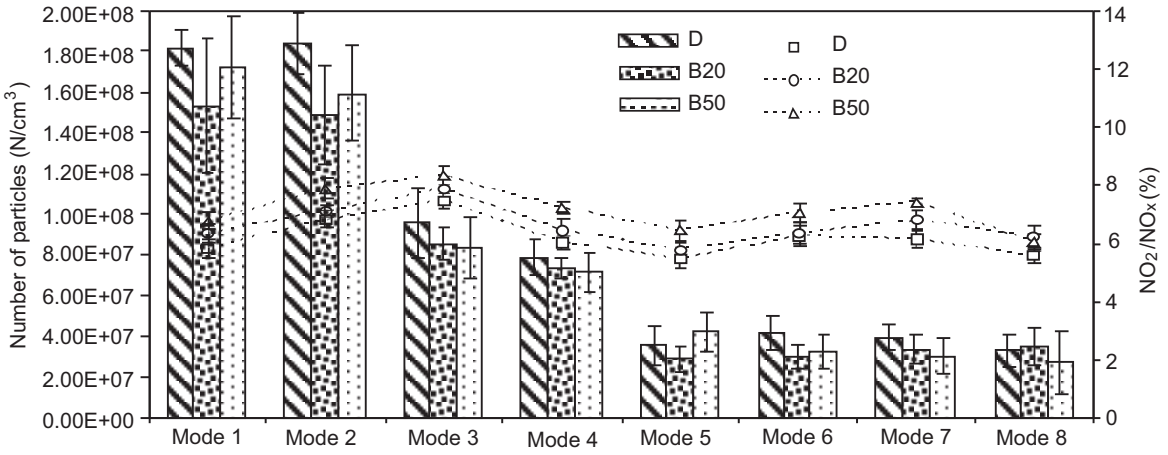

Fig. 3. Sub-50 nm aerosols and NO_2/NO_x ratio comparisons at different test modes.

ratios are higher in the case of B50 relative to B20 during all the cyclic modes except the idle mode. Biodiesel inherits oxygen content which promotes the oxidation of NO to NO_2, with the consequent higher NO_2/NO_x ratios. The elevated NO_2/NO_x ratio may further increase the combustion of soot and soluble parts of PM, as soot combustion is accelerated with NO_2 relative to oxygen itself (Setiabudi *et al.,* 2004). Thus presence of both oxygen (fuel-bound oxygen) and NO_2 are responsible for the controlling of over-50 nm aerosols in case of both B20 and B50 as compared to D. In addition to this, higher cetane number of biodiesel decreases the ignition lag/delay with the consequent earlier combustion of fuel with biodiesel and its blends relative to their counterpart diesel fuel. This further leads to higher MCP in the cylinder, and thus more complete combustion resulting in reduced PM emissions, particularly in over-50 nm aerosols. It has already been demonstrated that, PM is decreased up to 80% and 21% with neat biodiesel and B20, respectively (Shah *et al.,* 2009a). Moreover, the higher viscosity of biodiesel (7.1 mm^2/s) causes the reduction of fuel losses in the injector resulting in quicker development of pressure with improved injection timing (Tsolakis, 2006). Shah *et al.* (2010) have reported that higher fuel injection pressure with B20 causes a rapid increase of injection flow rate together with higher injection velocity, kinetic energy and momentum of droplet resulting in larger penetration distance in the combustion chamber. Consequently, better atomisation, and hence better air-fuel mixing takes place with biodiesel and its blends.

The elevated emissions at higher loads are most probably due to the incomplete combustion of the carbonaceous part of PM caused by the minimised relative air/fuel ratio λ (lambda) or rich mixture formation (Liu *et al.,* 2011). The higher pollutants at maximum speed modes, on the other hand, are attributed to higher soot formation because of the weak oxidation rate caused

by the decrease in temperature. It is well documented that turbulences inside the combustion chambers are increased at higher engine speeds which further cause the increase in heat losses (Collier *et al.,* 1995).

Moreover, the ELPI data reflects the relatively higher uncertainty levels. The possible reasons of this uncertainty may be one or more than one of the following factors: (i) the condensation of high concentrated and temperature exhaust, (ii) reduction in pressure of high effective particle air (HEPA), (iii) preheating of primary dilutor to a temperature less than 195 °C, (iv) variation in dilution ratio, (v) any problem in charging and collection mechanisms i.e., mishandling during particle charging, (vi) wrong inertial classification in a cascade impactor and (vii) the electrical detection of aerosol particles, etc.

Emissions of sub-50 nm aerosols. It is important to discuss the sub-50 nm aerosols of PM on account of their potential hazards to the environment and human beings. As the diameters of particles are decreased into nano-sizes, their probability to be inhaled is increased. Sub-50 nm aerosols are predominant at maximum load modes of both cyclic speeds (i.e. Mode 1 and Mode 5) with B50 relative to other two fuels as shown in Fig. 3. However, B20 gives a better control of the pollutants during these modes. Generally, both blends show diminished emissions of sub-50 nm aerosols, and relative reduction rate is 14-32% with B20 and 4-15.8% with B50. Contrary to the particle trends, NO_2/NO_x ratios reveal the order of magnitude as B50, B20, and then diesel. This leads to an interesting finding that unlike B20, B50 does not show much relevance to the NO_2/NO_x ratios. It has also been reported in previous study (Shah *et al.,* 2014) that sub-50 nm aerosols (nuclei mode particles) are not directly affected by NO_2/NO_x ratios, and thus remain higher with neat biodiesel, relative to diesel.

Neat biodiesel may promote the heterogeneous nucleation owing to oxygen enrichment (Shah *et al.,* 2009c). This phenomenon is more significant during higher load modes due to the burning of rich mixture. Although biodiesel has lower sulphur contents as compared to diesel, this available quantity along with that carried by lube oil was oxidised to sulphur dioxide (SO_2) in the presence of oxygen contents. Subsequently, SO_2 was converted to sulphur trioxide (SO_3), and then to sulphuric acid (H_2SO_4) nuclei in the presence of diluting air and water. Thus, the adsorption phenomenon of such inorganic nuclei was promoted leading to the proliferation of heterogeneous nucleation with higher level blends (Shah *et al.,* 2014). Kittelson (1998) has reported that nuclei mode particles are formed during the nucleation process caused by dilution and cooling of the engine exhaust. It has been experimentally proved earlier that the concentrations of nucleation mode particles are predominant with neat biodiesel and B20 relative to petroleum diesel (Shah *et al.,* 2009c)

Sulphates. It is pertinent to note that the maximum load modes at which emissions of sub-50 nm aerosols were higher with B50 as discussed earlier, the sulphates too remain elevated at the same as shown in Fig. 4. The relative increase is 9% and 13% at Mode 1 and Mode 5, respectively. However, these pollutants remain lower during all other cyclic modes with both blended fuels relative to their counterpart. The relative decrease varies by 3-12% with B20 and 4.5-16% with B50.

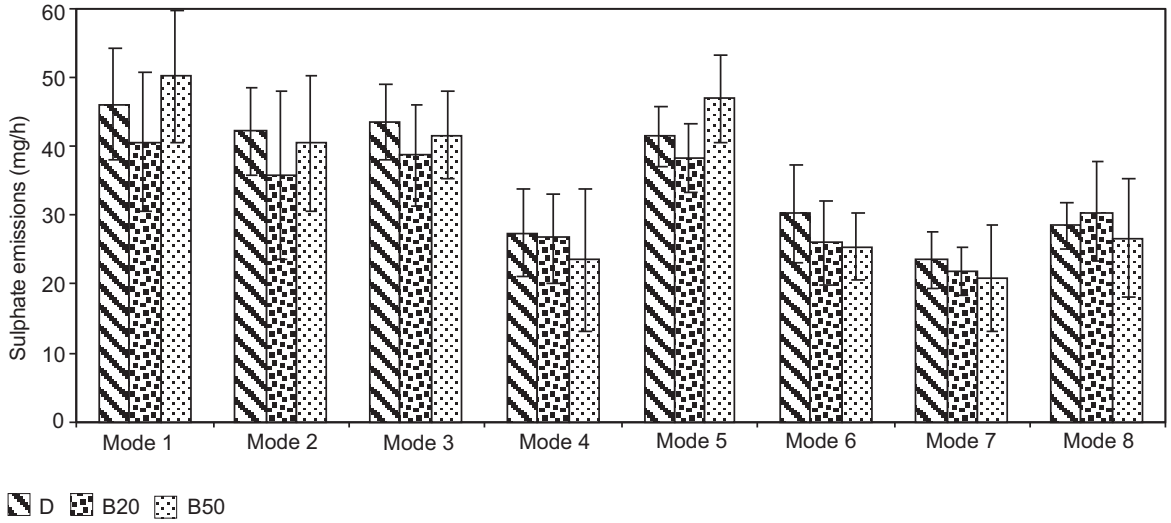

Fig. 4. Comparison of sulphate emissions at different test modes.

These findings i.e predominance of sulphate emissions at maximum load modes further ratifies the argument that, it is actually heterogeneous nucleation which increases both nuclei mode NP as well as sulphate emissions. Oxygen enrichment in biodiesel promotes the oxidation of sulphur (available in lube oil and in fuel as traces) to SO_2 in a very similar fashion as NO is oxidised to NO_2, and thus leads to the heterogeneous or inorganic nucleation. Consequently, the sulphate nano-particles are increased at maximum load modes in case of higher biodiesel blend B50 as compared to lower blend B20.

Meanwhile, the decrease in sulphate pollutants with both blends of biodiesel during all other test modes may be due to the more complete combustion owing to better physicochemical properties of biodiesel relative to conventional diesel. Thus the modes other than that at 100% load develop the temperatures in the combustion chamber which are prone to the decomposition of PM, especially to soot and sulphates.

Trace metals. Trace metal is an important class of pollu-tants which along with some other substances contribute 8% to total PM emissions (Agarwal, 2007). Although this percentage contribution to PM is low, the toxicity or perniciousness to human health associated with TME is significant (Becker *et al.,* 2005). Crust elements such as Al, Ca, Mg, Si and Fe contribute about 82% to total metals of petroleum diesel (Wang *et al.,* 2003). Figure5 presents the TME and their reduction rates with B20 and B50 relative to baseline measure-ments during the various cyclic modes. Both of the biodiesel blends give significant control over these pollutants, and the reduction rates vary by 42-57% with B20 and 64-80% with B50. It is quite obvious that higher blended fuel i.e. B50 gives substantial control over TME as compared to B20. Thus, higher the percentage of biodiesel in a blend, the greater will be the reduction in TME. This finding is consistent with the previous study (Shah *et al.,* 2014) that neat biodiesel presents 65% to above 85% reduction in TME. These reduction rates, of course, endorse that biodiesel is more benign to both environment and human health.

The study of the effect of biodiesel on TME has further been extended to individual species to gain a deep insight into the biodiesel role in the alteration of trace metal composition. Two important modes, i.e., Mode 3 (50% of full load at 2300 rpm) and Mode 7 (50% of full load at 1400 rpm), were selected for this purpose. It is clear that Ca and Fe are predominant components with diesel and B20, while Na is the dominant element in case of both blended fuels. B20 and B50 give a good control over Ca and Fe, but Na is increased with both the blends (Fig 6). The relative decrease in Ca is 53-70% and 68-79% with B20 and B50, respectively. Similarly, the relative decrease in Fe is up to 55% with B20 and 90% with B50 during the selected modes of the test cycle. The relative rise in Na, on the other hand, is up to 64.5% and 76% with B20 and B50, respectively.

The abatement in Ca with biodiesel blends may be due to the better physicochemical properties of biodiesel such as reduced ignition delay, improved cetane number, earlier start of injection, higher MCP, higher rate of pressure rise, better air-fuel mixing and heat release, and oxygen enrichment causing the better oxidation rate of Ca. It is

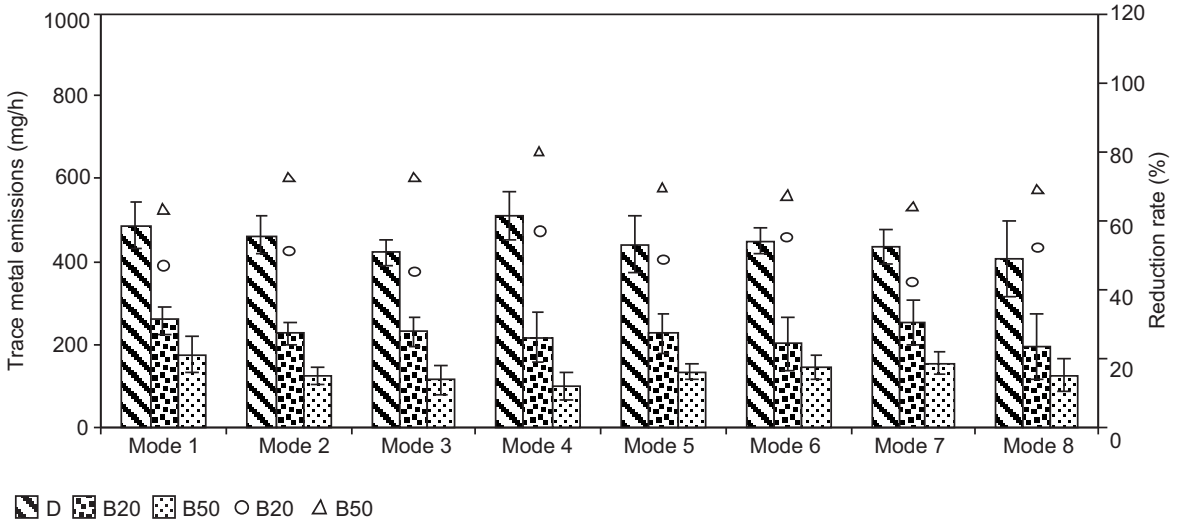

Fig. 5. Comparison of TME and reduction rate at various modes.

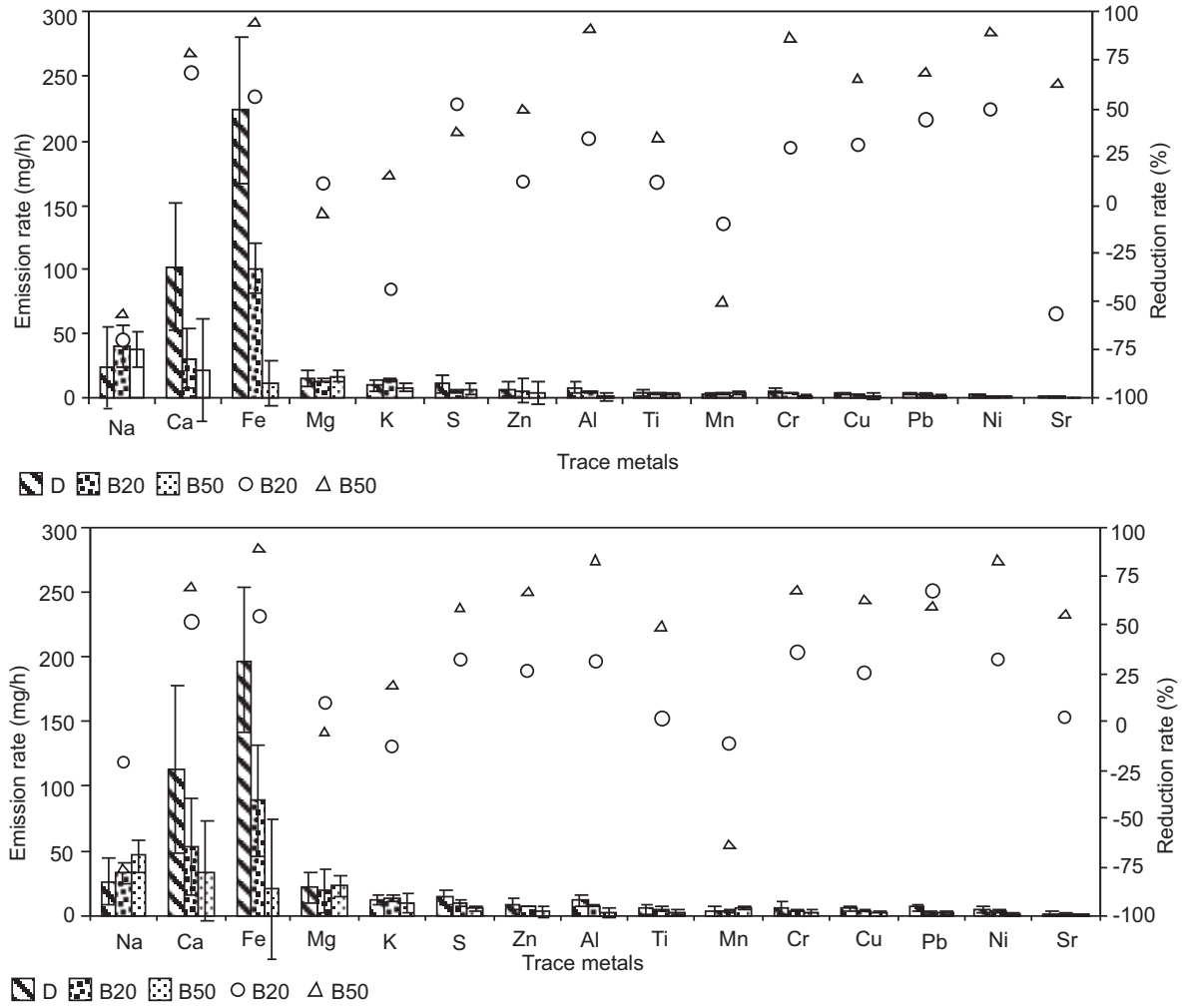

Fig. 6. Comparison of individual trace metals and their reduction rates at Mode 3 and 7.

conjectured that the higher content of Ca (i.e., > 1000 ppm) in lubricating oil along with other additives in petroleum diesel may have adversely affected the quality of fuel from Ca viewpoint, and thus lead to higher Ca emissions in this case. The signi-ficant decrease in Fe emission rates with these blends is probably due to the relative decrease in wear rates of the engine in case of B20 and B50. Agarwal (2007) is of the view that the wear rates of different parts of engine such as piston-rings, piston, cylinder-liner, etc. are remarkably decreased with biodiesel on account of additional lubricity possessed by it. The elevated rates of Na emissions with biodiesel blends, on the other hand, are ascribed to sodium hydroxide (NaOH) used as a catalyst during the transesterification process of biodiesel.

Conclusion

The effect of biodiesel on the PM composition constituted by nuclei and accumulation mode particles, sulphates, and TME was investigated. A turbocharged inter-cooled direct injection type compression ignition engine was connected to an AC electrical dynamometer to operate under the auspices of the Chinese steady state cycle on a test bench. The engine was first operated on commer-cial diesel, then on B20 and B50, respectively, to collect the required samples of pollutant for their subsequent analysis. According to the experimental results, over-50 nm aerosols were decreased by 8.7-47% and 6-51% with B20 and B50, respectively, as compared to baseline measurements on account of elevated NO_2/ NO_x ratios. The abatement of this category of pollutants remained remarkably at medium load modes. The sub-50 nm aerosols and sulphates were decreased by 14-32% and 3-12%, respectively, with B20, but increased with B50 during maximum load modes owing to higher percentage (by volume) of biodiesel which promoted the heterogeneous

nucleation. In addition to this, TME were highly reduced with B20 and B50 and the respective reduction rates varied by 42-57% and 64-80%. The most abundant TME such as Ca and Fe were highly reduced, while Na increased in case of blended fuels relative to diesel.

Acknowledgement

Authors are thankful to Dr. He Chao and Dr. Liu Zhi-Hua for their helping and encouraging attitude during the operation of ion chromatography and ICP-atomic emission spectroscopy. Our thanks are also due to the National Natural Science Foundation (NNSF) of China under grant # 50576063.

References

Agarwal, A.K. 2007. Biofuels (alcohols and biodiesel) applications as fuels for internal combustion engines. *Progress in Energy and Combustion Science,* **33:** 233-271.

Agarwal, A.K., Das, L.M. 2001. Biodiesel development and characterization for use as a fuel in compression ignition engine. *Journal of Engineering for Gas Turbines and Power,* **123:** 440-447.

Becker, S., Dailey, L.A., Soukup, J.M., Grambow, S.C., Devlin, R.B., Huang, Y.C. 2005. Seasonal variations in air pollution particle-induced inflamatory mediator release and oxidative stress. *Environment Health Perspective,* **113:** 1032-1038.

Burtscher, H. 2005. Physical characterization of particulate emissions from diesel engines: a review. *Journal of Aeosole Science,* **36:** 896–932.

Collier, A.R., Rhead, M.M., Trierand, C.J., Bell, M.A. 1995. Polycyclic aromatic compound profiles from a light-duty direct-injection diesel engine. *Fuel,* **74:** 362-367.

Donaldson, K., Li, X.Y., MacNee, W. 1998. Ultrafined (manometer) particle mediated lung injury. *Journal of Aerosol Science,* **29:** 553-560.

Dorado, M.P., Ballesteros, E., Arnal, J.M., Gomez, J., Gimenez, F.J.L. 2003. Testing waste olive oil methyl ester as a fuel in a diesel engine. *Energy and Fuels,* **17:** 1560-1565.

He, C., Ge, Y.S., Tan, J.W., You, K.W., Han, X.K., Wang, J.F., You, Q., Shah, A.N. 2009. Comparison of carbonyl compounds emissions from diesel engine fuelled with biodiesel and diesel. *Atmospheric Environment,* **24:** 3657-3661.

Jha, S.K., Fernando, S., Filip, T.S.D. 2008. Flame temperature analysis of biodiesel blends and components. *Fuel,* **87:** 1982-1988.

Karabektas, M.P., Ergen, G., Hosoz, M. 2008. The effects of preheated cottonseed oil methylester on the performance and exhaust emissions of a diesel engine. *Applied Thermal Engineering,* **28:** 2136-2143.

Kittleson, D.B. 1998. Engine and nanoparticles: a review. *Journal of Aerosol Science,* **29:** 575-588.

Lee, C.S., Park, S.W., Kwon, S. 2005. An experimental study on the atomozation and combustion characteristics of biodiesel-blended fuels. *Energy & Fuels,* **19:** 2201-2208.

Lim, M., Ayoko, G., Morawska, L., Ristovski Z., Jayaratne, E., Kokot, S. 2007. The effects of fuel characteristics and engine operating conditions on the elemental composition of emissions from heavy duty diesel buses. *Fuel,* **86:** 1831-1839.

Lin, Y.C., Lee, W.J., Wu, T.S., Wang, C.T. 2006. Comparison of PAH and regulated harmful matter emissions from biodiesel blends and paraffinic fuel blends on engine accumulated mileage test. *Fuel,* **85:** 2516-2523.

Liu, Z.H., Shah, A.N., Ge, Y.S., Ding, Y., Tan, J.W., Jiang, L., Yu, L., Zhao, W., Wang, C., Zeng, T. 2011. Effects of continuously regenerating diesel particulate filters on regulated emissions and number-size distribution of particles emitted from a diesel engine. *Journal of Environmental Sciences,* **23:** 798-807.

Rahman, H., Ghadge, S.V. 2007. Performance of compression ignition engine with mahua *(Madhuca indica)* biodiesel. *Fuel,* **86:** 2568-2573.

Setiabudi, A., Makkee, M., Moulijn, J.A. 2004. The role of NO_2 and O_2 in the accelerated combustion of soot in diesel exhaust gases. *Applied Catalysis B: Environmental,* **50:** 185-194.

Shah, A.N., Ge, Y., Shah, F.H., Mughal, H.U., Rahman, Z.U., Naveed, A. 2014. Effect of biodiesel on particulate numbers and composition emitted from turbocharged diesel engine. *International Journal of Environmental Science and Technology,* **11:** 385-394.

Shah, A.N., Ge, Y., Jiang, L. 2011. Impact of a urea-selective catalytic reduction system on volatile organic compound emissions from a diesel engine. *The Arabian Journal for Science and Engineering,* **36:** 891-901.

Shah, A.N., Ge, Y., He, C. 2010. Macroscopic spray characteristics of diesel and biodiesel-diesel blend: An experimental comparison. *Journal of Engineering & Applied Sciences,* **29:** 35-47.

Shah, A.N., Ge, Y., Tan, J.W., He, C. 2009a. Effects of biodiesel from soyabean oil on the exhaust emissions of a turbocharged diesel engine. *Pakistan Journal of Scientific and Industrial Research,* **52:** 217-227.

Shah, A.N., Ge, Y., Tan, J.W., Liu, Z.H. 2009b. Experimental investigation of VOCs emitted from DI-CI engine fuelled with biodiesel, diesel and biodiesel-diesel blend. *Pakistan Journal of Scientific and Industrial Research,* **52:** 158-166.

Shah, A.N., Ge, Y., Jiang, Shaikh, M.A. 2009c. An experimental study on number size distribution of particles emitted from a heavy duty CI engine fuelled with biodiesel and its 20% blend. *Mehran University Research Journal of Engineering & Technology,* **28:** 205-214.

Shah, A.N., Ge, Y., Tan, J.W., Liu, Z.H. 2008. An experimental investigation of PAH emissions from a heavy duty diesel engine fuelled with biodiesel and its blends. *Pakistan Journal of Scientific and Industrial Research,* **51:** 293-300.

Szybist, J.P., Song, J., Alam, M., Boehman, A.L. 2007. Biodiesel combustion, emissions and emission control. *Fuel Process Technology,* **88:** 679-691.

Tsolakis, A. 2006. Effects on particle size distribution from the diesel engine operating on RME-biodiesel with EGR. *Energy & Fuels,* **20:** 1418-1424.

Turrio-Baldassarri, L., Battistelli, C.L., Conti, L., Crebelli, R., De Berardis, B., Iamiceli, A.L., Gambino, M., Iannaccone, S. 2004. Emission comparison of urban bus engine fueled with diesel oil and biodiesel blend. *The Science of the Total Environment,* **327:** 147-162.

Usta, N. 2005. An experimental study on performance and exhaust emissions of a diesel engine fuelled with tobacco seed oil methyl ester. *Energy Conversion and Management,* **46:** 2373- 2386.

Wang, Y.F., Huang, K.L., Li, C.T., Mi, H.H., Luo, J.H., Tsai, P.J. 2003. Emissions of fuel metals content from a diesel vehicle engine. *Atmospheric Environment,* **37:** 4637-4643.

Wong, C.P., Chan, T.L., Leung, C.W. 2003. Characterization of diesel exhaust particle number and size distributions using mini-dilution tunnel and ejector-diluter measurement techniques. *Atmospheric Environment,* **37:** 4435-4446.

Zhao, H., Ge, Y., Wang, X., Tan, J., Wang, A., You, K. 2010. Effects of fuel sulfur content and diesel oxidation catalyst on PM emitted from light-duty diesel engine. *Energy & Fuels,* **24:** 985-991.

Pak. j. sci. ind. res. Ser. A: phys. sci. 2015 **58** (1) 26-33

Preparation of GF/Wollastonite Reinforced Epoxy Hybrid Composite: Mechanical Properties

Gowkanapalli Ramachandra Reddy[a], Mala Ashok Kumar*[b], Ati Ramesh[b], Mehaboob Basha[c], Nadadur Karthikeyan[b] and Kolimi Madhava Reddy[d]

[a]Department of Polymer Science & Technology, Krishnadevaraya University, Anantapur-515055, Andhra Pradesh, India

[b]Department of Mechanical Engineering, Dr. K.V. Subba Reddy Institute of Technology, Dupadu, Kurnool-518218, Andhra Pradesh, India

[c]Department of Mechanical Engineering, Govt. Polytechnic, Anantapur, India

[d]Department of Mechanical Engineering, P.V.K.K. Institute of Technology, Anantapur, Andhra Pradesh, India

(received March 18, 2013; revised March 30, 2014; accepted April 3, 2014)

Abstract. Performance of injection moulded short wollastonite fibre and chopped glass fibre reinforced hybrid epoxy composites was studied. The results showed that hybridisation of glass fibre and wollastonite was in congruence to epoxy glass fibre composite system. Effect of fibre length, fibre orientation in matrix and analysis and fracture surface was undertaken. The mechanical properties of injection moulded, chopped glass fibre/wollastonite/epoxy hybrid composites were investigated by considering the effect of hybridisation by these two fillers. It was observed that the tensile, flexural, and impact properties of the filled epoxy were higher than those of unfilled epoxy. The effect of filler on epoxy matrix subjected to the tensile strength and modulus was studied and compared with the rule of mixture. The actual results are marginally low as compared with the values obtained by the rule of hybrid mixtures (RoHM).

Keywords: hybrid fibres, wollastonite, glass fibre, mechanical properties

Introduction

The persistence of plastics in the environment, shortage of landfill space, concerns over emissions resulting from incineration, and hazards to human health as well as hazards to animals, birds, and fish from entrapment or ingestion of these materials have spurred the efforts to find more environment friendly alternative materials. Various organic/natural fillers reduce the quality of plastic matrix. The hybrid composites reduces pay load and increase in stiffness is important for certain applications for example, satellite and space craft systems. Scientists have explored advantages and disadvantages of hybrid effects in terms of mechanical properties in all these systems. Short fibre composites are attractive structural materials for their relatively ease of processability with respect to resulting flow field and cooling conditions. A complex microstructure may results in different fibre orientations at different points of moulded specimens. Microstructure characteristics can only explain the mechanical properties of short fibre composites. The hybridisation with small amounts of mineral fibres makes these glass fibre composites more suitable for technical applications.

In a hybrid system various mechanical properties like stiffness strength and fracture toughness depend on the characteristics of constituent fibres like fibre length and fibre volume fraction. When fibre length is smaller than critical fibre length, fibre pull out takes place but if fibre length is more than critical fibre length breaking of fibre occurs thus fracture mechanisms can be identified with the knowledge of critical fibre length. Epoxy (EP) resin is one of the most important classes of thermosetting polymers which are widely used as matrices for fibre reinforced composite materials and for structural adhesives. They are amorphous, highly cross-linked polymers and these polymers possess various desirable properties such as high tensile strength, modulus, uncomplicated processing and good thermal and chemical resistance and dimensional stability. However, it also leads to low toughness and poor crack resistance, which should be up graded before they can be considered for many end applications. But when filled with mineral and glass fillers, the mechanical properties improve to such an extent of engineering thus enabling them to use

*Author for correspondence;
E-mail: ashokkumarmala7@hotmail.com

in engineering applications. The typical reinforcing material used in polymer composites is glass fibre. It is a common reinforcement due to good strength properties, lower price and relatively good adhesion to matrix but now present minerals are in more demand because of a few drawbacks of glass fibres such as lower dispersion, lower thermal and chemical stability and liberation of large amount of heat while processing (Kumar *et al*., 2011a; 2011b; 2011c; 2010; Mishra and Aireddy, 2011; Dauda *et al*., 2009; Jayaramudu *et al*., 2009; Dani *et al*., 2008; John and Venkata, 2007). Wollastonite is a naturally occurring calcium silicate mineral. Earlier studies have shown that acicular wollastonite can be used as coreinforcer in short fibre composites (Padma and Venkata, 2009; Mohan *et al*., 2006). Use of wollastonite in high fraction will reduce the cost of composite and improve tensile strength, impact properties and dimensional stability and yield Rao *et al*. (2011). High aspect ratio (*15) resulting on these wollastonite composites to resist machining and thus has greater surface area, better stress propagation (Sreenivasan *et al*., 2011; Rao *et al*., 2010). Reinforcement with wollastonite increases the starting crystallisation temperature and induces a shorter processing time in injection moulding and thus the effect of crystallinity of the composite for this reason the reinforcement of rotational moulded articles with wollastonite is of interest for research. These materials exhibits increase in flexural modulus, HDT, superior dimensional stability, reduced cost and ease processability. Certain mechanical properties such as strength or modulus of a hybrid system consisting of two single systems can be predicted by the rule of hybrid mixtures (RoHM) as explained earlier (Reddy *et al*., 2010; Reddy *et al*., 2009; 2008a; 2008b; Rajulu and Devi, 2007). The present work aims to develop chopped glass fibre and particulate type wollastonite reinforced epoxy composite. The composites were prepared by extrusion compounding and using injection moulding techniques. In the present research, the effects of hybridisation by chopped glass fibre and wollastonite on the tensile and flexural properties of the hybrid EP/GF/W composite were made. Since the mechanical properties of glass fibres and wollastonite differ greatly, the hybrid effect would likely to exist for their hybrid reinforced composites. The hybrid effects have been calculated using the rule of hybrid mixtures for the tensile strength, modulus, flexural strength and modulus.

Materials and Methods

The epoxy (Araldite-LY 556 and Amine Hardener- HY 951) employed in this study was Ciba-Geigy of India Limited. In addition, the glass fibre (density: 350 g/m^2) was supplied by Saint Gobain Industries Ltd., Bangalore, India with an aspect ratio 250. The grade of wollastonite (W) used for preparing different compositions was Fillex-11AB3 (surface treated), supplied by Wolkem India Limited. The total fibre volume fraction was fixed at 40%. The compositions of prepared specimens are given in Table 1.

The extruder used was a twin screw extruder (JSW, Japan TEX-30A) with a diameter of 25 mm and machine capacity of 20 kg/h having single feeding point. The set point temperatures were between 165 and 220 °C for compounding. The composite was prepared by feeding the glass fibre and wollastonite in the polymer melt. The compounded extrudates were immediately quenched into water and cooled in air to ambient temperature. Then the extrudates strands were chopped into granules with the help of cutter and dried. All the specimens were then injection moulded using L&T injection moulding machine with the parameters listed in Table 2. Test specimens for the evaluation of mechanical properties were prepared. The tensile, flexural and impact properties were determined using 5 samples of each composition.

Tensile strength, three point bending tests were carried out at par with ASTM D 53455. Tensile and flexural tests were performed on Instron universal testing machine (3369). Impact strength of samples was measured on the model number of machine Zwick according to ASTM D 53433. All the tests were accomplished at a room

Table 1. Various compositions prepared specimens

Sample	EP (% by wt.)	GF (% by wt.)	W (% by wt.)
S_1	100	0	0
S_2	60	40	0
S_3	60	30	10
S_4	60	20	20
S_5	60	10	30
S_6	60	0	40

Table 2. Injection moulding machine parameters for EP/GF/W composites

Injection pressure (%)	Holding pressure (%)	Back pressure	Injection speed	Temperature (°C)	Pressure (N/mm^2)
65	65	5.0	70	150	170-200

temperature of 20 °C. At least, 5 samples were tested for each composition and results were averaged. Impact properties were measured in accordance with ASTM D256. The notched Izod test is best applied in determining the impact resistance for many parts with many sharp corners, such as ribs, intersecting walls and other stress concentrator components. The Izod strength of notched/unnotched specimens were conducted (the impact energy used to break a notched/unnotched specimen is divided by the thickness of the specimen at the notch), expressed in kilojoules per meter (kJ/m). Scanning electron microscopy (SEM) studies of the fractured surface of the tensile specimen were carried out on a Jeol (6380LA, Japan). The specimen was sputter-coated with gold to increase surface conductivity. The length of 400-500 glass and wollastonite fibres from each sample were measured separately and recorded with Axiovision Rel 4.6 software.

Results and Discussion

The results obtained from mechanical tests are shown in Table 3. The results are also obtained graphically in Fig. 1(a-b). It has been found from data that with the incorporation of 40% glass fibre (S_2), the tensile strength, tensile modulus values increased sharply when compared to unfilled material indicating the stiffening effect of glass fibre. On the other hand with the incorporation of wollastonite from 10-30% by wt., the above values were found to decrease gradually with respect to S_2, indicating lower stiffening effect of wollastonite in comparison to glass fibre. When compared $S_1$with S_6, it was observed that there is a little change in tensile strength value between S_1 and S_6, but the values of tensile modulus of S_6 had been found higher than that of S_1. The composites (S_2 to S_6) yield had lower values of tensile modulus. On the basis of the above results, it was concluded that the addition of wollastonite content by reducing glass fibre partially, the degree of amorphous nature of epoxy decreases. Tensile stress strain curves of hybrid composites exhibit brittle fracture and show linear deformation under high stress. This non-linear deformation behaviour may be related to (1) interfacial microfailure at the fibre ends would have occur in the composites, (2) the microfailure propagates along the fibre lengths, (3) plastic deformation bands in the matrix were observed, and (4) crack opening occurs in the band and the crack grows slowly through the band as observed by Rajulu and Devi (2007). Finally, the catastrophic crack propagation takes place through the matrix pulling out the fibres from the matrix. The curves shift from right side to left side as the relative

Table 3. Mechanical properties of EP/GF/W composites

Sample	Tensile strength (MPa)	Tensile modulus (MPa)	Elongation at max. force (%)
S_1	46.2	451.6	13.1
S_2	50.5	680.2	8.2
S_3	47.7	593.4	9.4
S_4	47.0	600.7	8.6
S_5	42.2	617.0	8.4
S_6	37.8	605.4	9.8

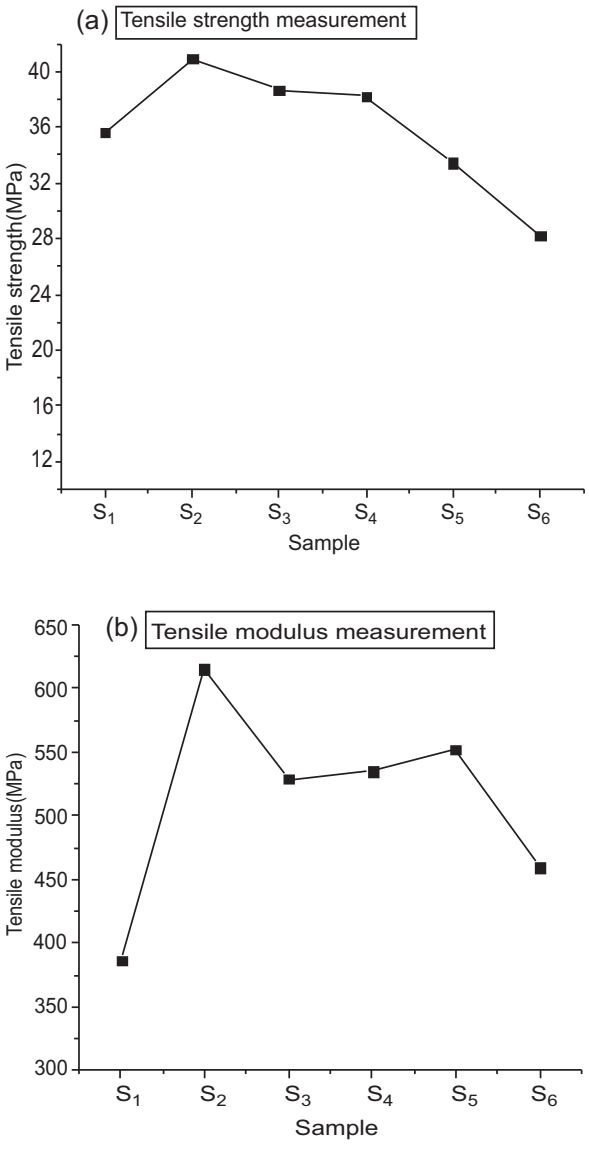

Fig. 1(a-b). Tensile (a) strength and (b) modulus measurements of samples.

wollastonite fibre volume fraction increases. This is due to the fact that the modulus of wollastonite fibres is higher than the matrix but when compared to the glass fibre composite, the modulus shows a slight change with the increase in relative wollastonite volume fraction (Reddy *et al*., 2009). Moreover, the failure strain of the hybrid composites increases with increase in relative wollastonite fibre volume fraction as shown in Fig. 2. This may be partially attributed to the less brittle nature of wollastonite fibre compared to glass fibre. Furthermore, as the wollastonite fibre volume increases there is no significant increase in the strength of the composites.

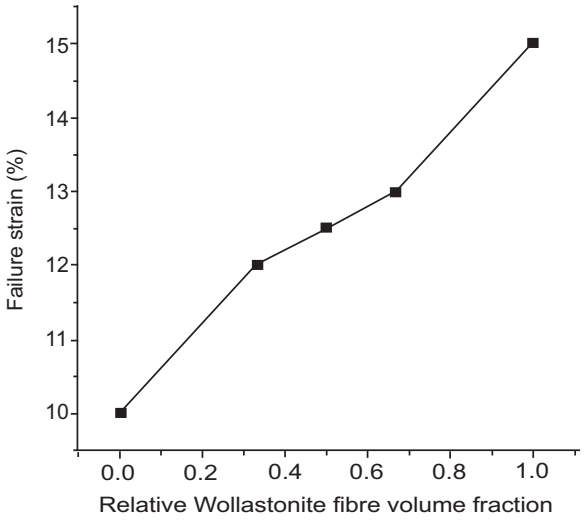

Fig. 2. Measurements of relative fibre volume fractions of failure strain of the samples.

Figure 3(a-b) represents the SEM micrographs of fracture surfaces of hybrid composites S_4 and S_6. The brittle fracture can be easily seen in the composites. It is observed that the short glass fibre and wollastonite were intimately mixed in the matrix and were distinguishable. Both the figures show that most of the glass fibres are pulled out and preferentially aligned in flow direction for these injection moulded specimens.

The orientation of fibres is observed morphologically on the specimen sections as shown in Fig. 3 which is the micrographs selected arbitrarily but is a typical one. For both single fibre reinforced and hybrid composites, the fibres are preferentially aligned along the flow direction. This has also been observed in earlier shortfibre studied (Kumar *et al*., 2011a; 2011b; 2011c). Fibre length measurements were performed by following manually fibre

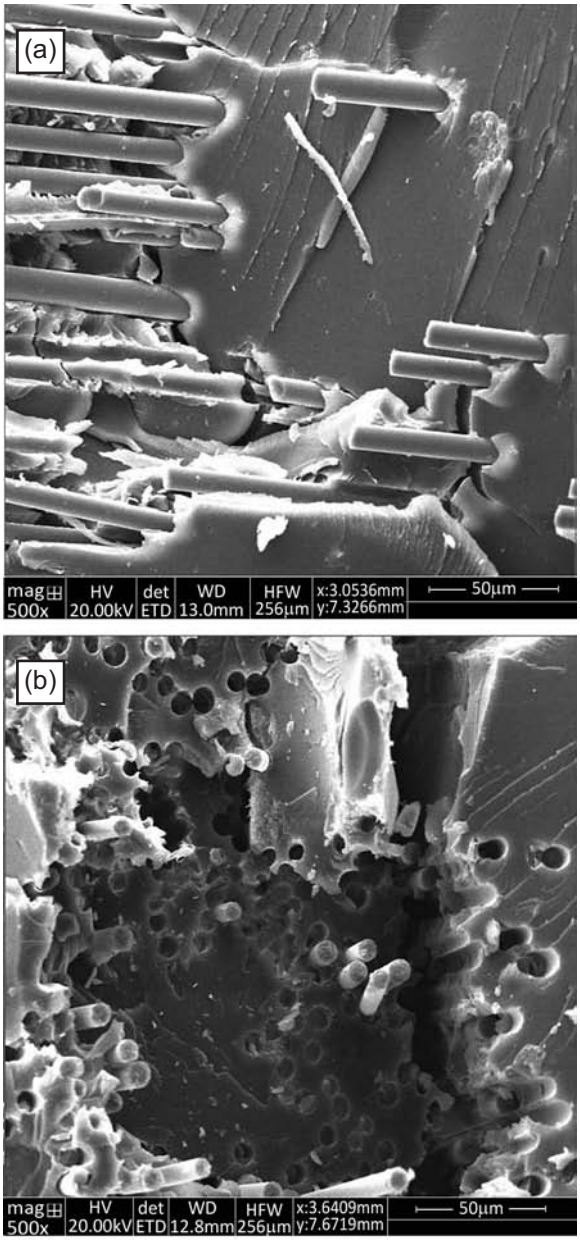

Fig. 3(a-b). SEM images of (a) sample S_4, and (b) sample S_6.

image traces from morphological pictures using Zeiss computerised microscope.

The effect of relative wollastonite fibre volume fraction on the mean wollastonite and glass fibre lengths is presented in Table 4 and Fig. 4, where the total glass and wollastonite fibre fraction is fixed at 40%. It is of interest to note while observing the trends in mean fibre lengths of both the fibres that with the increase of relative wollastonite fibre volume fraction decreases the mean

Table 4. Relative frequencies of EP/GF/W composites

Length classes (μm)	Vf(GF)=40% Vf(W)=0%	Vf(GF)=30% Vf(W)=10%		Vf(GF)=20% Vf(W)=20%		Vf(GF)=10% Vf(W)=30%		Vf(GF)=0% Vf(W)=40%
	GF	GF	W	GF	W	GF	W	W
0-2	0	0	0	0	0	0	0	0
2-4	0	0	0	0	0	0	0	0
4-6	0	0	0.04	0	0.04	0	0	0
6-10	0	0	0.18	0	0.04	0	0.12	0.14
10-20	0.10	0.06	0.40	0.08	0.18	0.08	0.22	0.24
20-40	0.16	0.16	0.44	0.06	0.24	0.04	0.32	0.28
40-60	0.2	0.14	0.04	0.16	0.28	0.14	0.28	0.18
60-80	0.22	0.36	0	0.18	0.08	0.18	0.08	0.1
80-100	0.16	0.08	0	0.18	0.1	0.16	0.1	0.1
100-120	0.16	0.18	0	0.22	0	0.28	0	0.04
120-140	0.04	0.06	0	0.08	0	0.08	0	0.04
140-160	0.06	0.06	0	0.14	0	0.14	0	0
160-180	0.04	0.04	0	0.04	0	0.04	0	0
180-200	0.04	0.06	0	0.04	0	0.04	0	0
200-260	0.04	0.04	0	0.04	0	0.04	0	0
>260	0	0	0	0	0	0	0	0
Mean fibre length(μm)	78.5	110.2	25.36	98.5	40.5	103.8	42.5	48.62

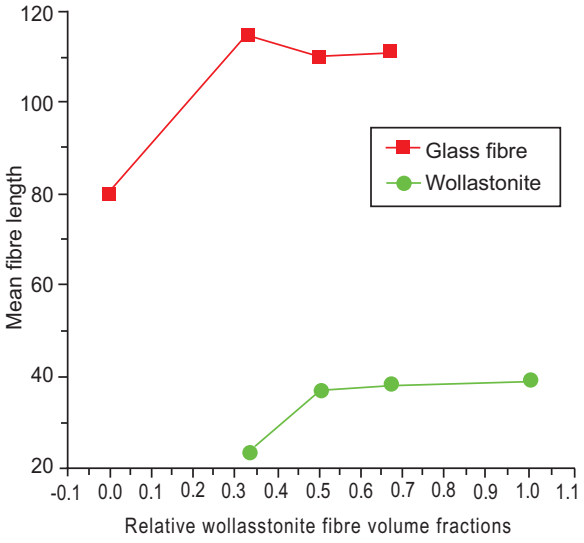

Fig. 4. Relative wollastonite fibre volume fraction Vf(wollastonite)/Vf(total).

fibre length relative than the wollastonite fibre due to wollastonite interaction. The glass and wollastonite fibre length distributions are presented in Fig. 5(a-b) which show that, fibre length distributions of both glass and wollastonite fibres shift towards left side as the relative wollastonite fibre volume fraction increases. This figure depicts the cumulative distribution of the fillers in matrix that leads to further study of the fibre distribution. Figure 5 show the results of the RoHM prediction and the strength of hybrid EP/GF/W composites.

Figure 6 shows the results of the tensile strength of the hybrid composite. It was observed that, ultimate strength was significantly improved by the incorporation of glass and mineral fibres. Since the fibres were preferentially aligned in flow direction for these injection moulded specimens (see SEMs), in broader view the fibre orientation can be assumed roughly unchanged with the fibre volume fraction. When the relative wollastonite fibre volume fraction increased, there is a slight variation in the mean glass and wollastonite fibre lengths. The changes in fibre length were considered to affect the strength of hybrid composites which was predicted using RoHM as described earlier by Reddy *et al*. (2011). The predicted values of the strength for hybrid composite are presented in Fig. 6a. It can be seen that the experimental values of the ultimate strength of the hybrid composite lie slightly above the predicted values. Thus strength studies exhibits a positive deviation from predicted volumes which is evident by fibre addition. Since the wollastonite fibre is slightly less stiff as compared to glass fibre and the mean aspect ratios of wollastonite fiber composites were lesser than those of glass fibers. Thus according to the stress

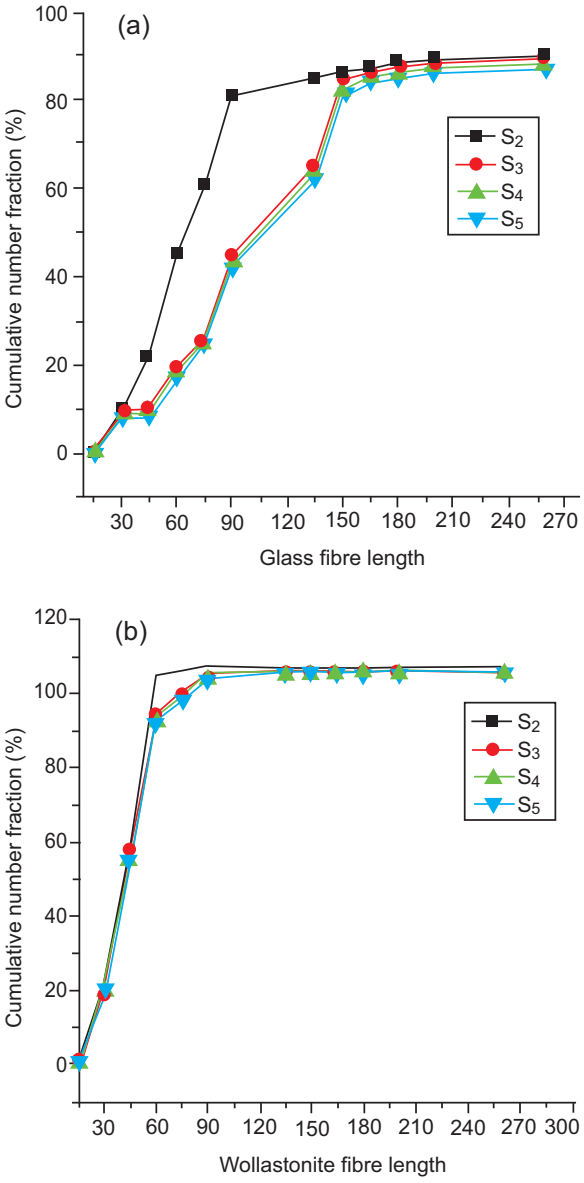

Fig. 5(a-b). (a) Glass fibre and (b) wollastonite fibre length distributions for hybrid, SGF/W/EP composites.

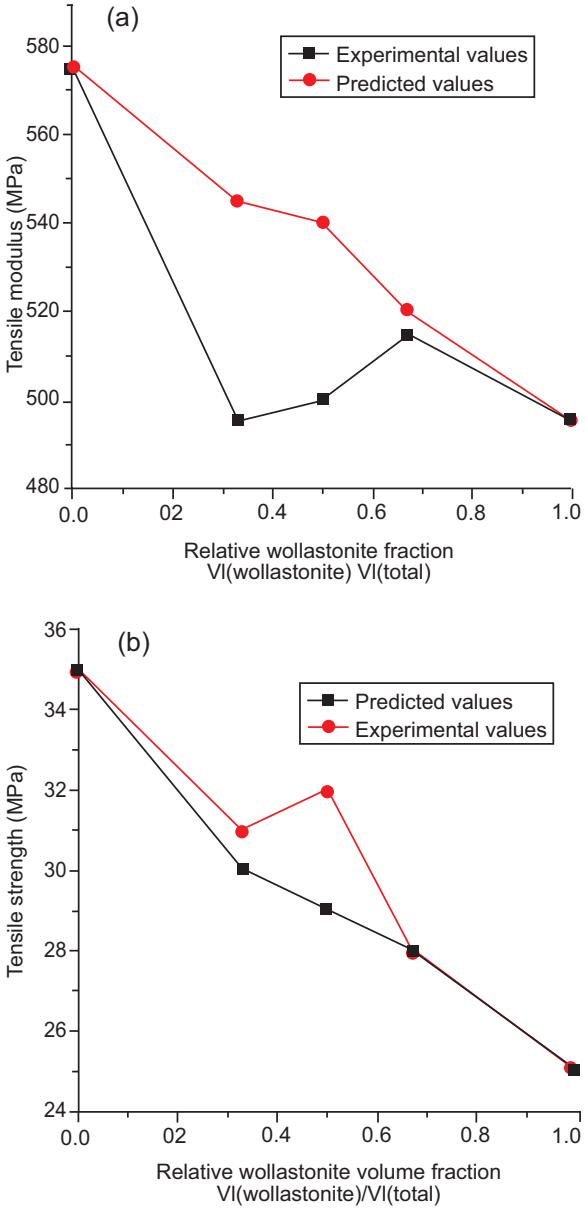

Fig. 6(a-b). Comparison of experimental values with predicted value.

transfer theory (Reddy *et al*., 2009) interfacial debonding would have taken place first at wollastonite fibre ends. Leading to micro crack creation, it was observed that wollastonite fibres are the source for the micro cracks. As the applied tensile strain or load is increased these cracks propagate along the fibre length and also across neighbouring matrix. In the presence of glass fibres these cracks would be bridged by these mineral fibres, allowing the wollastonite fibres to have a slightly larger contribution to the tensile strength of the hybrid composites than that of single wollastonite reinforced composites. As a result, a slight encouraging strength of hybrid composites is observed with the addition of these fibres. Figure 6(b) shows the case of tensile modulus. Since glass fibres are stiffer than wollastonite, modulus was observed to increase with the 100% relative volume of glass fibre and as wollastonite replaces glass fibre partially, composite modulus decreases with increasing relative wollastonite volume fraction. It can be observed from the figure that modulus of hybrid composites is greatly improved by

the addition of both glass fibres and wollastonite fibres (the matrix modulus is 386.3 MPa). The modulus decreases slightly with the increase in relative wollastonite volume fraction. The predicted values according to mixture rule lie above the experimental values and it indicates that the modulus exhibits a negative deviation from the mixture rule.

Conclusion

The mechanical properties of injection moulded hybrid epoxy composites reinforced with short glass fibres and wollastonite fibres have been investigated. The results have shown that the tensile strength, tensile modulus, flexural strength, flexural modulus and impact strength of hybrid composites are in close agreement with composites. The elongation at ultimate load and failure strain of the hybrid composites increases slightly with increase in relative wollastonite fibre volume fraction. The effects of fibre reinforced have been studied on the tensile properties of the hybrid composites. A positive effect had been observed in the ultimate strength while negative effect was noted for the tensile modulus.

Acknowledgement

Authors pay gratitude for Department of Polymer Science and Technology, and Department of Pharmacy at S. K. University Anantapur, India for providing instruments.

References

Dani, J., Rajulu, A.V., Guduri, B.R. 2008. Tensile properties of polycarbonate-coated natural fabric hildegardia populifolia. *Journal of Reinforced Plastics and Technology*, **27:** 1833-1838.

Dauda, S.B., Olutunde, O., Prasad, P. 2009. Characterizing mechanical properties of braided and woven textile composite beams. *Applied Composite Materials*, **16:** 15-21.

Jayaramudu, J., Reddy, O.K., Maheswari, U.C., Reddy, J.P.D., Rajulu, V.A. 2009. Tensile properties and thermal degradation parameters of polyalthia cerasoides natural fabric reinforcement. *Journal of Reinforced Plastics and Composites*, **28:** 2177-2181.

John, K., Naidu, V.S. 2007. Chemical resistance of sisal/glass reinforced unsaturated polyester hybrid composites. *Journal of Reinforced Plastic Composites*, **26:** 373-376.

Kumar, A.M., Reddy, R.G., Reddy, H.G., Chakradhar, K.V.P., Reddy, N.B., Reddy, S.N. 2011a. Mechanical properties of randomly oriented short sansevieria trifasciata fibre/epoxy composites. *International Journal of Fibre and Textile Research*, **1:** 6-10.

Kumar, A.M., Reddy, G.R., Reddy, H.K., Reddy, V.M.Y., Reddy, R.P., Reddy, S.N. 2011b. Fabrication and performance of hybrid betel nut (*Areca catechu*) short fibre/*Sansevieria cylindrica (agavaceae)* composite. *The Indian Journal of Materials Science*, **53:** 375-386.

Kumar, A.M., Reddy, H.K., Reddy, G.R., Reddy, V.M.Y., Reddy, S.N. 2011c. Tensile, thermal properties & chemical resistance of epoxy/hybrid fibre composites (glass/jute) filled with silica powder. *Indian Journal of Macromolecules*, **24:** 241-249.

Kumar, A.M., Reddy, G.R., Bharathi, S.Y., Naidu, S.V., Naidu, N.P.V. 2010. Frictional coefficient, hardness, impact strength and chemical resistance of reinforced sisal-glass fiber epoxy hybrid composites. *Journal of Composite Materials*, **46:** 3195-3202.

Mishra, S.C., Aireddy, H. 2011. Evaluation of dielectric behavior of bio-waste reinforced polymer composite. *Journal of Reinforced Plastics & Composites*, **30:** 134-141.

Mohan, T.P., Ramesh, K.M., Velmurugan, R. 2006. Thermal, mechanical and vibration characteristics of epoxy-clay nanocomposites. *Journal of Material Science*, **41:** 5915-5925.

Padma, V.T., Naidu, V.S. 2009. Chemical resistance and tensile properties of sisal/glass fibres. *Indian Journal of Fibre and Textile Research*, **23:** 128-132.

Rajulu, V.A., Devi, R.R. 2007. Tensile properties of ridge gourd/phenolic composites and glass/ridge gourd/phenolic hybrid composites. *Journal of Reinforced Composites and Plastics*, **26:** 629-638.

Rao, R.H., Kumar, A.M., Reddy, R.G. 2011. Hybrid composites: Effect of fibers on mechanical properties. *International Journal of Macromolecular Science*, **1:** 9-14.

Rao, R.H., Rajulu, V.A., Reddy, R.G., Reddy, H.K. 2010. Flexural and compressive properties of bamboo and glass fiber-reinforced epoxy hybrid composites. *Journal of Reinforced Plastics and Composites*, **29:** 1446-1450.

Reddy, R.G., Kumar, A.M., Chakradhar, K.V.P. 2011. Fabrication and performance of hybrid betel nut (*Areca catechu*) short fiber/sansevieria cylindrica

(agavaceae) epoxy composites. *International Journal of Materials and Biomaterials Applications*, **1:** 6-13.

Reddy, V.S.E., Rajulu, V.A., Reddy, H.K., Reddy, R.G. 2010. Chemical resistance and tensile properties of glass and bamboo fibres reinforced polyester hybrid composites. *Journal of Reinforced Plastics and Composites*, **29:** 2119-2123.

Reddy, V.G., Rani, S.T., Rao, C.K., Naidu, V.S. 2009. Flexural, compressive and interlaminar shear strength properties of kapok/glass composites. *Journal of Reinforced Plastics and Composites*, **28:** 1665-1677.

Reddy, V.G., Naidu, V.S., Rani, S.T. 2008a. Impact properties of kapok based unsaturated polyester hybrid composites. *Journal of Reinforced Plastics and Composites*, **27:** 1789-1804.

Reddy, V.G., Naidu, V.S., Rani, S.T. 2008b. Kapok/glass polyester hybrid composites: tensile and hardness properties. *Journal of Reinforced Plastics and Composites*, **27:** 1775-1787.

Sreenivasan, V.S., Somasundaram, S., Ravindran, D., Manikandan, V., Narayanasamy, R. 2011. Micro-structural physico-chemical and mechanical characterization of *Sansevieria cylindrica* fibres: an exploratory investigation. *Materials and Design*, **32:** 453-461.

Pak. j. sci. ind. res. Ser. A: phys. sci. 2015 **58**(1) 34-40

Manufacturing of Kevlar/Polyester Composite by Resin Transfer Moulding using Conventional and Microwave Heating

Iram Abdullah
Department of Polymer Engineering, National Textile University, Faisalabad, Pakistan

(received May 20, 2013; revised December 22, 2013; accepted January 07, 2014)

Abstract: Microwave heating was incorporated into the resin transfer moulding technique. Polytetrafluoroethylene (PTFE) mould was used to cure the composite panel. Through the use of microwave heating, the mechanical and physical properties of produced Kevlar fibre/polyester composites were compared to those manufactured by conventional resin transfer moulding. The flexural modulus and flexural strength of 6-ply conventionally cured composites was 45% and 9% higher than the flexural modulus and flexural strength of 6-ply microwaved cured composites, respectively. However, 19% increase in interlaminar shear strength (ILSS) and 2% increase in compressive strength was observed in 6-ply microwave cured composites. This enhancement in ILSS and compressive strength is attributed to the better interfacial bonding of polyester resin with Kevlar fibres in microwaved cured composite, which was also confirmed *via* electron microscopy scanning. Furthermore, the microwave cured composite yielded maximum void contents (3%).

Keywords: microwave curing, resin transfer moulding, polymer matrix composites, mechanical properties

Introduction

Resin transfer moulding (RTM) technique has been used more than 50 years for the manufacturing of fibre-reinforced composite materials. Their high strength-to-weight and stiffness-to weight ratio have led to their applications and uses in lots of major industries, and among these automotive and aerospace industry taking the larger part (Reia da Costa *et al*., 2012; Mouton *et al*., 2010; Harper, 2009; Potter, 1999). However, their high operational cost involved has restricted their wider use in industry and considerable efforts have been made to develope cost effective routes for curing of RTM composites.

RTM involves injecting a liquid thermosetting resin into a closed mould containing a dry fibre preform. Air and excess resin are purged through peripheral vents. The mould heating system raises the temperature of the mould body and the heat is transferred to the resin by conduction, initiating the exothermic reaction. Completion of the cure sequence is signalled by the cure at the injection gate. This is direct consequence of the thermal quench in that region and variation in chemical 'age' across the laminate (Johnson *et al*., 1998). Process developments involving zone heated moulds, phased initiator resin systems and pre-heating the resin with microwave radiations have been used to compensate for thermal quench and have provided significant reductions in the cycle time (Agius *et al*., 2013; Johnson *et al*., 1998). Microwave radiation generates uniform heat within the material through conversion of electrostatic energy to thermal energy rather than heat transfer through conduction and convection (Thostenson and Chou, 1999). This made it attractive to be used for curing composites. Several attempts have been made to use microwave radiation for the curing of epoxy resin (Varaporn and Kaew, 2005; Zhou, *et al*., 2003; Boey and Yap, 2001; Fu and Hawley, 2000; Bai *et al*., 1995; Wei *et al*., 1993; Marand *et al*., 1992; Majovic and Wijaya, 1990a) and epoxy composites (Chaowasakoo and Sombatsompop, 2007; Rao *et al*., 2006; Varaporn and Dumrong, 2006; Nightingale and Day, 2002; Yue and Looi, 1995). It offers several advantages such as rapid, volumetric curing, energy saving, reduced processing time and improved processing control (Yusoff *et al*., 2007; Davies *et al*., 2007; Zhou *et al*., 2003; Ku *et al*., 2002; Bykov *et al*., 2001; Mijovic and Wijaya, 1990b). However, very little research work is available in which microwave radiation is used for curing RTM composites and it has not been fully exploited. Previously microwave radiation has been used for the curing of carbon/epoxy composite and it had substantially reduced the cure cycle time,

E-mail: i_tayyab@hotmail.com

energy requirements and operational costs. Furthermore, the stronger adhesion at the interface improved the stress transfer between the carbon fibre and the epoxy matrix (Papargyris *et al*., 2008). Consequently, the interlaminar shear strength for the microwave cured composite was improved. Microwave curing also forms a different molecular structure of polymer as compared with the conventional curing.

The aim of the present work is to incorporate microwave heating into the resin transfer moulding technique and to compare the overall physical and mechanical properties of the fabricated Kevlar/polyester composites with those obtained by conventional thermal resin transfer moulding. This is an attempt to assess if microwave radiation is also as efficient and feasible power source for curing Kevlar/polyester composite as it proved to be effective for the curing of carbon/epoxy composite.

Materials and Methods

The resin system used in this study was Norpol 420-100, supplied by Rachold Chemicals. This resin system contains 75% polyester resin and 25% styrene with no added accelerator. Benzoyl peroxide obtained from Aldrich was used as 1% by the weight of resin as an initiator. Unidirectional high modulus aramid fibre roving UT-A 300/500P supplied by Heinsco, was used as reinforced material.

Resin transfer moulding (RTM) processing. ***Conventional thermal RTM processing.*** Conventional thermal RTM processing was based on the Hypaject 3/6 Mark II RTM injection system (Plastech) as illustrated systematically in Fig. 1. The system comprising of an inlet valve, a heated homogeniser, a pneumatic valve, a metal

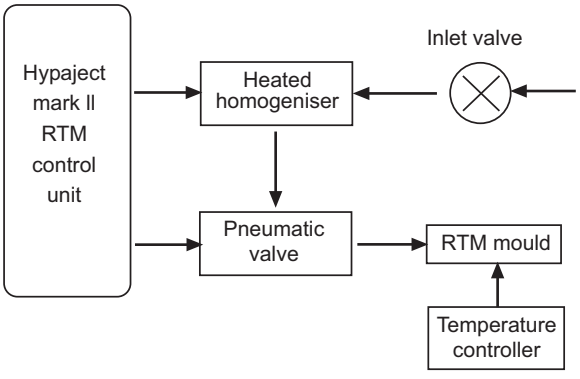

Fig. 1. Schematic diagram of conventional thermal RTM processing (black arrows indicate resin flow, grey arrows indicate process control).

mould with 8 electric-cartridge heaters giving a total power output of 2 KW, two K-type thermocouples and two PID temperature controllers. Prior to the curing process, the metal mould was coated with Frekote 44-NC release agent. The fibres were then placed inside the mould cavity (200 × 300 × 3 mm dimensions) and the mould was inclined at 45° from horizontal in a steel stand in order to minimise air entrapment during the injection.

The resin was drawn into the homogeniser through the inlet valve and left for 10-15 min under vacuum in order to remove any air bubbles created at initial resin-hardener mixing stage. The resin was then injected under low pressure (0.3 bar) into the pre-heated mould through the inlet valve. After completion of injection stage, the resin loaded mould was heated for 45 mins at 120 °C. The cure kinetic study on Norpol 420-100 unsaturated polyester resin showed that 95% of resin cures at 120°C The temperature controller maintained the cure temperature. Through this technique the following composites were prepared:

1. 5 ply Kevlar/polyester composite,
2.5 ply Kevlar/polyester composite with preheated mould at 50 °C for 30 min,
3. 6 ply Kevlar/polyester composite with preheated mould at 50 °C for 30 min,

Microwave RTM processing. In microwave RTM processing microwave radiation was employed in order to cure the composite. A polyethylene tetrafluoroethylene (PTFE) mould of cavity dimensions of 200 × 200 × 3 mm was used. Preparation of mould prior to resin injection involved applying Chemlease C15 sealer agent and PMR Chemlease release agent. The fibres were then placed inside the cavity and the mould was again inclined at 45° from horizontal during resin injection, which was carried out using Hypaject RTM system.

The microwave RTM heating equipment comprises a network analyser (Hewlett Packard HP8720ET) used as the power source, a travelling wave tube amplifier, an isolator, a multimode microwave applicator (Brass cavity), a PTFE mould and 4 fluoroptic probs (Luxtron Corp) connected to Luxtron 790 fluoroptic thermometer. The microwave system set up is shown in Fig. 2.

A computer control system was employed to ensure uniform heating and maintaining a stable cure temperature. Temperature stability was achieved by adjusting the microwave power while uniformity of the electric field distribution within the applicator was provided by

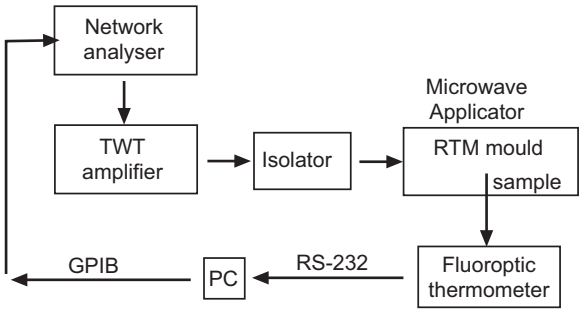

Fig. 2. Schematic digrarm of microwave RTM processing (Black arrows indicate microwave power flow, grey arrows indicate process control/temperature measurements).

varying the excitation frequency. Different excitation frequencies ranging from 6-8 GHz were used for processing. It was observed that 7.339 GHz was the best frequency for microwave to cure the polyester/ Kevlar composite with less noise ratio and 5 W power was reflected back to the amplifier.

Microwave power (180 W) and frequency (7.339 GHz) was adjusted via a general purpose interface bus (GPIB) connection between the computer and the NA to raise the temperature of the mould from 27 °C to 120 °C in 60 min. The computer control system was designed in such a way that the NA would continuously step through the excitation frequencies, while simultaneously regulating the microwave power in order to maintain the 120 °C cure temperature for 45 mins. The sample temperature was constantly monitored by the computer *via* a serial connection with the fluoroptic thermometer. A typical 6-ply Kevlar/polyester microwave cured composite was prepared through this technique.

Mechanical testing. ***Differential scanning calorimetry (DSC).*** Differential scanning calorimetric studies were carried out on a TA instrument MDSC 2920 to ensure that the fabricated composite panels were fully cured. Small size samples (10 mg) were heated from 0 to 300 °C at 20 °C/min in an inert nitrogen atmosphere. Samples were taken from different locations on each composite panel.

Flexural modulus. The flexural properties of composite samples were determined according to British Standard test method BS 2782: Part 3: Method 335A. The apparatus used was an Instron 1122 equipped with a three point bend jig. 6 samples (60 mm × 10 mm) of each composite panel were tested and an average value was taken.

Interlaminar shear strength. Interlaminar shear testing of composite samples was conducted on an Instron 1122 with a load cell of 2 KN according to British Standard method BS 2782: Part 3: Method 341A: 1977. 6 samples of each (60 mm × 10 mm) composite panel were tested and average values were taken.

Compressive strength. 63 mm long/ 0.5 mm thick steel tabs were adhered on each composite sample of 140 mm/ 6 mm/3.3 mm dimension. The compressive test was carried out on an Instron 1185. The load cell was 50 KN and the crosshead speed was 5 mm/min.

Quantitative microstructural analysis. Small fractions from the panels were cut and potted in epoxy resin. Each sample was first grinded using diamond grinder/polisher with metlap fluid dispenser and then polished for 10-20 mins using Mastertex cloth platen with an $AlSiO_2$ abrasive of 1m dimension.

Microstructural analysis was done using image analysis system. Images were acquired using a stero zoom microscope and a CCD black and white camera. On computer screen circumstance of the voids was manually traced out with a light pen. The computer programme 'Genias' was used to calculate the void contents. The following equation was used to calculate percentage void contents.

% age void content = [High-lighted area / total area of picture] × 100

Scanning electron microscopy (SEM). Small fractions of fractured surfaces from mechanically tested samples were placed on metal stubs using double sided carbon tabs. The stubs with the fractured surfaces were then coated with a thin layer (0.1 mm) of gold using Edwards S150B sputter and examined for fibre-matrix inter-laminar strength using Philips ×L30 FEG SEM micro-scope.

Resuts and Discussion

The cured cycle employed for both conventional thermal and microwave RTM processing was 120 °C for 45 min. DSC results confirmed that the composites panels fabricated with these profiles were fully cured as shown in Table 1. The quality of composite panel prepared through RTM processing depends upon the stiffness of the mould. The mould must resist all the loads; loads arise from the pressure required to compact the reinforcement and from the pressure of the resin injected into the mould. An additional pressure is also generated from the expansion of resin due to temperature changes.

Table. 1. Mechanical and physical properties of Kevlar/polyester composites produced by conventional thermal and microwave RTM processing

Properties	5-Ply conventional thermal RTM	5-Ply preheated conventional thermal RTM	6-Ply preheated conventional thermal RTM	6-Ply microwave RTM
Degree of cure (%)	99.6	99.5	99.8	99.5
Void contents Vv (%)	0.49	0.45	0.47	3.4
Flexural modulus (GPa)	17.9 ± 2.9	17.3 ± 1.9	26.4 ± 1.6	14.4 ± 4
Flexural strength (MPa)	378 ± 55	404 ± 28	441 ± 13	401 ± 24
ILSS (MPa)	21.8 ± 3.3	22.3 ± 3.3	23.9 ± 1.2	28.5 ± 4
Compressive strength (MPa)	156.5 ± 4.5	161.4 ± 5.7	177.6 ± 13	181.6 ± 23

This additional pressure in PTFE mould was delayed to zero during curing due to the lower stiffness of the mould. The deflection of mould from the centre caused shrinkage induced voidages (Fig. 3a-b), therefore, the void contents of microwave assisted RTM composite are much higher than the void contents of conventional RTM composite samples as shown in Table 1. The surface quality of microwave assisted RTM composite is also poor as compared with the surface quality of conventional RTM composite panel as shown in Fig. (4a-b).

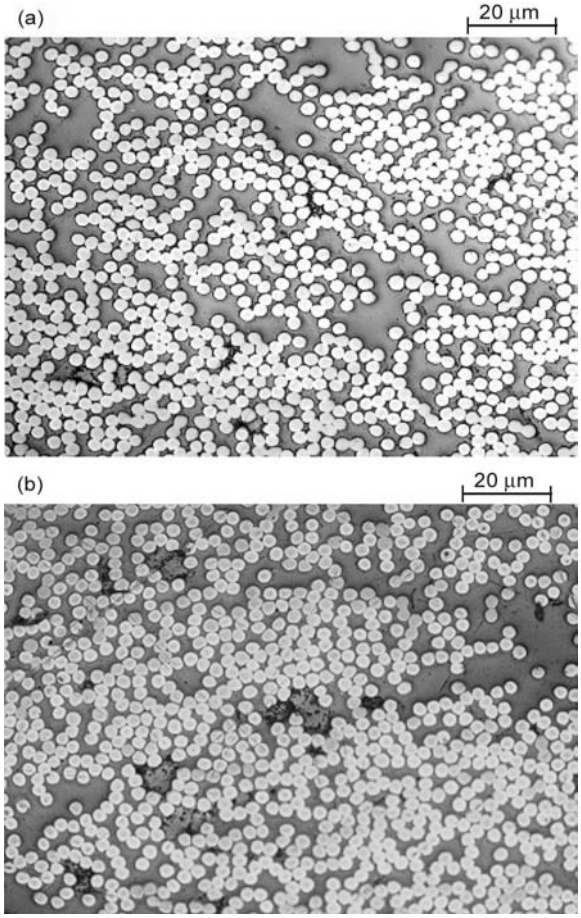

Fig. 3(a-b). Optical micrographs showing at same magnification voids in 6-Ply (a) conventional thermally cured RTM composite (b) microwave cured RTM composite.

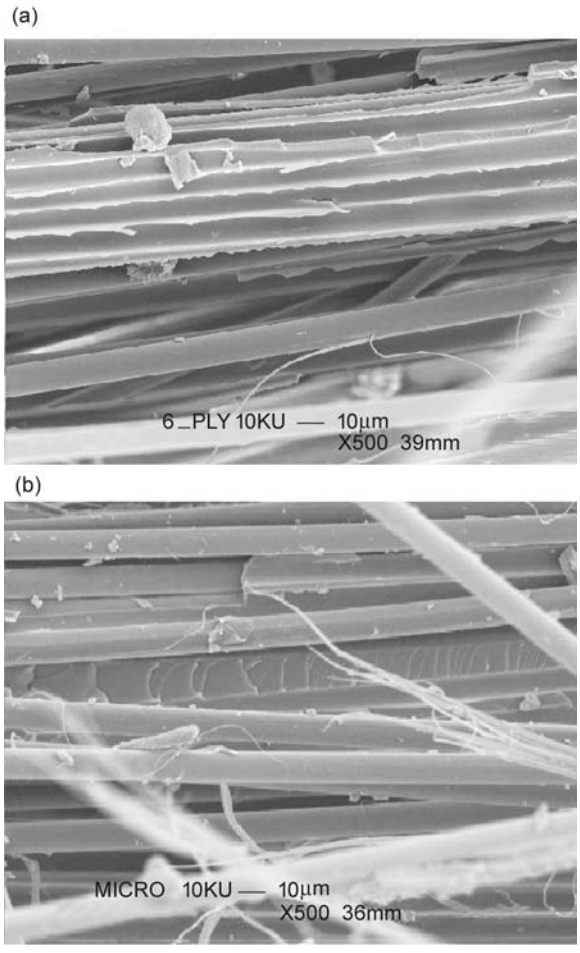

Fig. 4(a-b). (a) Conventional thermally cured RTM composite panel, (b) microwave cured RTM composite panel.

The comparison of flexural mechanical properties of the manufactured composites (Table 1) shows that the flexural modulie of 6-ply microwave cured composite is lower than the 6-ply thermally cured composite. The flexural strength of microwave cured composite is slightly less than conventionally thermally cured composite. However, no distinctive improvement in the flexural modulie and strength of 5-ply conventional thermally cured composite can be concluded; both 5-ply composites exhibit the same flexural properties. The value of the interlaminar shear strength obtained for microwave cured composite is found to be slightly higher than those cured thermally, possibly signifying that the microwave curing improves the interfacial bonding between the Kevlar fibre reinforcement and polyester matrix. The fracture surfaces of composite samples subjected to interlaminar shear strength testing were also examined using scanning electron microscopy. Representative topographic features of both types of composites are shown in Fig. 5a-b. It can be seen from the fractured surfaces of the composites that in both conventionally cured and microwaved composites the fibres are pulled-out of the matrix system. However, in microwave cured composite resin traces are present on the fibre surfaces (Fig. 5b) as opposed to clean fibres present in thermally cured composite (Fig. 5a), which indicates that interfacial bonding in microwave cured composite may be slightly better than the interfacial bonding produced in conventionally cured composite. The smooth surface and inert chemical structure of Kevlar fibre prevents its interfacial bonding with most of the resins used in composites (Gu *et al.,* 2012; Jia *et al*., 2011). The better compression strength value of microwave cured composites compared with the conventionally cured composites also indicated that either the microwave cured specimen exhibit better interface than conventionally cured specimen or the strength of the matrix in microwave cured specimen is high.

Generally, microwave heating is regarded as a volumetric heating technique in which the microwaves interact with the material and heat is generated directly as a result. Hence, heating is efficient because energy is deposited directly into the material and the effects of convection and conduction heat transfers are less significant than with some other heating techniques. In Kevlar/polyester composite; Kelvar is a low conductive fibre. The dielectric loss of composite is dominated by the dielectric properties of polyester matrix. Polyester molecules were heated directly inside the network structure; the induced

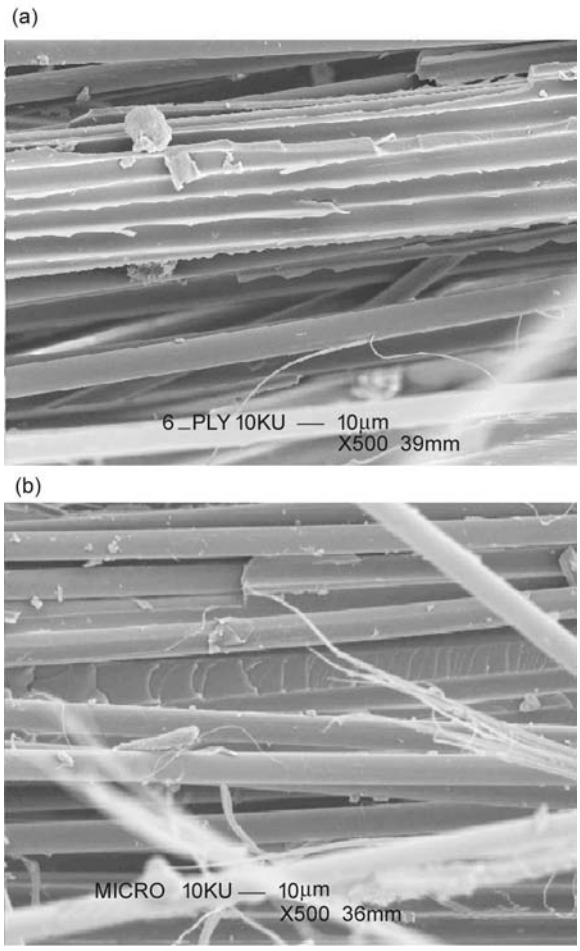

Fig. 5(a-b). SEM micrographs after interlaminar shear strength; (a) conventionally cured specimen (b) microwave cured specimen.

polymer polarisation along the applied electromagnetic field greatly increased the molecular mobility. This led to an increase in crosslinking inside the microgels. Kevlar fibres were heated in contact with polyester resin through conduction. The increased crosslinking created strong bonding at the fibre/matrix interface. The higher crosslinking is expected to improve the mechanical properties of microwave cured Kevlar/ polyester composites. The interlaminar shear strength (ILSS) increased by 19% and compressive strength was increased by 2%, however, this increase was not profound as it comes in the range of experimental errors. No increase in flexural modulus and flexural strength is observed due to high void contents. The improvement in flexural strength and modulie can be achieved by selecting better mould material which must have dimensional stability to withstand the temperature and pressure cycle during processing. The reduction in void

contents may further improve the mechanical properties of microwave cured composite.

Conclusion

In this study, the conventional resin transfer moulding (RTM) technique incorporated with microwave heating was presented. Composites were produced by both conven-tional thermal and microwave RTM processing in order to compare their physical and mechanical properties. The curing profile employed in conventional thermal and microwave RTM processing was 45 mins at 120 °C. DSC analysis of samples taken from different panel locations confirmed that the composites were fully cured, validating the uniformity of the microwave field inside the applicator. Mechanical testing showed lower values of flexural modulie and flexural strength for microwaved composite as compared with the conventional thermally cured composites. The inter-laminar shear strength and compressive strength of the composites produced by microwave RTM processing was found to be higher than that of the thermally cured composites. This enhancement is suggested to be mainly attributed to the better interfacial bonding between the fibre surface and matrix. The microwave cured compo-sites exhibited higher void content values than those cured conventionally. PTFE mould was too soft to remain in shape while curing of resin.

The results presented in this work underline the potential of microwave heating in improving composites process-ing and manufacturing. Despite the defects in mould used for microwave curing, the mechanical and physical properties of the microwave cured composites were found to be comparative and, in some cases, superior compared to the thermally cured composite. Further research is necessary in order to understand and explain the differences in the reaction mechanism between thermally and microwave cured composites. Optimisation of material and processing parameters is also required to achieve better mechanical properties, surface of composite panel and reduction in processing cost.

Acknowledgement

The Material Science Centre, UMIST, Manchester UK, is gratefully acknowledged for technical support.

References

Agius, S.L., Magniez, K.J.C., Fox, B.L. 2013. Cure behaviour and void development within rapidly cured out-of-autoclave composites. *Composites Part B,* **47:** 230-237.

Bai, S.L., Djafari, V., Andreani, M., Francois, D. 1995. A comparative study of the mechanical behaviour of an epoxy resin cured by microwaves with one cured thermally. *European Polymer Journal*, **31:** 875-884.

Boey, F.Y.C., Yap, B.H. 2001. Microwave curing of an epoxy-amine system: Effect of curing agent on the glass-transition temperature. *Polymer Testing*, **20:** 837-845.

Bykov, Y.V., Rybakov, K.I., Semenov, V.E. 2001. High temperature microwave processing of materials. *Journal of Physics D: Applied Physics*, **34:** R55-75.

Chaowasakoo, T., Sombatsompop, N. 2007 Mechanical and morphological properties of fly ash/epoxy composites using conventional thermal and micro-wave curing methods. *Composite Science and Technology*, **67:** 2282-2291.

Davies, L.W., Day, R.J., Bond, D., Nesbitt, A., Ellis, J., Gardon, E. 2007. Effect of cure cycle heat transfer rates on the physical and mechanical properties of an epoxy matrix composite. *Composite Science and Technology*, **67:** 1892-1899.

Fu, B., Hawley, M.C. 2000. Comparative study of continuous-power and pulsed-power microwave curing of epoxy resins. *Polymer Engineering and Science*, **40:** 2133-2143.

Gu, R., Yua, J., Hua, C., Chena, L., Zhua, J., Hub, Z. 2012. Surface treatment of para-aramid fiber by Argon dielectric barrier discharge plasma at atmospheric pressure. *Applied Surface Science*, **258:** 10168-10174.

Harper, A. 2009. RTM-past present and future. *Rein-forced Plastics*, **11/12:** 30-33.

Jia, C., Chena, P., Liua, W., Li, B., Wang, Q. 2011. Surface treatment of aramid fiber by air dielectric barrier discharge plasma at atmospheric pressure. *Applied Surface Science*, **257:** 4165-4170.

Johnson, M.S., Rudd, C.D., Hill, D.J. 1998. Microwave assisted resin transfer moulding. *Composites* Part A: *Applied Sciences and Manufacturing*, **29A:** 71-86.

Ku, H.S., Siores, E., Taube, A., Ball, J.A.R. 2002. Productivity improvement through the use of indus-trial microwave technologies. *Computer and Indus-trial Engineering*, **42:** 281-290.

Marand, E., Baker, K.R., Graybeal, J.D. 1992. Compari-son of reaction mechanisms of epoxy resins undergoing thermal and microwave cure from in Situ measurements of microwave dielectric proper-ties and infrared spectroscopy. *Macromolecules*, **25:** 2243-2252.

Mijovic, J., Wijaya, J., 1990a. Comparative calorimetric study of epoxy cure by microwave vs thermal energy. *Macromolecules*, **23:** 3671-3674.

Mijovic, J., Wijaya, J. 1990b. Review of cure of polymers and composites by microwave energy. *Polymer Composite,* **11:** 184-191.

Mouton, S., Teissandier, D., Sébastian, P., Nadeau, J.P. 2010. Manufacturing requirements in design: The RTM process in aeronautics. *Composites*: *Part A,* **41:** 125-130.

Nightingale, C., Day, R.J. 2002. Flexural and interlaminar shear strength properties of carbon fibre-epoxy composites cured thermally and with microwave radiation. *Composites* Part A: *Applied Sciences and Manufacturing*, **33:** 1021-1030.

Papargyris, D.A., Day, R.J., Nesbitt, A., Bakavos, D. 2008. Comparison of the mechanical and physical properties of a carbon fibre epoxy composite manufactured by the resin transfer moulding using conventional and microwave heating. *Composites Science and Technology*, **68:** 1854-1861.

Potter, K.D. 1999. The early history of resin transfer moulding process for aerospace applications. *Composites Part A: Applied Sciences and Manufacturing*, **30A:** 619-621.

Reia da Costa, E.F., Skordos, A.A., Partridge, I.K., Rezai, A. 2012. RTM processing and electrical performance of carbon nanotube modified epoxy/fibre composites. *Composites Part A, Applied Science and Manufacturing,* **43:** 593-602.

Rao, R., Rao, S., Sridhara, B. 2006. Studies on tensile and interlaminar shear strength properties of thermally cured and microwave cured glass/epoxy composites. *Journal of Reinforced Plastics Composites*, **25:** 783-795

Thostenson, E.T., Chou, T-W. 1999. Microwave processing: Fundamentals and applications. *Composites Part A: Applied Sciences and Manufacturing*, **30:** 1055-1071.

Varaporn, T., Dumrong, J. 2006. Comparison between microwave and thermal curing of glass fiber-epoxy composites: Effect of microwave heating cycle on mechanical properties. *Journal of Applied Polymer Science*, **102:** 1059-1070.

Varaporn, T., Kaew, S.T. 2005. Comparison of microwave and thermal cure of epoxy-anhydride resins: Mechanical properties and dynamic characteristics. *Journal of Applied Polymer Science*, **97:** 1442-1461.

Wei, J., Hawley, M.C., Delong, J.D. 1993. Comparison of microwave and thermal cure of epoxy resins. *Polymer Engineering and Sciences*, **33:** 1132-1140.

Yue, C.Y., Looi, H.C. 1995. Influence of thermal and microwave processing on the mechanical and interfacial properties of a glass/epoxy composite. *Composites*, **26:** 767-773.

Yusoff, R., Aroua, M.K., Nesbitt, A., Day, R.J. 2007. Curing of polymeric composites using microwave resin transfer moulding (RTM). *Journal of Engineering Science and Technology*, **2:** 151-163.

Zhou, J., Shi, C., Mei, B. 2003. Research on the technology and the mechanical properties of microwave processing of polymer. *Journal of Material, Process and Technology*, **137:** 156-158.

Pak. j. sci. ind. res. Ser. A: phys. sci. 2015 **58** (1) 41-45

Water Characterisation of Coal Mining Areas of Chakwal, Punjab, Pakistan

Syed Mahmood Arshad[a], Syed Muhammad Tariq[a], Muhammad Shahzad[a]*, Muhammad Zubair Abu Bakar[b] and Muhammad Waqas[a]

[a]Mining Engineering Department, University of Engineering & Technology Lahore, Pakistan
[b]Geological Engineering Department, University of Engineering & Technology Lahore, Pakistan

(received July 1, 2013; revised February 7, 2014; accepted February 8, 2014)

Abstract. Discharged water from mines shows alteration in its physical properties and may be acidic depending upon the concentration of heavy metals and sulphate ions, which pose hazardous effects on groundwater and ecosystem. This paper deals with the characterisation of water being affected by coal mining in the Basharat area of Punjab. Total eleven samples were collected from different water sources including groundwater, mine outflows, mine inflows and surface water in the vicinity of Hassan Kishor Coal Mine. All samples except that of groundwater showed higher turbidity, lower pH values and higher total solid contents. Higher concentration of iron and copper in all samples indicate higher acid mine drainage (AMD). Relatively larger concentration of calcium in groundwater as compared to its presence in other samples demonstrates quashing effect of overlying limestone to the AMD.

Keywords: water pollution, groundwater, coal mine, acid mine drainage

Introduction

The rapid growth of population particularly in developing countries such as Pakistan demands more natural resources for the fulfillment of needs of human beings. These large quantities of natural resources are obtained through increased mining activities and amplified rate of extraction. The growing mining activities are vigorously endangering the environment (Monjezi *et al*., 2009). Mining adversely affects the environment during all of its stages even after the completion of mining operation (Singh *et al*., 2011; Younger *et al*., 2002). Its major negative impacts include changes in hydrology, lithology, topography, ecology, land-use distribution and visual degradation, socio-economic statistics and atmosphere (Singh, 2008). Probably the most severe damage occurs to the groundwater regime of the area. Generally, water is contaminated either physically or chemically by taking up impurities. This contaminated water enteres the water cycle and causes hazardous effects on living things, land and atmosphere. Extent of water contamination is primarily dependent upon composition of ore deposits and its surrounding geology, structural features of the area, hydrology and climate of the mining region (Dold and Fontbote, 2001).

Coal mining adversely affects the hydrology of the area. Acid generation through oxidation of sulphur-bearing minerals such as pyrite in coal mines is one of the major causes of water contamination (Tiwary, 2000). The amount of acidity produced from a coal mine mostly depends on the sulphide contents, age of the deposit, alkalinity producing minerals and waste volumes (Gomes *et al*., 2011). Manganese, iron and aluminium are found to be the major elements, which constitute acidity in coal mine drainages (Skousen *et al*., 1998). Normally sulphide minerals react with oxygen and water to produce sulphuric acid and iron sulphide or iron hydroxide. Reaction of pyrite with oxygen and water is discussed by many researchers (Banks *et al*., 1997; Zaihua *et al*., 1991; Powell, 1988). The reduced pH values cause further dissolution of various minerals and toxic metals into water (Tiwary, 2000). Lead, arsenic and nickel are frequently found toxic metals in coal mine drainages (Younger and Sapsford, 2004).

The aquatic life is adversely affected by the acid-generation. Not only the lower pH values harm organisms but release of heavy metals into water severely damages the aquatic biota, wild life and land fertility for vegetation (Tiwary, 2000). Besides, acid mine drainage in appropriate physical conditions like temperature and turbidity of water play significant role in limiting the growth of living things (Kumar and Kakrani, 2000). This study aims to physically and chemically characterise water samples collected from different sources in and around coal mines in Basharat area, Punjab. These samples

*Author for correspondence; E-mail: m.shahzad87@uet.edu.pk

were particularly evaluated for their acidity due to contamination in the form of dissolved metal contents.

Materials and Methods

Location and geology of the study area. Water samples were collected from different sources in and around of Hassan Kishor Coal Mine situated in Basharat area which is 17 km north-east of Choa Saiden Shah and 40 km south-east of Chakwal (Fig. 1). The stratigraphic sequence of the area is given in the Fig. 2.

Sample collection. Total eleven water samples were collected in pre-cleaned air tight bottles washed by nitric acid prior to sampling from different sources including mine inflows (I1 and I2), mine outflows (O1, O2, O3), groundwater outlets (G1, G2) and surface flows (S1, S2, S3) and labeled as shown in Fig. 3.

Each sample from a particular source was collected from different locations. I1 and I2 were collected from two different points within the mine, while I3 was sampled from a little inrush of water in the midway of the main incline. O1, O2 and O3 were collected from

Fig. 1. Location map of Hassan Kishor Coal Mine. (www.maps.google.com).

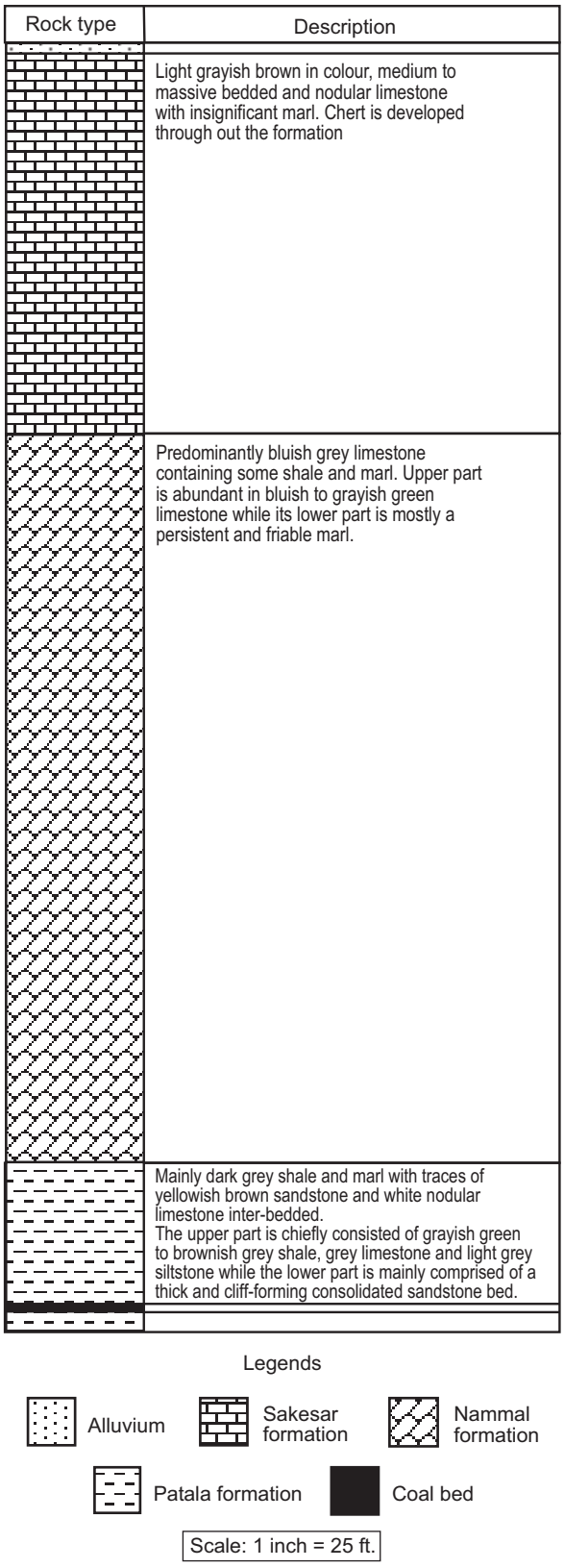

Fig. 2. Stratigraphic sequence of the study area (Ibrahim, 2009).

Fig. 3. Water samples collected from Basharat area near Hassan Kishor Coal Mine.

sump-1 situated down the main incline, discharged water by pump and sump-2 located in midway of the incline, respectively. G1 was collected from a well nearby the mine portal while G2 was sampled from a well far away from mine. S1, S2 and S3 were collected from three different surface sources located in different directions to the mine. In order to find out the potential of coal to pollute water, a sample C1 was prepared in the laboratory by adding 7 liter distilled water in 2 kg crushed coal having particle size less than 4 mm. The mixture was allowed for 24 h and then the polluted water was filtrated through a 150 micron sieve to get the desired water sample.

Methodology. Colour of all water samples was noted before and after exposure of 24 h to fresh air to get an idea of oxidation (Fig. 4).

Mercury thermometer calibrated in degree Celsius was used to measure temperature of the water samples on-site. pH and turbidity (haziness of a fluid due to invisible suspended particles) of all samples were measured by using ELE pH meter and ELE turbidity meter, respectively. The Lovibond SesnsoDirect Con200 electrical conductivity meter was used to determine the electrical conductivity of water samples in µS and mS (micro and milli Siemens). Total solid (TS) and total dissolved solids (TDS) were determined by using conventional heating methods. ELE Paqualab Photometer was utilized to find out concentrations of metals such as calcium, magnesium, zinc, and copper as well as sulphate ions.

Iron concentration was estimated indirectly by using following stoichiometric relation (Younger *et al*., 2002)

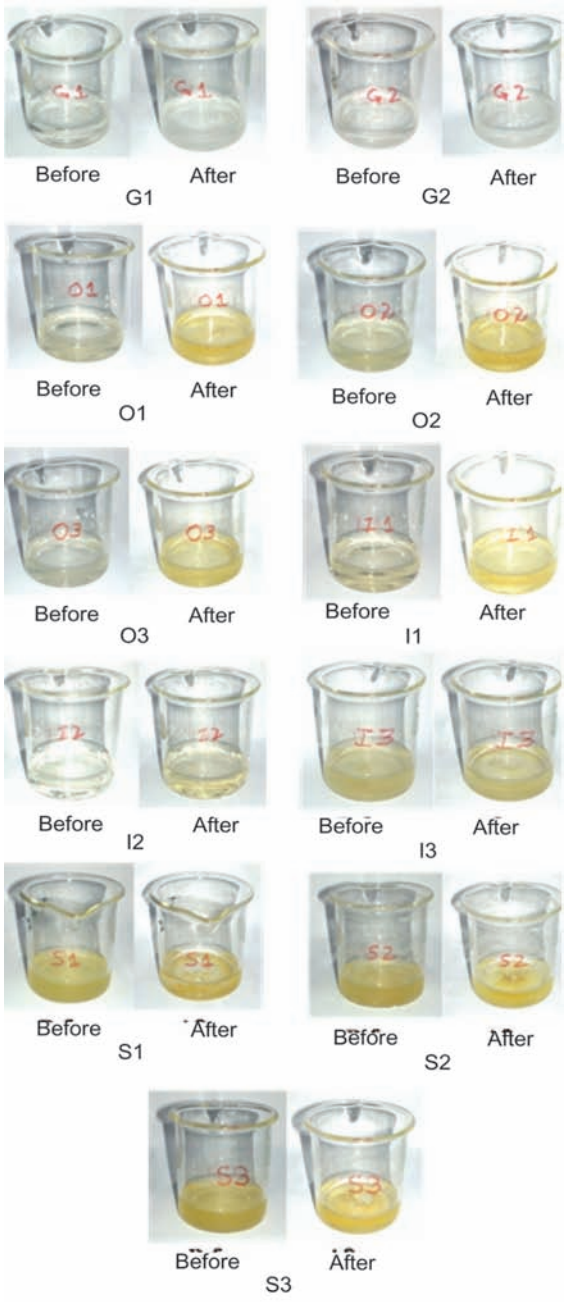

Fig. 4. Colour of the water samples before and after one day exposure to fresh air.

assuming that pyrite content (FeS_2) is the only source of sulphate and iron ion production in coal mines.

$$2FeS_2(s) + 7O_2 + 2H_2O \rightarrow 2Fe^{+2} + 4SO_4^{-2} + 4H^+$$

Results and Discussion

Groundwater samples showed a slight increase in turbidity while a dramatic increase in turbidity was

Table 1. Characteristics of water samples collected from in and around the vicinity of Hassan Kishor coal mine

Sample	Temperature	pH	Conductivity	Turbidity	Concentrations (mg/L)							
limit**	(°C) (on-site)	6-9	(mS)	(ftu)	Total solids	TDS	Ca	Mg	Fe*	Zn	Cu	SO_4^{2-}
	---		---	5	(200***+3500)	3500	--	--	8.0	5.0	1.0	600
G1	16	6.35	7.72	1.151	530	460	153	1.0	60	0.00	1.28	207
G2	16	6.46	7.33	1.152	760	530	415	7.0	60	0.00	0.72	207
O1	21	2.23	66	4.85	6530	5130	14	12.5	63	0.11	11.75	215
O2	21	2.31	67	4.77	6800	4500	14	5.0	60	0.06	11.75	207
O3	21	2.31	71	4.7	5730	5000	0	0	63	0.08	10.53	215
I1	23	2.27	20.37	5.12	5060	4500	56	0	63	0.03	10.53	215
I2	23	2.32	6.64	5.29	6130	4500	56	0	63	0.01	10.53	215
I3	17	6.29	403	0.882	830	460	0	6.0	74	0.50	4.48	254
S1	19	2.36	396	2.76	3260	2200	0	5.0	80	0.97	7.58	267
S2	19	2.34	493	2.82	3200	2460	0	7.0	74	1.13	6.91	254
S3	19	2.43	592	2.87	3530	1730	0	10.0	74	0.86	7.22	254
C1	22	5.63	412	1.039	2630	860	0	12.5	88	0.03	11.75	302

* = iron concentration is calculated from sulphate ion concentrations by using stoichiometric relation assuming that pyrite is the only source of iron and sulphate ions; ** = after national environmental quality standards (NEQS, 1997); *** = total suspended solid limit.

observed for the samples of mine outflows, surface water and mine inflows. All samples except groundwater showed yellow coloured precipitates after exposure of 24 h to fresh air. The yellowish colour of water is likely due to the formation of iron hydroxide [$Fe(OH)_3$], which is commonly found in the water bodies near coal mining areas. Generally, when iron is introduced into the natural water, it becomes hydrolysed and forms precipitate of iron hydroxide. Iron in coal mines normally results from pyrite contents in the coal (Sewer and Singh, 2004).

The results of temperature, pH, turbidity, total solids, total dissolved solids, and metal, and sulphate concentrations are shown in the Table 1. pH values of the water samples vary between 2.27 and 6.46. All samples except that of groundwater showed low pH values which indicate acidity of the water. This water may flow to rivers or streams where it can be hazardous to aquatic life since it facilitates leaching of toxic metals into the water (Sewer and Singh, 2004). Moreover, high acidity limits the amount of nutrients in the water which usually are required for vegetation (Ezeigbo and Ezeanyim, 1993).

The analysis of mine outflows and inflows revealed higher total solid (TS) and total dissolved solid (TDS) beyond the standard limits (NEQS, 1997). These solid materials may be present in the form of insoluble suspended mineral particles and soluble ions of metals and sulphate. The suspended particles are harmful for aquatic life as they reduce the availability of light and dissolved oxygen in water which is necessary for photosynthesis.

Although sulphate ions in all water samples are found to be within limits which vary between 207 and 302 mg/L, they may combine with water to form sulphuric acid or can attach to calcium ions to form gypsum sludge. Copper and iron concentrations vary from 0.72 to 11.75 mg/L and 60 to 88 mg/L, respectively. These concentrations are very high which are responsible for acidity of water. Concentration of calcium, magnesium and zinc vary from 0 to 415, 0 to 12.5 and 0 to 1.13 mg/L, respectively. Higher concentration of calcium and magnesium are the root causes of water hardness which may affect health of living bodies if used for drinking purposes.

Conclusion

Most of the water samples were found to be severely affected by impurities. These impurities appeared in the form of suspended and dissolved solids. Elevated concentrations of iron, copper and sulphate in most of the water samples had caused considerable reduction in pH value of water making it highly acidic. However, it was found that groundwater was not much affected yet as it showed the pH value in the prescribed safe limits (6-9). It was concluded that geological formations such as limestone present in the study area is natural treatment process of the mine discharged water. This

was confirmed by the presence of large amount of calcium ions and relatively low concentrations of iron, copper and sulphate ions in the groundwater samples. Moreover, characteristics of the water extracted from coal samples in the laboratory clearly revealed that the coal seam had fair tendency to produce acid mine water.

References

Banks, D., Younger, P.L., Arnesen, R.T., Iversen, E.R., Banks, S.B. 1997. Mine-Water Chemistry: the Good, the Bad and the Ugly. *Environmental Geology*, **32:** 157-174.

Dold, B., Fontbote, L. 2001. Element cycling and secondary mineralogy in porphyry copper tailings as a function of climate, primary mineralogy and mineral processing. *Journal of Geochemical Exploration*, **74:** 3-55.

Ezeigbo, H.I., Ezeanyim, B.N. 1993. Environmental pollution from coal mining activities in the Enugu area Anambka State Nigeria. *Mine Water and the Environment*, **12:** 53-61.

Gomes, C.J., Mendes, C.A.B., Costa, J.F.C.L. 2011. The enviroenmental impacts of coal mining: A case study in Brazil's Sangao Watershed. *Mine Water and the Environment*, **30:** 159-168.

Ibrahim, S.M. 2009. *Stratigraphy of Pakistan*, pp. 25-39, Geological Survey of Pakistan.

Kumar, U., Kakrani, B. 2000. *Water Environment and Pollution*, Agrobios Publisher, Jodhpur India.

Monjezi, M., Shahriar, K., Dehghani, H., Namin, F.S. 2009. Environmental impact assessment of open pit mining in Iran. *Environmental Geology*, **58:** 205-216.

NEQS, 1997. *Pakistan Environmental Legislation and The National Environmental Quality Standards*, pp. 1-7, Government of Pakistan, October 1997.

Powell, J.D. 1988. Origin and influence of coal mine drainage on streams of the United States. *Environmental Geology and Water Sciences*, **11:** 141-152.

Singh, A.K., Mahato, M.K., Neogi, B., Mondal, G.C., Singh, T.B. 2011. Hydrogeochemistry, elemental flux, and quality assessment of mine water in the Pootkee-Balihari mining area, Jharia coalfield, India. *Mine Water and the Environment*, **30:** 197-207.

Singh, G. 2008. Environmental Impact Assessment of Mining Projects. In: *Proceedings of International Conference on TREIA-2008* at Nagpur, Nov. 23-25.

Skousen, J., Rose, A., Geidel, G., Foreman, J., Evans, R., Hellier, W. 1998. *Handbook of Technologies for Avoidance and Remediation of Acid Mine Drainage*, 1st edition, Morgantown, WV: National Mine Land Reclamation Center, West Virginia, Virginia University, Virginia, USA, June 1, 1998.

Swer, S., Singh, O.P. 2004. Status of Water Quality in Coal Mining Areas of Meghalaya, India. In: *Proceedings of the National Seminar on Environmental Engineering with Special Emphasis on Mining Environment*, March, 19-20.

Tiwary, R.K. 2000. Environmental impact of coal mining on water regime and its management. *Water, Air and Soil Pollution*, **132:** 185-199.

www.maps.google.com

Younger, P.L., Sapsford, D.J. 2004. *Evaluating the Potential Impact of Opencast Coal Mining on Water Quality (Groundwater Regulations 1998): An Assessment Framework for Scotland*, Newcastle University, Newcastle upon Tyne: Scottish Environment Protection Agency (SEPA).

Younger, P.L., Banwart, S.A., Hedin, R.S. 2002. Mine Water: Hydrology, Pollution, Remediation. In: *Environmental Pollution*, B. J. Alloway and J. T. Trevors (eds.), vol. **5,** 1st edition, Kluwer Academic Publishers, Dordrecht, The Netherlands.

Zaihua, L., Daoxian, Y., Zhaoli, S. 1991. Effect of coal mine waters of variable pH on spring-water quality: A case study. *Environmental Geology and Water Sciences*, **17:** 219-225.

Pak. j. sci. ind. res. Ser. A: phys. sci. 2015 **58** (1) 46-50

Characterisation and Identification of Taraxerol and Taraxer-14-en-3-one from *Jatropha tanjorensis* (Ellis and Saroja) Leaves

Sunday Olusegun Oladoye*, Ezekiel Temidayo Ayodele, Misbaudeen Abdul-Hammed and Olajumoke Tolulope Idowu

Department of Pure and Applied Chemistry, Ladoke Akintola University of Technology, P.M.B. 4000, Ogbomoso, Oyo State, Nigeria

(received September 3, 2013; revised January 31, 2014; accepted February 12, 2014)

Abstract. *Jatropha tanjorensis* leaves were collected, air dried and pulverised. The pulverised sample was extracted with solvents (*n*-hexane, ethylacetate and ethanol) of varying polarity to obtain the crude extracts. Repeated column and thin layer chromatographic separation of the crude extracts afforded two compounds which were characterised by their IR, MS, ^{1}H and ^{13}C-NMR spectral data. Comparison of the data with literature confirmed the compounds to be taraxerol and taraxer-14-en-3-one.

Keywords: *Jatropha tanjorensis*, taraxerol, taraxer-14-en-3-one, chromatography

Introduction

Jatropha tanjorensis is a plant in the Euphorbiaceae family. It is a perennial herb which is a hybrid specie with phenotypic character between *Jatropha curcas* and *Jatropha gossypifolia* (Prabakan and Sujatha, 1999). The plant is widely cultivated in Nigeria primarily for fencing, as a source of leafy vegetable and for medicinal purpose (Oboh and Masodje, 2009; O'Hara *et al*., 1998).

The leaf extract of the plant is employed traditionally in the treatment of anaemia, diabetes and cardiovascular diseases (Iwalewa *et al*., 2005; Olayiwola *et al*., 2004). Studies have been carried out to validate these claims of the traditional uses. The leaf extract has been shown to have hypoglycaemic properties (Olayiwola *et al*., 2004).

The antioxidant potential of the plant leaf has also been a subject of several studies (Atansuyi *et al*., 2012; Omobuwajo *et al*., 2011; Omoregie and Osagie, 2011) and all these studies confirmed the antioxidant properties of this plant. Toxicity studies have also been carried out on the leaf extract of *J. tanjorensis* with animal models, to ascertain its safety while, some of the studies suggest that it may not be safe (Oyewole *et al*., 2012; Ogoruvwe and Kori-Siakpere, 2012; Igbinaduwa *et al*., 2011; Akhigbe *et al*., 2009). Others suggested, it is safe for human consumption (Omobuwajo *et al*., 2011; Orhue *et al*., 2008).

*Author for correspondence; E-mail: oluoladoye@yahoo.co.uk

The antimicrobial potential of this plant has also been evaluated in several studies (Arun *et al*., 2012; Viswanathan *et al*., 2012; Sekaran, 1998) and the results showed excellent broad spectrum antimicrobial activity against the tested organisms.

Phytochemical analysis of the leaf extract revealed the presence of saponins, cardiac glycosides, flavonoids, terpenoids and tannins (Oyewole and Akingbala, 2011). However, except for the recent work of Viswanathan *et al*. (2012) who reported the isolation of friedelin, β-amyrin, stigmasterol and R(+)-4-hydroxyl-2-pyrrolidinone from the leaf extract of *J. tanjorensis*, there has been no other report in the literature on isolation and characterisation of the phytochemical constituents of this plant. Hence, this study was taken for isolation and characterisation of two terpenoid compounds, taraxerol and taraxer-14-en-3-one, from this plant.

Materials and Methods

Plant material. Fresh leaves of *J. tanjorensis* were collected in the month of April 2012 from Ladoke Akintola University of Technology (LAUTECH.), Ogbomoso, Nigeria. Identification was done in the Department of Pure and Applied Biology, LAUTECH. Harvesting was done with hands properly protected with glove to avoid contact with the milky sap of the plant which causes irritation and itching on contact with the skin.

Sample preparation. The leaves were air dried at room temperature for about two months. Thereafter, the dried leaves were pulverised.

Extraction and isolation. Pulverised sample 755 g was successively extracted with three solvents of varying polarity (*n*-hexane, ethylacetate and methanol), at room temperature (Taylor *et al*., 1983).

The crude *n*-hexane extract (13 g) was subjected to silica gel column chromatography and the column eluted with either one or a mixture of two of *n*-hexane, ethylacetate and methanol. Elution was done by gradually increasing the polarity of the solvent system starting with 100% *n*-hexane. The eluents were collected in fractions of 200 mL each. A total of 50 fractions were collected and analysed by thin layer chromatography, fractions with similar TLC profile were pooled together and concentrated to dryness *in vacuo*. Rechromatography of fraction 21 gave compound 1 (100 mg) as a white crystalline solid.

Fractions 24 to 29 were combined and rechromatographed using the solvent system as stated above and fractions collected at 15 mL interval, compound 2 (65 mg) crystallised out of fraction 10 of this column.

Melting points were determined on a Kofler apparatus and are uncorrected. IR spectra were recorded by using a Thermo Nicolet 5700 FT-IR spectrometer, in $CHCl_3$. ^1H and ^{13}C NMR spectra were recorded in $CDCl_3$ on an Agilent DD2 400 NMR spectrometer at 400 MHz and 100 MHz, respectively. The chemical shifts as δ-values are reported in parts per million (ppm) relative to teteramethylsilane (TMS, δ=0) as internal standard.

The positive and negative ion high resolution ESI mass spectra were obtained from a Bruker Apex III Fourier transform ion cyclotron resonance (FT-ICR) mass spectrometer (Bruker Daltonics, Billerica, USA) equipped with an infinity cell, a 7.0 Tesla superconducting magnet (Bruker, Karlsruhe, Germany), an RF-only hexapole ion guide and an external electrospray ion source (Agilent, off axis spray). Nitrogen was used as drying gas at 150 °C. The sample solutions were introduced continuously via a syringe pump with a flow rate of 120 μL/h. The data were acquired with 512 k data points; zero filled to 2048 k by averaging 16 scans and evaluated using the Bruker XMASS software (Version 7.0.8).

The electrospray (ESI) mass spectra were performed on a SCIEX API-3200 instrument (Applied Biosystems, Concord, Ontario, Canada) combined with a HTC-XT autosampler (CTC Analytics, Zwingen, Switzerland). The samples were introduced via auto sampler and loop injection. All solvents used for extraction and column chromatography were General Purpose Reagent (GPR), redistilled before use. Column chromatography was carried out on Merck Si gel 60, while thin layer chromatography (TLC) were done with aluminium sheet pre coated with normal phase silica gel 60 F254 (Merck, 0.20 mm thickness). The TLC was run using suitable solvent systems. Spots were located on the developed TLC plates by visualisation under ultraviolet light at 254 and 366 nm.

Results and Discussion

There are few reports on the isolation and characterisation of the phytochemical constituents of *J. tanjorensis*, however, a recent study reported the isolation of friedelin, B-amyrin, stigmasterol and R-(+)-4-hydroxyl-2-pyrrolidinone from the leaf extract of the plant (Viswanathan *et al*., 2012). These phytoconstituents present in the methanol extract were suggested to be responsible for the broad spectrum antimicrobial activity of the plant. Now, two compounds are isolated and reported in this work.

The infra red spectrum of compound 1 (Fig. 1) (m.p 238-240 °C) revealed absorptions at 3048.7 cm^{-1} and 3007.7 cm^{-1} due to =C–H of alkene, 2956.7, 2913.8 and 2847.9 cm^{-1} due to C–H stretch of alkane; 1706 cm^{-1} due C=O strectching vibration and at 1471, 1461 and 1447 cm^{-1} as a result of the bending vibrations of =C–H. The ESI MS of the compound gave its molecular mass as 424 corresponding to the molecular formula $C_{30}H_{48}O$. The mass spectrum of the compound showed intense peaks at m/z 300, 285 and 204. Table 1 showing the ^1H

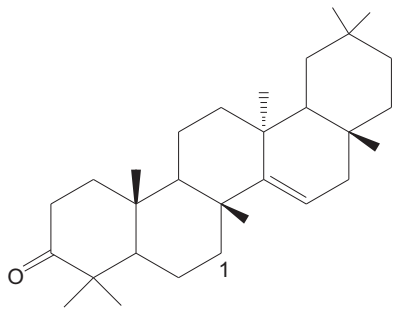

Fig. 1. Structure of Taraxer-14-en-3-one.

Table 1. ^{1}H and ^{13}C NMR data for compound 1

Position	δC (ppm)	C type	δH(ppm)
1	38.3	CH_2	1.90; 1.60
2	34.1	CH_2	2.60 ; 2.36
3	217.5	C=O	-
4	47.6	C	-
5	55.8	CH	1.90
6	19.9	CH_2	1.75 ; 1.60
7	35.1	CH_2	1.70 ; 1.60
8	38.9	C	-
9	48.7	CH	1.70
10	35.8	C	-
11	17.4	CH_2	1.70 ; 1.60
12	37.68	CH_2	1.70; 1.60
13	37.72	C	-
14	157.6	C=	-
15	117.2	HC=	5.57
16	36.6	CH_2	2.10 ; 1.85
17	37.5	C	-
18	48.8	CH	1.70
19	40.6	CH_2	1.70; 1.50
20	28.8	C	-
21	33.6	CH_2	1.75; 1.60
22	33.1	CH_2	1.75 ; 1.60
23	26.1	CH_3	0.99
24	21.5	CH_3	0.99
25	14.8	CH_3	1.03
26	29.9	CH_3	1.14
27	25.6	CH_3	1.14
28	29.8	CH_3	1.03
29	33.3	CH_3	0.83
30	21.3	CH_3	0.83

and ^{13}C-NMR spectra data for compound 1, the ^{1}H NMR spectrum shows a double doublet of an olefinic proton at δ5.57 ppm among other signals confirming the olefinic double bond while the ^{13}C-NMR confirms a total of thirty carbon atoms, eight of which are methyl carbons, ten methylene carbons, four methine carbons and eight quartenary carbons including carbonyl at δ217.5 ppm and the unsaturated carbon atoms at δ157.6 and 117.2 ppm.

The Infra red spectra of compound 2 (Fig. 2) (M.pt 277–280 °C) revealed, among others, a broad absorption band centred at 3843.0 cm^{-1} due to O-H stretching vibration, absorptions at 3052.6 cm^{-1} due to =C-H stretching vibration, absorptions at 2914.0 and 2848.0 cm^{-1} due to C-H stretching vibration of alkanes and at 1641 cm^{-1} due to C=C stretching vibrations. The ESI MS of the compound gave a molecular mass of 426 corresponding

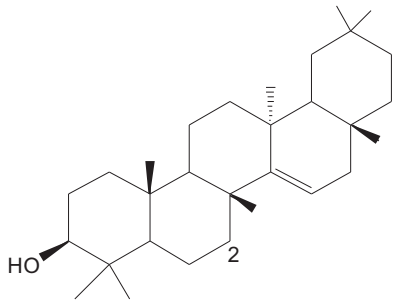

Fig. 2. Structure of Taraxerol.

Table 2. ^{1}H and ^{13}C NMR data for compound 2

Position	δC (ppm)	C type	δH (ppm)
1	37.7	CH_2	1.60; 1.15
2	27.2	CH_2	1.60; 1.40
3	79.1	C—OH	3.2, 3.6
4	39.0s	C	-
5	55.5	CH	1.40
6	18.8	CH_2	1.60; 1.15
7	35.1	CH_2	1.95; 1.60
8	38.8	C	-
9	48.8	CH	1.40
10	35.8	C	-
11	17.5	CH_2	1.15
12	37.7	CH_2	1.15
13	37.6	C	-
14	158.1	C=	-
15	116.9	HC=	5.5
16	36.7	CH_2	2.01; 1.95
17	38.0	C	-
18	49.3	CH	1.40
19	41.3	CH_2	1.15
20	28.8	C	-
21	33.7	CH_2	1.15
22	33.1	CH_2	1.15
23	28.0	CH_3	0.82
24	15.44	CH_3	0.82
25	15.4	CH_3	0.99
26	29.9	CH_3	1.10
27	25.9	CH_3	1.10
28	29.8	CH_3	0.99
29	33.3	CH_3	0.82
30	21.3	CH_3	0.82

to a molecular formula of $C_{30}H_{50}O$. The mass spectrum of the compound also showed intense peaks at m/z 302 and 204. The ^{1}H NMR of compound 2 confirmed the presence of OH group in the compound through the double doublet centred at δ3.20 ppm, the methylene group is also confirmed through the double doublet at δ5.50 ppm. The ^{13}C NMR spectrum revealed a total of thirty carbon atoms distributed as follows: 8 methyl, 10 methylene, 5 methine and 7 quartenary carbons as presented in Table 2. The spectra characteristics of these compounds confirm compound 1 to be taraxer-14-en-3-one while compound 2 as taraxerol. These interpretations are in excellent agreement with the literature data for these compounds isolated and characterised from *Myrica rubra* and *Euphorbia pubescens* (Valente *et al*., 2004; Sakurai *et al*., 1987).

Acknowledgement

The support of Ladoke Akintola University of Technology, Ogbomoso, Nigeria through Senate Research Grant is appreciated. The Authors are also grateful to Prof. Dr. Ludger Wessjohann and Dr. Katrin Franke of Leibnitz Institute of Plant Biochemistry, Halle- Saale, Germany for measurement of the spectroscopic data of the compounds.

References

Akhigbe, A.O., Idu, M., Orhue, E.S., Ataman, J.E., Ehimwenman, S.O. 2009. Effect of *Jatropha tanjorensis* J.I. Ellis and Soroja leaves in rabbits: Biochemistry and ultrasonography. *Research Journal of Medicinal Plant*, **3:** 29-33.

Arun, K.P., Ravichandran, N., Vajrai, R., Brindha, P. 2012. Studies on micromorphological standardization, antimicrobial efficacy and nutritional values of *Jatropha tanjorensis*. *International Journal of Pharmacy and Pharmaceutical Sciences*, **4:** 139-142.

Atansuyi, K., Ibukun, E.O., Ogunmoyole, T. 2012. Antioxidant properties of free and bound phenolic extract of the leaves of *Jatropha tanjorensis in vitro*. *Journal of Medicinal plants Research*, **6:** 4667-4674.

Igbinaduwa, P.O., Usifoh, C.O., Ugwu C.C. 2011. Phytochemical analysis and toxicological evaluation of the methanolic extract of *Jatropha tanjorensis* leaf. *Journal of Pharmacy & Bioresources*, **8:** 86-91.

Iwalewa, E.O., Adewunmi, C.O., Omisore, N.O.A., Adebanji, O.A., Azike, C.K., Adigun, A.O., Olowoyo, O.G. 2005. Pro- and antioxidant effects and cytoprotective potentials of nine edible vegetables in South West. *Journal of Medicinal Food*, **8:** 539-544.

O'Hara, M.D., Kiefer, K., Farrell, T., Kemper, K. 1998. A review of twelve commonly used medicinal herbs. *Archives of Family Medicine*, **7:** 523-536.

Oboh, F.O.J., Masodje, H.I. 2009. Nutritional and antimicrobial properties of *Jatropha tanjorensis* leaves. *American-Eurasian Journal of Scientific Research*, **4:** 7-10.

Ogoruvwe, O.J., Kori-Siakpere, O. 2012. Alterations in the activities of the nitrogenous waste of *Clarias Gariepinus* after intramuscular injection with aqueous extracts of *Jatropha tanjorensis* leaves. *Journal of Pharmacy and Biological Sciences*, **2:** 35-38.

Olayiwola, G., Iwalewa, E.O., Omobuwajo, O.R., Adeniyi, A.A., Verspohl, E.J. 2004. The antidiabetic potential of *Jatropha tanjorensis* leaves. *Nigerian Journal of Natural Products and Medicine*, **8:** 55-58.

Omobuwajo, O.R., Alade, G.O., Akanmu, M.A., Obuotor, E.M., Osasan, S.A. 2011. Microscopic and toxicity studies on the leaves of *Jatropha tanjorensis*. *African Journal of Pharmacy and Pharmacology*, **5:** 12-17.

Omoregie, E.S., Osagie, A.U. 2011. Effect of *Jatropha tanjorensis* leaves supplement on the activities of some antioxidant enzymes, vitamins and lipid peroxidation in rats. *Journal of Food Biochemistry*, **2:** 409-424.

Orhue, E.S., Idu, M., Ataman, J.E., Ebite, L.E. 2008. Haematological and histopathological studies of *Jatropha tanjorensis* (Ellis and Soroja) leaves in rabbits. *Asian Journal of Biological Sciences*, **1:** 84-89.

Oyewole, O.I., Oladipupo, O.T., Atoyebi, B.V. 2012. Assessment of renal and hepatic functions in rats administered methanolic leaf extract of *Jatropha tanjorensis*. *Annals of Biological Research*, **3:** 837-841.

Oyewole, O.I., Akingbala, P.F. 2011. Phytochemical analysis and hypolipidemic properties of *Jatropha tanjorensis* leaf extract. *European Journal of Medicinal Plants*, **1:** 180-185.

Prabakan, A.J., Sujatha, M. 1999. *Jatropha tanjorensis*, Ellis and Soroja, a natural interspecific hybrid occurring in Tamil Nadu, India. *Genetic Resources and Crop Evolution*, **46:** 213-218.

Sakurai, N., Yaguchi, Y., Inoue, T. 1987. Triterpenoids from *Myrica rubra*. *Phytochemistry*, **26:** 217-219.

Sekaran, R. 1998. Antimicrobial action of the leaf extract of *Jatropha tanjorensis*. *Ancient Science of Life*, **18:** 50-51.

Taylor, M.D., Smith III, A.B., Furst, G.T., Gunasekara, S.P., Bevelle, C.A., Cordell, G.A., Farnsworth, N.R., Kupchan, S.M., Uchida, H., Branfman, A.R., Dailey Jr., R.G., Sneden, A.T. 1983. New anti-leukemic Jatrophone derivatives from *Jatropha gossypiifolia*: Structural and stereochemical assignment through nuclear magnetic resonance spectroscopy. *Journal of American Chemical Society*, **105:** 3177-3183.

Valente, C., Pedro, M., Duarte, A., Nascimento, M.S.J., Abreu, P.M., Ferreira, M.J.U. 2004. Bioactive diterpenoids: A new jatrophane and two ent-abietanes, and other constituents from *Euphorbia pubescens*. *Journal of Natural Products*, **67:** 902-904.

Viswanathan, M.B., Jeya Ananthi, J.D., Sathish-Kumar, P. 2012. Antimicrobial activity of bioactive compounds and leaf extracts in *Jatropha tanjorensis*. *Fitoterapia*, **83:** 1153-1159.

Pak. j. sci. ind. res. Ser. A: phys. sci. 2015 **58** (1) 51-58

Environmental Impact Assessment of Trace Metal Deposition Around the Petrol Filling Stations

Durdana Rais Hashmi*, Akhtar Shareef, Farooq Ahmad Khan and Alia Bano Munshi
Centre for Environmental Studies, PCSIR Laboratories Complex, Karachi-75280, Pakistan

(received October 3, 2013; revised February 26, 2014; accepted March 11, 2014)

Abstract. The wide use of petroleum products causes contamination of air, water, soil and plants. The present study was conducted to monitor the trace metal deposition in road side soil around the petrol filling stations along the busy roads of Karachi, Pakistan. Total 21 road side soil samples were collected from selected locations of busy roads. The soil samples were digested using acid digestion method and atomic absorption spectrophotometer (AAS) was used for the elemental analysis. Results of the study showed that concentration of lead was highest in the soil samples ranging from 41.3 to 361 mg/kg, then copper from 23.0 to 101 mg/kg, manganese from 36.2 to 125.0 mg/kg and zinc from 27.5 to 213.0 mg/kg, respectively. The correlation-coefficient (r) was also calculated between the metals in soil samples. The correlation matrix showed that all the pollution is coming from the same source. The gravitational sedimentation and impact on vegetation of coarse fraction is responsible for the high lead contamination of vegetation and soils. Collected data showed that, almost all the pollution being generated by automobile exhaust in urban areas of Karachi. The soil acts as an important sink for pollutants released through different activities.

Keywords: petrol filling stations, trace metals, soil, vehicular traffic, acid digestion

Introduction

Air pollution has become a serious environmental issue, mainly due to the presence of toxic trace metals in the atmosphere as a consequence of rapid industrialisation and increased transportation during recent years. Pollution of soils by trace metals is a serious environmental issue. Determination of the trace metal contents of various environmental materials such as soil, natural water, plants, dust etc., have been performed by various researchers (Malakotian *et al.,* 2009; Vinodhini and Narayanan, 2009; Kalantari and Ghaffari, 2008; Karabassi *et al.,* 2008; Itoh *et al.,* 2006; Krolak, 2000; Soylak *et al.,* 2000).

Trace metals have been added into urban soils through urban waste, chemical industries (Chaoyang *et al.,* 2009) and most importantly through the vehicular emission (Xia *et al.,* 2011). The urban road side soil has been recognised as an important repository of trace metals.

Environmental measurements revealed the higher concentrations of metals in road side soil near the petrol filling stations, and most of the signs could be attributed due to petrol fumes (Das *et al.,* 1991). Lead, copper, manganese and zinc are the major metal pollutants of the roadside environment and are released during different operations of the road transport such as combustion, component wear, fluid leakage and corrosion of the metals. Lead is one of the most important trace metals in Pakistani environment because of the extensive use of lead tetraethyl as gasoline additive, since early years of the 20th century until 2005, when this compound was prohibited and the unleaded petroleum introduced. According to Fernandez and Ramirez (2002), the concentration of lead in solid particles from roads of the city of Caracase ranged between 5.500 to 13.000 µg/g, respectively. Carrasquero (2006) reported the levels of lead from 2.000 to 4.000 µg/g in urban soils near the most transited streets and avenues.

Majority of the trace metals are toxic to the living organisms, and can impair important biochemical processes posing a threat to human health, plant growth and animal life (Silva *et al.,* 2005; Jarup, 2003; Michlake, 2003).

Zinc is a trace element that is essential for human health. When people absorb too little quantity of zinc they can experience a loss of appetite, decreased sense of taste and smell, slow wound healing and skin sores. Zinc-shortage can even cause birth defects. Although humans can handle proportionally large concentrations of zinc, too much zinc can still cause eminent health problems, such as stomach cramps, skin irritations, vomiting, nausea and anemia. Very high levels of zinc can damage the pancreas and disturb the protein metabolism, and cause arteriosclerosis. Extensive exposure to zinc can cause respiratory disorders.

*Author for correspondence; E-mail: drhpak@yahoo.com

In the work place environment, zinc contagion can lead to a flu-like condition known as metal fever. Zinc can be a danger to unborn and newborn children (Hussein *et al.,* 2012). Similarly, higher concentration of Pb, Cu and Mn can cause serious health issues in human beings.

Long-term exposure to copper can cause irritation of the nose, mouth and eyes and it causes headaches, stomachaches, dizziness, vomiting and diarrhoea. Intentionally high uptakes of copper may cause liver and kidney damage and even death. Industrial exposure of copper fumes, dusts, or mists may result in metal fume fever with atrophic changes in nasal mucous membranes. Chronic copper poisoning results in Wilson's disease (Araya *et al.,* 2008).

Manganese effects occur mainly in the respiratory tract and in the brain. Symptoms of manganese poisoning are hallucinations, forgetfulness and nerve damage. Manganese can also cause Parkinson, lung embolism and bronchitis. When men are exposed to manganese for a longer period of time they may become impotent. A syndrome that is caused by manganese has symptoms such as schizophrenia, dullness, weak muscles, headaches and insomnia. Chronic manganese poisoning may result from prolonged inhalation of dust and fume. The central nervous system is the chief site of damage from the disease, which may result in permanent disability. Symptoms include languor, sleepiness, weakness, emotional disturbances, spastic gait, recurring leg cramps, and paralysis (Nagatomo *et al.,* 1999).

Studies have shown that, such pollutants can be harmful to the road side vegetation, wildlife and the neighbouring human settlements (Turer and Mynard, 2003; Caselles, 1998; Ferretti *et al.,* 1995; Iqbal *et al.,* 1994; Ndiokwere, 1984; Khan and Frankland 1983). It is evident that the urban soil containing the trace metals poses a serious threat to the safety of the human life by ingestion and inhaling (Wei and Yang, 2010) and through the direct contact with the soil on the road sides contaminated by trace metal (Yang *et al.,* 2011; 2010). It links to effects on the skin and penetration into the body tissues also causing genetic modification and affected intelligence of young children (Sims, 1990).

Transportation sources contribute 60-70% of the total aerial burden in Karachi. Over the last 20 years, the number of motor vehicles has risen from 0.8 million to nearly 5 million; an average growth rate in excess of 14%. The highest rise was in two-stroke vehicles (1,751%), while diesel vehicle numbers were three times higher in 2005 than in 1980 (Colbeck *et al.,* 2010). The main source of lead pollution is the emissions from automobile exhausts. Airborne lead is typically present in vehicular exhaust emissions in the form of particles, which have diameter of less than 1 μm and therefore, may be transported to large distance in the atmosphere between one and 4 weeks lifetime depending on climatic factors. The current emission of lead from automobile exhausts is around 7000 tonnes annually. 10% of this level is fallen out as dust on road side and remaining in airborne until it is washed out of the air by rain or it can be removed by contact with vegetation or soil.

The world's petrol consumption is about 84.2 million barrels per day (in 2010). Only United States (North America) consumes 27 million barrels per day (27.3% of the world total), Asia consumes 29 million barrels per day whereas, Pakistan is the 36th biggest consumer of petrol (CIA, 2013).

Very little work has been carriedout in Karachi to assess the contribution of emission sources of trace metals to the total aerial burden and their accumulation in road side soils due to petrol filling stations of the city.

The aim of this study is to determine the concentrations of airborne trace metals lead (Pb), copper (Cu), manganese (Mn) and zinc (Zn) near the petrol filling stations as indicators of the impact produced by the emission of vehicles. This information will be useful to evaluate the potential risk on the habitants of this city.

Materials and Methods

Sampling. For collection of soil samples, 21 locations were selected on the main roads, round abouts and open places near petrol filling stations along the busy roads of Karachi. Table 1 indicating the sampling points along with sample code, Global positioning system (GPS location) and local locations. Soil samples were collected from a depth between 5-10 cm (Marjanovic *et al.,* 2009; Gadkari and Pervez, 2008). The samples were stored in polyethylene bags then treated and analysed separately. The samples were prepared and analysed by AAS for trace elements Pb, Cu, Mn and Zn, respectively.

Reagents. All the experiments were performed with analytical reagent grade chemicals. Distilled and de-ionised water was used for dilution and preparation of reagents and standards. Reference standards were prepared from BDH spectrosol AA standard (1000 mg/L).

Sample preparation. Samples were dried at 120 °C and homogenised, passed through 0.5 mm size sieve. One gram portion of prepared soil samples was gently refluxed

Table 1. Soil sample codes and their locations

Sample code	Local locations	GPS locations	
		Lat	Long
S-1	Shell Petrol Pump	24.9359	67.0727
S-2	PSO Petrol Pump	24.9368	67.0744
S-3	PSO Petrol Pump	24.9255	67.0656
S-4	PSO Petrol Pump	24.9018	67.0455
S-5	Shell Petrol Pump	24.9157	67.0626
S-6	PSO Petrol Pump	24.8923	67.0437
S-7	Shell Petrol Pump	24.8801	67.0389
S-8	PSO Petrol Pump	24.8786	67.0473
S-9	Shell Petrol Pump	24.8806	67.0436
S-10	Caltex Petrol Pump	24.8895	67.0364
S-11	Shell Petrol Pump	24.9179	67.0971
S-12	Caltex Petrol Pump	24.9034	67.0548
S-13	Shell Petrol Pump	24.8831	67.0500
S-14	PSO Petrol Pump	24.9109	67.0307
S-15	PSO Petrol Pump	24.9029	67.0024
S-16	Shell Petrol Pump	24.8918	66.9887
S-17	PSO Petrol Pump	24.8873	67.0330
S-18	Caltex Petrol Pump	24.8556	67.0385
S-19	Caltex Petrol Pump	24.8503	67.0303
CS-20	PSO Petrol Pump	24.9431	67.0952
CS-21	Shell Petrol Pump	24.9467	67.1392

with 2 M nitric acid for 30 min. After cooling the contents were filtered through Whatman 42 into a graduated 50 mL flask and diluted up to the mark. All the glasswares were extensively soaked in diluted HNO_3 and rinsed with double distilled water.

Apparatus. Analysis was performed on atomic absorption spectrophotometer (Hitachi Z-8000), with Zeeman effect background correction. The spectrophotometer was equipped with a graphite furnace, a microprocessor and a built in printer.

Metal analysis. Determination of Cu, Mn and Zn were carried out by flame atomic absorption spectrophotometer (FAAS) whereas Pb was carried out by electro-thermal atomic absorption spectrophotometer (ETAAS), employing the standard addition technique. Measurement was made by using the hollow cathode lamp for the metals Pb, Cu, Mn and Zn, respectively.

Triplicate readings were taken on each sample by AAS, and the mean values of each sample readings were used to calculate results. The working conditions and detection limits for the detected elements by atomic absorption spectrophotometer are presented in Table 2. Accuracy was also monitored by spike with Cu, Mn and Zn in the level of 1.0 mg/L each, whereas Pb in the level of 20 µg/L, respectively. Five soil samples were spiked with Pb, Cu, Mn and Zn to determine the recovery. The average recovery for each metal i. e., Pb, Cu, Mn, and Zn are also given in Table 2.

Results and Discussion

Statistical parameters pertaining to the soil samples for trace metals in the form of range, mean, median and standard deviation are presented in Table 3. Correlation coefficient matrix are also presented in Table 4. The average concentration of lead, copper, manganese and zinc for each of 21 locations is presented in Fig. 1. The level of all investigated ions in soil samples were found at mg/kg.

Figure 1 shows the mean values of total average concentration of lead, copper, manganese and zinc at selected locations in Karachi. The highest average concentration of lead was found to be 361 mg/kg at location S-17; whereas, the lowest concentration was recorded as 70 mg/kg near location S-19, respectively. The mean values

Table 2. Working condition for detected elements and the recovery of metals added to the soil samples by atomic absorption spectrophotometer

Parameters	Pb	Cu	Mn	Zn
Slit (nm)	1.3	1.3	1.3	1.3
Wave length (nm)	283.3	324.8	279.3	213.9
Drying temperature (°C)	80-120	-	-	-
Ashing temperature (°C)	400	-	-	-
Atomisation temperature (°C)	2000	2300	2300	2300
% Recovery of metal added	95.5%	99.6%	98.0%	97.2%

Table 3. Average metal concentration (mg/kg) in soil samples collected from road side near petrol filling stations in Karachi

Metal	Range (mg/kg)	Mean	Median
Pb	41.3 - 361.0	126.5	109.0
Cu	23.0 - 101.0	75.8	76.0
Mn	36.2 - 125.0	73.7	69.0
Zn	27.5 - 213.0	97.6	91.0

Table 4. Correlation coefficient in soil samples collected from petrol filling stations in Karachi

Metals	Pb	Cu	Mn	Zn
Pb	1.00	-	-	-
Cu	0.613	1.00	-	-
Mn	0.703	0.627	1.00	-
Zn	0.850	0.671	0.822	1.00

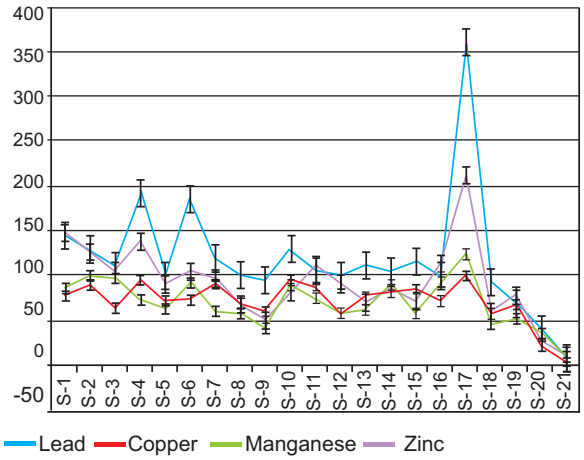

Fig. 1. Concentration of trace metals in soil samples near petrol filling stations.

of total average concentration of lead (Fig. 1) shows that, relatively high concentration of lead was found at locations S-4 (201 mg/kg), S-6 (187 mg/kg) and S-17 (361 mg/kg). These locations of road side filling stations are surrounded by high traffic density and there are several automobile workshops and large parking places for hundred of rickshaws near these filling stations. Moreover, during the period of survey, civil works for bridges was also under progress at these locations.

The lowest lead level at S-19 was found to be 70 mg/kg (Fig. 1). The low values obtained here may be because the location is relatively open place and situated at the intersection of very wide road having large round about. Lead has been found to be one of the major toxic elements generated through the motor vehicle exhaust using leaded gasoline. It is non degraded pollutant and it not only accumulates in the body but also modifies itself as it moves through biological cycles and food chain.

In the last decades, much attention has been directed towards lead in the road side environment as a result of its widespread use as an anti-knocking agent in gasoline (Turer and Mynard, 2003; Hafen and Brinkmann, 1996; Weheeler and Rolfe, 1979; Davis and Holmes, 1972). In the recent years, however, the lead content in gasoline markedly decreased after the introduction of the regulations requiring the reduction in the lead content from 0.64 g/L in 1966 to 0.14 g/L in 1986. This decrease has reduced the addition of lead to the environment by motor vehicles. However, the previously deposited lead remains a major contaminant of the road side environments. Although the lead content in gasoline is minimised these days, the increased traffic has caused an increase in the lead emission in the road side environment (Jones *et al.,* 1991).

Relatively high concentration of zinc was found at location S-1(149 mg/kg), S-4 (159 mg/kg) and S-17 (213 mg/kg), respectively. The maximum concentration of zinc in the soil was found to be 213 mg/kg, at location S-17 and lowest 51.0 mg/kg at location S-8 (Fig. 1). The highest concentration of zinc in soil at location S-17 may be due to the fact that this area is mostly surrounded by automobile workshops and has high traffic density. Most of the vehicles (60%) plying on the roads are using old and out dated imported tyres. These tyres are prone to tear off quickly as compared to new tyres and add more zinc in the soil as zinc is the component of tyres (Howard *et al.,* 1984). The average concentration of lead, copper, manganese and zinc are of the same order of magnitude. These metals are released during different operations of the road transport such as combustion, component wear, fluid leakage and corrosion of batteries and metallic parts such as radiators etc. (Dolan *et al.,* 2006).

Many studies on trace metal concentration in urban soil have been undertaken in various metropolitan cities (Table 5). Table 3 shows that, in the present studies, average concentration of Pb was recorded in the range of 41.3 to 361.0 mg/kg with mean value of

Table 5. Average metal concentration (mg/kg) in urban soils from different cities across the world

City	Pb	Cu	Mn	Zn	Reference
		(mg/kg)			
Galway	58.0	27.0	539.0	85.0	Zhang, 2006
Hong Kong	88.1	16.2	-	103.0	Celine *et al.,* 2006
Madrid	22.0	14.0	249.0	50.0	De-Miguel *et al.,* 2007
Hangzhou	46.2	36.6	415.3	116.1	Hasan *et al.,* 2008
Belgrade	298.6	46.3	417.6	174.2	Mirjanvi *et al.,* 2009
Yorkshire	25.0	15.5	-	56.7	Khalid *et al.,* 2006
Karachi	120.9	72.4	70.7	93.5	Present study

126.5 mg/kg which is higher than that reported from Galway 58.0 mg/kg (Zhang, 2006), Hong Kong 88.1 mg/kg (Celine, 2006), Madrid 22.0 mg/kg (De-Miguel *et al.,* 2007) and Hangzhou city 46.2 mg/kg (Hasan, 2008) and lower from Belgrade 298.6 mg/kg (Marjanovic *et al.,* 2009).

Concentration of Cu in different urban soil from various cities had been reported to be in the range 10-50 mg/kg. In the urban soil samples of Galway the concentration of Cu was 27 mg/kg, in Hong Kong 16.2 mg/kg, in Madrid 14 mg/kg, in Hangzhau 36.6 mg/kg and in Belgrade 46.3 mg/kg.

Average concentration of Cu in the soil samples recorded in the present study was 23.0 mg/kg (Table 3), which is higher than that reported from Hong Kong 16.2 mg/kg, Madrid 14 mg/kg and lower from the soil samples of other cities compared with whereas, the concentration of Mn in different urban soil samples is in the range of 250-550 mg/kg (Table 5). In the present study, the mean concentration of Mn is 73.7 mg/kg (Table 3), which is lower from all other cities compared in this study (Table 5) whereas, the concentration of Zn in this study was recorded in the range of 27.5-213.0 mg/kg with the mean value of 97.6 mg/kg Table 3 which is higher from Galway 85.0 mg/kg and Madrid 50.0 mg/kg and lower from Hangzhou 116.1 mg/kg, Hong Kong 103.0 mg/kg and Belgrade 174.2 mg/kg compared in this study (Table 5).

Location number SC-21 is located about 20 km away from the city centre in the down wind direction. This location was used as control site in this investigation. The highest concentration of lead found at selected locations was more than 50 times greater than the lead found at control site (Locations No: SC-21). The high increase in the concentration of lead at selected locations is due to very high number of vehicles plying at the intersections of filling stations than the control site filling station. The average concentration of lead at control location was found to be 9 mg/kg, Cu 5 mg/kg, Mn 14 mg/kg and Zn 12 mg/kg, respectively. The analysis for soil sample from other locations when compared with the control location (SC-21) shows that almost all the pollution (>90%) near petrol filling stations is being generated due to higher density of vehicular exhaust and leakage of petrol fumes during filling of vehicles and scratching of vehicles tyres on roads. The study conducted to compare road side soils of northern England also shows ten time greater concentration of lead in the soil samples collected along busy roads of petrol filling stations then the control location concentration (Akbar *et al.,* 2006).

The climate of Karachi is tropical and dominated by the monsoon region. The average rain fall in Karachi amounts to about 20 mm and wind direction is SW in summer, and during winter it is usually in the NE. Wind velocity is 10 m/sec during the June-July and 3.5 m/sec from January to March. Because of the dry climate in Karachi lead contamination in the soil is not easily eliminated nor fixed.

Table 4 presents the matrix correlation for all the variables. The correlation coefficient is statistically significant when the values are above + 0.5. The Table 4 clearly shows that the values are positive and approximately all the values are above + 0.5.

Lead in the form of tetraethyl lead acetate is used as anti-knocking agent in petrol. It shows good relation with Cu, Mn and Zn. As the samples of soil were collected from petrol filling stations therefore, the source of trace metals in soil may be vehicular traffic. Lead is anti knocking agent in petrol and copper is the component of engine; hence both are directly related in automobiles and have good agreement in correlation coefficient matrix. Manganese shows the lowest correlation coefficient with all the metals studied. Although it is the component of tyres, but the values show that the correlation of manganese with other metals is not statistically significant. Zinc shows highest correlation with copper. The sources of these metals may also be the motor vehicles. Lead, cadmium, copper, and zinc are the major metal pollutants of the roadside environments and are released from fuel burning, wear out of tyres, leakage of oils, and corrosion of batteries and metallic parts such as radiators etc. (Dolan *et al.,* 2006).

A hospital survey was carried out to assess the impact of pollution on human health (Table 6). Seven hospitals were visited to collect the data about patient suffering from various diseases due to inhalation, during the study period 2009-2010.

Survey of hospitals shows that, the number of patents suffering from air pollution related diseases to that of allergic diseases is about 3:1. The number of male cases as compared to females regarding air pollution allergies, mainly related to chest infections is in the ratio o 2.4:1. This may be due to an extensive exposure of male to the polluted air and professional hazards as compared to females who are mostly house wives and remain indoor.

Table 6. Number of patients suffering from atmospheric pollution related diseases in hospitals of study area

Hospitals	Diseases	Number of cases			Male female ratio
		Male	Female	Total	
Kiran Hospital	Chest infection	12,218	5,479	17,697	2.2 :1
	Cancer	137,232	75,488	212,720	1.8 :1
	Heart ailment	6,487	3,743	10,230	1.7 :1
	Allergy	5,631	2,054	7,685	2.7 :1
	T.B	6,231	3,125	9,356	2.0 :1
	Pulmonary diseases	20,432	9,288	29,720	2.2 :1
Darul Sehat Hospital Gulistan-e-Jauhar	Chest infection	47,738	21,862	69,600	2.2 :1
	Cancer	16,572	7,828	24,400	2.1 :1
	Heart ailment	19,381	9,419	28,800	2.1 :1
	Allergy	7,123	4,189	11,312	1.7 :1
	T.B	9,421	4,127	13,548	2.3 :1
	Pulmonary diseases	85,525	38,875	124,400	2.2 :1
Ashfaq Memorial Hospital Gulshan-e-Iqbal	Chest infection	98,288	54,132	152,420	1.8 :1
	Cancer	69,375	36,145	105,520	1.9 :1
	Heart ailment	328,320	172,800	501,120	1.9 :1
	Allergy	8,421	3,715	12,136	2.3 :1
	T.B	10,220	6,012	16,232	1.7 :1
	Pulmonary diseases	111,822	48,618	160,440	2.3 :1
Abbasi Shaheed Hospital Nazimabad	Chest infection	86,196	49,644	135,840	1.7 :1
	Cancer	7,008	2,672	9,680	2.6 :1
	Heart ailment	117,961	54,423	172,384	2.2 :1
	Allergy	4,614	1,987	6,601	2.3 :1
	T.B	11,503	5,712	17,215	2.0 :1
	Pulmonary diseases	97,960	50,480	148,440	1.9 :1
Imam Clinic North Nazimabad	Chest infection	135,021	61,425	196,446	2.2 :1
	Cancer	3,212	1,704	4,916	1.9 :1
	Heart ailment	123,760	81,345	205,105	1.5 :1
	Allergy	3,614	1,287	4,901	2.8 :1
	T.B	15,503	8,712	24,215	1.8 :1
	Pulmonary diseases	99,543	39,021	138,564	2.6 :1
Shahrukh Hospital North Nazimabad	Chest infection	26,201	12,103	38,304	2.2 :1
	Cancer	712	324	1,036	2.2 :1
	Heart ailment	2,427	987	3,414	2.5 :1
	Allergy	1,614	680	2,294	2.4 :1
	T.B	7,503	2,712	10,215	2.8 :1
	Pulmonary diseases	17,960	7,480	25,440	2.4 :1
Taj Medical Complex Sadar	Chest infection	115,021	47,425	162,446	2.4 :1
	Cancer	9,503	3,712	13,215	2.6 :1
	Heart ailment	143,660	61,245	204,905	2.3 :1
	Allergy	2,427	787	3,214	3.1 :1
	T.B	1,614	580	2,194	2.8 :1
	Pulmonary diseases	91,543	40,021	131,564	2.3 :1
Total		2,126,517	1,043,367	3,169,884	2.0 :1

Few decades ago only industrial emissions was considered as an important risk factor for lung cancer but nowadays polluted air due to vehicular exhaust is the most important factor for lung cancer and other types of chest infections and pulmonary diseases. People in developing countries are commonly exposed to very high levels of pollution for 3-10 h daily over many years. The number of lung cancer cases by air pollution, are also on the increase and mostly male cases due to outdoor exposure in air. The worst affected age group for this disease was between 50 – 60 years, now reducing to 35-55 years. This is also mainly due to increasing air

pollution level but some other factors are also involved like personal hygiene, social activity, socio economic conditions, mental worries and smoking etc.

Conclusion

Trace metal contamination in the soil samples collected from main roads petrol filling stations along the busy roads of Karachi shows that growing number of vehicles, leaded gasoline consumption and poor conditions of the roads are major cause of high concentration of lead and other trace metals level in Karachi. Soil acts as an important sink for pollutants released through industrial discharge and other human activities. It is suggested that in the polluted areas such species of the plants should be grown which not only clean the atmosphere but also grow well in the polluted atmosphere as a permanent source of cleaning the environment around the filling stations.

References

Akbar, K.F., Hale, W.H.G., Headley, A.D., Athar, M. 2006. Heavy metal contamination of roadside soils of northern England. *Soil & Water Research,* **1:** 158-163.

Araya, M., Olivares, M., Pizarro, F. 2008. Copper in Human Health. *International Journal of Environment and Health,* **1:** 608-620.

Carrasquero-Durán, A. 2006. Determination of Lead Contamination Levels in Soils and Dust of Streets of Maracay, *Agronomia Tropica,* **56:** 252-273.

Caselles, J. 1998. Levels of Lead and other metals in citrus along a motor road. *Water, Air and Soil Pollution,* **105:** 593-602.

Celine, S.L., Xiangdong, L., Wenzhong, S., Sharon, C.C., Iain, T. 2006. Metal contamination in urban, suburban and country park soils of Hong Kong: a study based on GIS and multivariate statistics. *Science of the Total Environment,* **356:** 45-61.

Chaoyang, W., Cheng, W., Linsheng,Y. 2009. Characterising spatial distribution and sources of heavy metals in the soils from mining-smelting activities in Shuikoushan, Hunan Province, China. *Journal of Environmental Sciences,* **21:** 1230-1236.

CIA, 2013. The World Factbook, https://www.cia.gov/library/publications/the world-factbook. does/obdyouknow.html.

Colbeck, I., Nasir, Z.A., Ahmed, S., Ali, Z. 2010. The state of ambient air quality in Pakistan-a review, *Environmental Science and Pollution Research,* **17:** 49-63.

Das, M., Bhargava, S.K., Kumar, A., Khan, A., Bharti, R.S., Pangtey, B.S., Rao, G.S., Pandya, K.P., 1991. An investigation of environmental impact on health of workers at retail petrol pumps. *Annals of Occupational Hygien,* **35:** 347-352.

Davies, B.E., Holmes, P.L. 1972. Lead contamination of roadside soil and grass in Birmingham, England in relation to naturally occurring levels. *The Journal of Agricultural Science,* **79:** 479-484.

De-Miguel, E., Iribarren, I., Chacon, E., Ordonez, A., Charlesworth, S. 2007. Risk-based evaluation of the exposure of children to trace elements in playgrounds in Madrid (Spain). *Chemosphere,* **66:** 505-513.

Dolan, L. M. J., Van Bohemen, H., Whelan, P., Akbar, K.F., Malley, V., O-Leary, G., Keizer, P.J. 2006. Towards the sustainable development of modern road ecosystem. In: *The Ecology of Transportation Managing Mobility for Environment,* J. Davenport, and J.L. Davenport (eds.), pp. 275-331, Springer, The Netherlands.

Ferretti, M., Cenni, E., Bussotti, F., Batistoni, P. 1995. Vehicle induced lead and cadmium contamination of roadside soils and plants in Italy. *Journal of Chemistry and Ecology,* **11:** 213-228.

Fernández, R., Ramírez, A. 2002. Geoquímica de la contaminación urbana. *Ciencia,* **10:** 94-101.

Gadkari, N., Pervez, S. 2008. Source apportionment of personal exposure of fine particulates among school communities in India. *Environmental Monitoring Assessment,* **142:** 227-241.

Hafen, M.R., Brinkmann, R. 1996. Analysis of lead in soils adjacent to an interstate highway in Tampa, Florida. *Journal of Environmental Geochemistry and Health,* **18:** 171-179.

Hasan, S.A., Hayat, S., Ali, B., Ahmad, A. 2008. 28-Homobrassinolide protects chickpea (*Cicer arietinum*) from cadmium toxicity by stimulating antioxidants. *Journal of Environmental Pollution,* **151:** 60-66.

Hussein, F.A., Bade, A.A., Mousa, A.K. 2012. Effect of the zinc on the some of blood parameter and some organs in local duck (*Anas plater* Hycous) *Bas. J. Vetenity Research,* **11:** 103-115.

Iqbal, M.Z., Shafiq, M., Ali, S.F. 1994. Effect of automobile pollution on seed germination and branch length of some plants. *Turkish Journal of Botany,* **18:** 475-479.

Itoh, Y., Miura, S., Yoshinaga, S. 2006. Atmospheric lead and cadmium deposition within forests in the Kanto district, Japan. *Journal of Forest Research,*

11: 137-142.

Jarup, L. 2003. Hazards of heavy metal contamination. *Brazilian Medical Bulletin,* **68:** 167-182.

Jones, K. C., Symon, C., Tylor, P.J.L., Walsh, J., Johnston, A.E. 1991. Evidence for a decline in rural herbage lead levels in UK. *Atmospheric Environment. Part A. General Topics,* **25:** 361-369.

Kalantari, N., Ghaffari, S. 2008. Evaluation of toxicity of heavy metals for *Escherichia coli* growth. *Iranian Journal of Environmental Health Sciences & Engineering,* **5:** 173-178.

Karabassi, A.R., Nouri, J., Mehrdadi, N., Ayaz, G.O. 2008. Flocculation of heavy metals during mixing of freshwater with Caspian Sea water. *Environmental Geology,* **53:** 1811-1816.

Khan, D.H., Frankland, B. 1983. Effects of cadmium and lead on plants with particular reference to movement of metals through soil profile and plant. *Plant and Soil,* **70:** 335-345.

Krolak, E. 2000. Heavy metals in falling dust in Eastern Mazowieckie Province, *Polish Journal of Environmental Studies,* **9:** 517-522.

Malakoutiaa, M., Nouri, J., Hossini, H. 2009. Removal of heavy metals from paint industries waste water using Leca as an available adsorbent. *International Journal of Environmental Science and Technology,* **6:** 183-190.

Marjanović, M.D., Vukč ević, M.M. Antonović, D.G., Dimitrijević, S.I., Jovanovic, D.M., Matavulj M.N., Ristic, M.D. 2009. Heavy metal concentration in soils from parks and green areas in Belgrade. *Journal of the Serbian Chemical Society,* **74:** 697-706.

Mielke, H.W., Blake, B., Burroughs, S., Hassinger, N. 1984. Urban lead levels in Minneapolis: The case of the Hmong children. *Environmental Research,* **34:** 64-76.

Michalke, B. 2003. Element speciation definitions, analytical methodology, and some examples. *Journal of Ecotoxicology and Environmental Safety,* **56:** 122-139.

Nagatomo, S., Umehara, F., Hanada, K. 1999. Manganese intoxication during total parental nutrition. *Journal of Neurological Sciences,* **162:** 102-105.

Ndiokwere, C.L. 1984. A study of heavy metal pollution from motor vehicle emissions and its effect on roadside soil vegetation and crops in Nigeria. *Environmental Pollution,* **(B)7:** 247-254.

Silva, A.L.O., Barrocas, P.R.G., Jacob, S.C., Moreira, J.C. 2005. Dietary intake and health effects of selected toxic elements. *Brazilian Journal of Plant Physiology,* **17:** 79-93.

Sims, R.C. 1990. Soil remediation techniques at uncontrolled hazardous waste sites. A critical review. *Journal of Air and Waste Management Association,* **40:** 704-732.

Soylak, M., Narin, I., Elci, L., Dogan, M. 2000. Lead concentration of dust samples from Nigde City-Turkey. *Fresenius Environmental Bulletin,* **9:** 36-39.

Turer, D.G., Maynard, B.J. 2003. Heavy Metal contamination in highway soils. Comparison of Corpus Christi, TX and Cincinnati, OH shows organic matter is key to mobility. *Clean Technology and Environmental Policy,* **4:** 235-245.

Vinodhini, R., Narayanan, M. 2009. The impact of toxic heavy metals on the hematological parameters in common crap (*Cyprinus carpio* L.). *Iranian Journal of Environmental Health and Science and Engineering,* **6:** 23-28.

Wei, B., Yang, L. 2010. A review of heavy metal contaminations in urban soils, urban road dusts and agricultural soils from China. *Micro Chemical Journal,* **94:** 99-107.

Wheeler, G.L., Rolfe, G.L. 1979. Relationship between daily traffic volume and the distribution of lead in roadside soil and vegetation. *Environmental Pollution,* **18:** 265-274.

Xia, X., Chen, X., Liu, R., Liu, H. 2011. Heavy metals in urban soils with various types of land use in Beijing. *Journal of Hazardous Material,* **186:** 2043-2050.

Yang, Z., Lu, W., Long, Y., Baoand, X., Yang, O. 2011. Assessment of heavy metals contamination in urban topsoil from Changchun City, China. *Journal of Geochemical Exploration,* **108:** 27-38.

Zhang, C. 2006. Using multivariate analyses and GIS to identify pollutants and their spatial patterns in urban soils in Galway, Ireland. *Environmental Pollution,* **142:** 501-511.